UNIVERSITY OF
BELGRADE

Faculty of Mechanical Engineering

Mohammed Alazeezi

Design and Optimization of Dual-Propellant Grains of Solid Rocket Motors

Doctoral Dissertation

Belgrade, 2024

УНИВЕРЗИТЕТ У БЕОГРАДУ

МАШИНСКИ ФАКУЛТЕТ

Mohammed Alazeezi

Пројектовање и оптимизација двокомпонентних погонских пуњења ракетних мотора са чврстом погонском материјом

докторска дисертација

Београд, 2024.

Mentor:
Dr. Predrag Elek, Full Professor
University of Belgrade – Faculty of Mechanical Engineering

Commission members:

Dr. Aleksandar Simonović, Full Professor
University of Belgrade – Faculty of Mechanical Engineering

Dr. Aleksandar Milivojević, Associate Professor
University of Belgrade – Faculty of Mechanical Engineering

Dr. Saša Živković, Research Assistant
Military Technical Institute, Belgrade

Defense date:

Ментор:
др Предраг Елек, редовни професор
Универзитет у Београду – Машински факултет

Чланови комисије:

др Александар Симоновић, редовни професор
Универзитет у Београду – Машински факултет

др Александар Миливојевић, ванредни професор
Универзитет у Београду – Машински факултет

др Саша Живковић, научни сарадник
Војнотехнички институт, Београд

Датум одбране:

Title of doctoral dissertation:
Design and Optimization of Dual-Propellant Grains of Solid Rocket Motors

Abstract:

Attaining an accurate burnback analysis and internal ballistics model of a solid propellant rocket motor is a crucial factor of having a precise performance prediction of the rocket motor. A successful design of the motor depends solely on the first calculations of the internal ballistics which lead to designing the rocket motor components accordingly. The main objective that shall be kept in mind throughout the whole development cycle of a rocket motor is to deliver a product that meets the user system requirements. Grain's geometry, propellant's composition and nozzle's geometry are the main parameters that influence the chamber pressure value which they all have an interchangeable relation.

The work of this dissertation focused on solving a complex propellant grain shape that consists of two propellants with each propellant has its own composition characteristics. The equations were solved numerically through writing a MATLAB program that integrates the given inputs, burning surface area formulas and internal ballistics equations. This tool would help in simulating the rocket motor performance in different temperature conditions. An essential part of developing the MATLAB program is determining what happens at each step of the burning surface area during the combustion. Thus, the thrust and pressure values were calculated at each step and the values get carried out to the next phase of calculations. The program split mainly in four sections. The first one introduces the programs' inputs and assumptions, the second section introduces the original grain model calculations, the third section introduces the optimized model calculations, and the last section acts as hub collecting all the simulation outputs and make them presentable.

A static test was conducted on a 128 mm solid propellant rocket motor that has two-propellant grain and the thrust and pressure profiles versus time were obtained. The static test was performed on three different temperatures which are ambient at 21 ^{o}C, cold at -41 ^{o}C and hot at 51 ^{o}C. The static test results showed oscillations in the profile which could indicate some level of instability in the rocket motor performance. In order to solve this issue, the burn back analysis model of the tested propellant grain had to be found to understand the grain's progression. Once that was done, the cause of the oscillations was identified which led to developing and optimized grain shape that could eliminate the serrated curve from the original grain shape. The program assisted to validate the burnback analysis model of the original and optimized grains against the results form static test.

The primary objective of this work was to build a simplified tool that could solve such grain shapes with the two propellants. Further work was to be done to verify the optimized model and validate its outputs.

Key words:
rocket propulsion, solid propellants, two-component propellant, burning surface area, operating chamber pressure, thrust of rocket motor, rocket motor static test

Scientific field: Mechanical engineering

Scientific subfield: Weapon systems

UDC: 623:621.454:621.453/.457

Наслов докторске дисертације:
Пројектовање и оптимизација двокомпонентних погонских пуњења ракетних мотора са чврстом погонском материјом

Резиме:

Тачно моделирање сагоревања и унутрашњебалистичког процеса ракетног мотора са чврстом погонском материјом је кључан фактор за прецизно предвиђање перформанси ракетног мотора. Успешно пројектовање мотора зависи првенствено од основних прорачуна унутрашње балистике који даље следствено воде ка пројектовању појединих компоненти ракетног мотора. Главни циљ који треба имати на уму током целог развојног циклуса ракетног мотора је добијање производа који испуњава системске захтеве корисника. Геометрија погонског пуњења, састав погонске материје и геометрија млазника су главни параметри који утичу на вредност притиска у комори, при чему су сви ови параметри међусобно повезани.

Истраживање у овој дисертацији усмерено је на моделирање сагоревања чврстог погонског пуњења сложеног облика које се уз то састоји од две погонске материје различитог састава и карактеристика. Једначине које дефинишу промену површине сагоревања пуњења су нумерички решене применом програма у Matlab-у који интегрише задате улазе, изазе за површине сагоревања, као и унутрашње балистичке једначине. Овај алат омогућава одређивање параметара перформанси ракетног мотора у различитим условима амбијенталне температуре. Суштински део развоја поменутог програма је одређивање егзактне геометрије сагоревања двокомпонентног пуњења веома сложене степенасте геометрије. Дакле, вредности радног притиска и потиска су израчунате у сваком кораку и пренете у следећу фазу прорачуна. Програм је подељен четири основне целине од којих се у првој уводе улазне величине и претпоставке програма, други одељак се односи на методу прорачуна параметара перформанси ракетног мотора са изворним степенастим обликом погионског пуњења, трећи део је посвећен анализи сагоревања поједностављене оптимизоване геометрије пуњења, док последњи део има фукцију чворишта које прикупља све излазе симулације и омогућава њихову презентацију.

Статички тестовима експериментално је испитан ракетни мотор са чврстом погонском материјом пречника 128 мм који има двокомпонентно погонско пуњење и добијени су профили потиска и притиска у зависности од времена. Статички тест је изведен на три различите амбијенталне температуре: нормални услови подразумевају 21°C, доња температурска граница је -41°C, док је горња 51°C. Резултати статичког испитивања очекивано су показали осцилације у временским профилима притиска и потиска, што би указује на одређени ниво нестабилности у перформансама ракетног мотора. Да би се решио овај проблем, најпре је формиран модел прорачуна сагоревања тестираног погонског пуњења да би се разумела еволуција горућих површина и одредили параметри перформансе. Када је то урађено, идентификован је узрок осцилација, што је омогућило развој оптимизованог облика пуњења који би могао елиминисати тестерасте криве пртиска и потиска карактеристичне за оригинални облик пуњења. Развијени програм је омогућио да се валидира модел анализе сагоревања оригиналног и оптимизованог погонског пуњења у односу на резултате статичких испитивања.

Примарни циљ овог рада био је да се направи једноставан инжењерски алат који омогућава анализу и моделирање ракетних мотора са двокомпонентним погонским пуњењем. Даљи рад би између осталог требало да се фокусира на верификацију оптимизованог модела погонског пуњења кроз поређење са експрименталним резултатима.

Кључне речи:
ракетни погон, чврсте погонске материје, двокомпонентно гориво, површина сагоревања, радни притисак ракетног мотора, потисак ракетног мотора, статичко испитивање ракетног мотора

Научна област: машинско инжењерство

Ужа научна област: војно машинство – системи наоружања

UDC: 623:621.454:621.453/.457

Table of Contents

List of Figures

List of Tables

Acronyms

Nomenclature

A	Burning surface area	[m^2]
A_c	Cylindrical burning surface area	[m^2]
A_l	Lateral burning surface area	[m^2]
A_f	Burning surface area of fast burning propellant	[m^2]
A_s	Burning surface area of slow burning propellant	[m^2]
A_{se}	Burning surface area of the edge	[m^2]
A_t	Throat area	[m^2]
A_e	Nozzle exit area	[m^2]
a	Axial burned edge of the slow fuel	[m]
b	Burn rate coefficient	[m/s/Pa^n]
b_f	Burn rate coefficient of fast burning propellant	[m/s/Pa^n]
b_s	Burn rate coefficient of slow burning propellant	[m/s/Pa^n]
c	Radial burned edge of the slow fuel	[m]
c^*	Characteristic velocity	[m/s]
c_F	Thrust coefficient	[-]
D	Outer diameter of both propellants	[m]
D_f	Inner diameter of the fast burning propellant	[m]
D_s	Inner diameter of the slow burning propellant	[m]
e	Length of the burned edge of slow fuel	[m]
e_s	Burning slope	[m]
F	Thrust	[N]
I_t	Total impulse	[Ns]
I_s	Specific impulse	[m/s]
k	Adiabatic gas constant	[-]
L_f	Length of the fast burning propellant	[m]
L_s	Length of the segment	[m]
L_{slope}	Slope length	[m]
$\dot{m}$	Mass flow rate	[kg/s]
$\dot{m}_f$	Mass flow rate of fast burning propellant	[kg/s]
$\dot{m}_s$	Mass flow rate of slow burning propellant	[kg/s]
m_p	Propellant mass	[kg]
n	Burn rate exponent	[-]
n_f	Burn rate exponent of fast burning propellant	[-]
n_s	Burn rate exponent of slow burning propellant	[-]
p_0	Chamber pressure	[Pa]
p_e	Nozzle exit pressure	[Pa]
p_a	Atmospheric pressure	[Pa]
R	Gas constant	[$Jkg^{-1}K^{-1}$]
r	Burning rate	[m/s]
T_c	Burning temperature	[K]
t_b	Burning time	[s]

V_1	Volumetric loading fraction	[-]
V_p	Propellant's grain volume	[m^3]
V_a	Chamber pressure volume	[m^3]
w	Web	[m]
ρ_p	Propellant density	[kg/m^3]
ρ_f	Fast burning propellant density	[kg/m^3]
ρ_s	Slow burning propellant density	[kg/m^3]
σ_p	Temperature sensitivity of burning rate	[K^{-1}]
π	Temperature sensitivity of the pressure	[K^{-1}]
ϵ	Expansion ratio	[-]

Acknowledgment

In the name of Allah, this dissertation would not have been possible without the United Arab Emirates and its leadership for giving me the opportunity and a healthy environment to pursue my higher studies at the University of Belgrade – Faculty of Mechanical Engineering. Words cannot express my gratitude for the endless support that I have received not only on the PhD studies, but even for Bachelor and Master studies during the past 13 years of being abroad.

I am especially indebted to Halcon and all my colleagues, who have been supportive of my career goals and who worked actively to provide me with the protected academic time to pursue my higher studies goals. This dissertation and the research behind it would not have been possible without the exceptional support offered by my organization. I am also grateful for the insightful comments offered by my colleagues. The expertise and generosity of one and all have improved this dissertation in innumerable ways and saved me from many errors.

I would also like to express my great appreciation to Prof. Predrag Elek for his valuable and constructive suggestions during the planning and development work of this dissertation. As my supervisor during the master's and PhD studies, he has taught more than I could ever give him credit for here. The continuous unwavering guidance and support have been invaluable, and this dissertation work has not been possible without Prof. Elek.

I want to take this opportunity to express gratitude to my friends and the people whom I came across during this journey for graciously helping me and leaving a great impact on this journey of completing my dissertation.

Lastly, but most importantly, nobody has been more important to me in the pursuit of this dissertation than the members of my family. I would like to show my appreciation and thank my parents, whose guidance and love are with me in whatever I pursue. They are the ones who provide me with unending inspiration. I am deeply grateful to my siblings for their never-ending support and unconditional care during this intense dissertation period.

1. Introduction

1.1 Literature review

1.1.1 Propulsion

Propulsion, in its broadest sense, is the act or process of pushing or pulling an object at rest in order to change its position. The object's position is changed by applying a force to it which changes its speed or overcome a drag force that is applied to it [1]. There are different forms of propulsion systems which are defined based on the energy source that they provide. The systems that drive the vehicles to which they are linked are known as propulsion systems. Propulsion systems, under this concept, are many and diverse, beginning with our muscles, which we use to move ourselves while walking, running, swimming, and so on. Consider traditional reciprocating engines, such as steam-powered external combustion piston engines or petroleum-fueled internal-combustion piston engines. Internal combustion piston engines power vehicles, ships, locomotives, and tiny low-speed aircraft, whereas steam engines propel locomotives and ships. The reciprocating engines that power trains and vehicles have a different propulsion theory than ships and low-speed aircraft. The wheels, propelled by the engine, seek to push the road or rails through friction in the former.

The vehicles to which the wheels are linked are moved in the reverse way driven by the reactive force (Newton's Third Law). The propellers pull in and push (accelerate) the fluid stream (water in ships, air in aircraft) to a speed higher than the velocity in ships and low-speed aircraft; that is, the fluid's momentum rate at exit is larger than the fluid's momentum rate at arrival to the propellers. Vehicles are again pushed or propelled by the reactive force. Nozzles accelerate "closed" streams and expel them as jets, whereas propellers accelerate "open" streams. The thrust is generated primarily by the difference in momentum rates at the entry and exit of the propulsion systems, whether they be propellers or nozzles. The momentum rates at the propeller's entry and departure must be considered in the case of propellers. However, we must consider the momentum rates at the entry and exit of the jet propulsion engine in the case of jet propulsion systems [2].

Thrust is the force produced by propulsion systems. There are multiple principles of propulsion systems, and rocket propulsion is one of the main ones.

1.1.2 Rocket propulsion

All the rocket propulsion systems are explained by Newton's third law of motion which states that there is always an equal and opposite reaction for every action. There are several types of rockets which are classified based on the stored fuel and oxidizer, and the most common ones are liquid propellant rocket motors, solid propellant rocket motors and hybrid rockets. The liquid propellant rocket motors store the fuel and oxidizer in two separate tanks where they are both injected into the combustion chamber. Injecting the fuel and oxidizer to the combustion chamber is controllable which gives liquid rocket motors an advantage over the solid propellant rocket motors [3]. Liquid propellants are usually used when it is required to have high performance and controllability of the rocket motor. Liquid propellant mixtures often provide higher performance than solid propellant mixtures by a ratio of 1.7, and it is common to have a combination of oxygen

and hydrogen. As discussed before, the liquid propellants are stored in two separate tanks, so they are either pushed into the combustion chamber, so it's called a pressurized feeding system or pumped into the combustion chamber then it works on the turbopump feeding system principle [4]. On the other hand, solid propellant rocket motors cannot be controlled once they are ignited since they store the fuel and oxidizer in the same combustion chamber [5]. Hybrid rockets fall in between the liquid rockets and solid rockets when it comes to performance and complexity. This type of rocket has the oxidizer stored in a separate tank than the fuel where the fuel is solid propellant stored in the chamber. It has the possibility of controlling the thrust during the flight mission [6]. These types of rockets are usually used for applications such as missiles or space shuttles. Figure 1 shows the main differences between the three rocket propulsion systems.

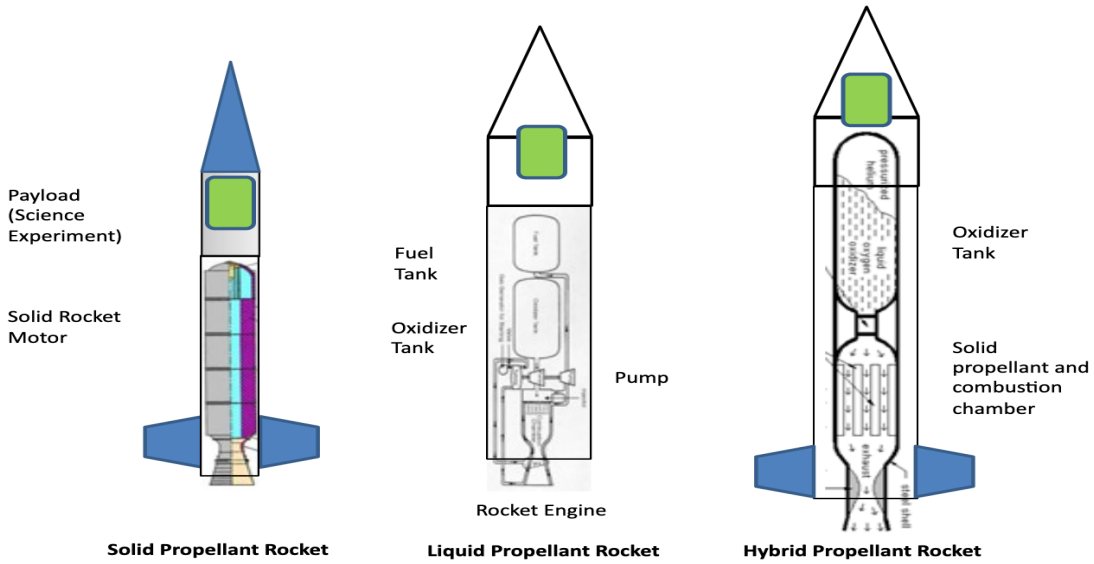

Figure 1 Rocket propulsion types [7]

1.1.3 Solid propellant rocket motors

Solid propellant rocket motors (SPRM) rely on solid propellants to deliver the needed energy to generate the needed thrust [8]. The main components of the solid propellant rocket motors are illustrated in Fig. 2.

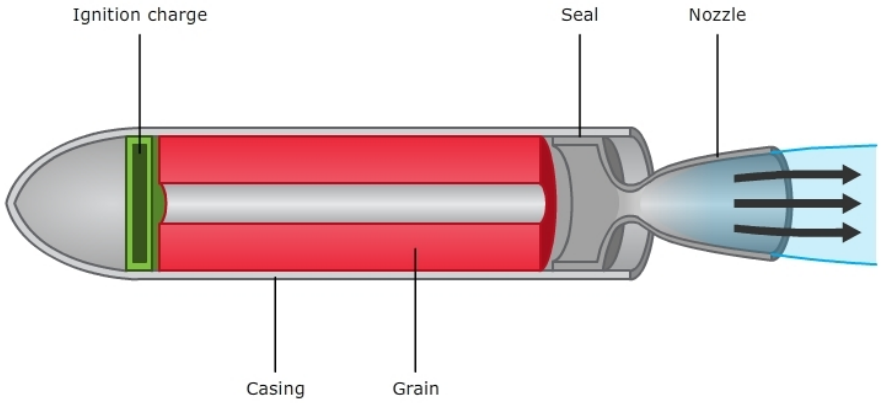

Figure 2 Schematic view of solid propellant rocket motor [9]

- Propellant grain:

The propellant grain is the main component that forms the rocket motor which its combustion provides the required energy of generating thrust. Two elements could influence the propellant grain selection, which are the propellant composition and the grain shape. The solid propellant composition selection will be discussed further in chapter 3.

- Combustion chamber/case:

The rocket motor combustion chamber or called the case as well has two primary functions. The first one is to house all the components that it holds the closure and igniter at one end and the nozzle at the other end. The second one is basically acting as a combustion chamber where the propellants' combustion occurs and containing the hot gasses before propelling them through the nozzle. The shape of the case is often cylindrical, but spherical cases are seen in some applications. The shape of the case usually takes the outer shape of the propellant grain. Maximum expected operating pressure (MEOP) must be taken into consideration when designing the case because it has to withstand high chamber pressure. That being said, it is necessary to use a proper material for the case in order to secure a safe operation of the rocket motor. Different materials are used such as aluminum alloy, high strength heat treated steels or enhanced fiber composite which each one of them has its own advantages and disadvantages. For example, fiber composite has a great advantage on reducing the case weight. However, steel is by far the most commonly used material due to its good characteristics and low cost of production compared to the other types of materials. Rocket motor cases are qualified to be used after conducting hydrostatic tests on them to ensure that they meet their design requirements [10].

Casings are often constructed of metal alloys. Titanium alloys and aluminum alloys are employed in smaller rockets, whereas nickel alloy steels are used in larger rockets [11]. They are made into cylindrical shells with expanded ends for joints. For specialized casing, sophisticated welding and heat treatment equipment and methods have been developed. Quality guarantee tests for hardness, durability, weld soundness and hydraulic pressure are performed on the casings. Thermal insulation is installed on the inside of the casings to protect them from hot gases. End covers, nozzles, and handles are all included in the casing. Composite materials, such as fiber-reinforced plastic (FRP), can also be used for casings. This type of enclosure is light but strong.

High specific strength, high specific modulus, manufacturing ease, ease of access and service conditions are the key criteria used to choose materials for SRM components. The materials used in rocketry are classified as follows: architectural metallic materials, composite materials, thermo-structural materials, thermal protection materials, special materials, and chemicals. The materials used in SRM casing are shown in Table 1 [12].

Certain metal enclosures suffer from stress-corrosion cracking, which can lead to sudden collapse with no visible signs of imminent disaster. The emphasis put on lightweight thin metal casings exacerbates stress corrosion and progression of cracks, which typically begins with a

fault in the metal and ends with a breakdown at a level of stress below the metal's yield strength. The casings are made of composites, which have the benefit of being lighter.

Table 1 Applications of different materials in the motor casing

No.	Materials	Applications
1	Low case Carbon Steel (15 CDV6)	Used in solid rocket motor case
2	Maraging Steel (M250) with high strength and high toughness	Used in booster solid rocket motor case
3	Titanium Alloy (Ti-6Al-4V)	Used in high-pressure gas bottles
4	Aluminum Alloys (AA 2219, AA2014, AA6061)	Used in liquid propellant tanks, engine components, airframe in reusable launch vehicles
5	Magnesium/ Mg-Lithium alloys	Used in upper stage structures like payload adopter, avionic decks, equipment bay structure.
6	Carbon Fiber / Silicon Carbide Ceramic Matrix	Used in nose-cap of heat-shield, leading edge and control surface of Rocket Launching Vehicle (RLV)
7	Different coating materials (Rajesh et al., 2017)	Used for protection and imparting certain characteristics to surfaces, potting of connectors

The researchers in [13] assessed several motor case materials to the composites in Table 2.

Table 2 Physical properties of different materials used for motor casing

	D6AC Steel	Maraging Steel	Glass-filament Composite (s-2)	Organic filament composite (Kevlar)	Intermediate-modulus polyacrylonitrile carbon fiber
Tensile Strength [MPa]	1586	1724	1172	827.4	1551
Density [g/cm^3]	7.883	8.00	1.993	1.356	1.55
Elastic Modulus [GPa]	199.5	189.1	31.72	75.84	172.4

- Nozzle:

In rocket engines, the high-energy product gases generated in the combustion chamber are propelled through the nozzle. The nozzle is a critical part, and one should be careful when designing it. Generally, the nozzle consists of three main parts which are the convergent part, throat and divergent part. The combustion products have a high temperature and low velocity at the convergent part of the nozzle. The gasses accelerate through the throat to reach higher

velocities while the pressure and temperature get reduced. This process basically translates the thermal energy of gasses to kinetic energy using the most common shape of nozzles which is de Laval nozzle or known as convergent-divergent nozzle Fig. 3.

Expansion is the process of converting combustion's thermal energy into kinetic energy in order to propel an item ahead. To put it another way, the hot gases produced by the combustion of fuel inside a jet or rocket engine are expelled via a nozzle to generate thrust. The form of the nozzle is crucial to the expansion process. As the high-temperature flow cools, it expands against the nozzle's walls, creating a force that propels the vehicle forward. Because the excess nozzle wall is wasted and does not provide any more thrust, this "pinching" of the flow diminishes efficiency. To avoid this needless wall, the nozzle could have been shorter.

Under-expanded flow regime describes the circumstance in which the ambient air pressure is lower than the exit pressure. The flow continues to extend outward after leaving the nozzle in this scenario. Because the external expansion exerts no stress on the nozzle wall, this behavior affects efficiency. As a result, this energy cannot be turned into thrust and is wasted. The nozzle should have been longer to catch and turn this expansion into thrust. On the other hand, a convergent-divergent nozzle endures an over-expansion flow when the exit pressure is less than the ambient pressure due to several conditions such as a large exit area comparing to the optimum, nozzle working at low altitudes and when the chamber pressure is low right after the ignition. The desired design condition of a nozzle is when full expansion of combustion product is achieved using so-called adapted nozzle. In this condition, the exit pressure equals the ambient pressure which results in a maximum thrust that could be reached.

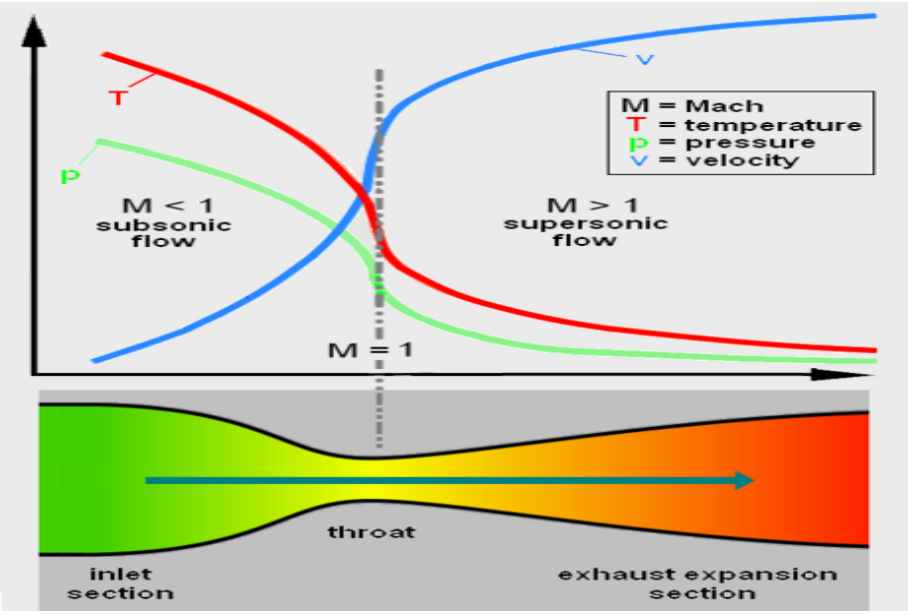

Figure 3 An illustration of de Laval nozzle [14]

To date, three principal types of nozzles have been used: the cone, the bell or contoured, and the annular or plug.

i. Conical Nozzle:

For its easiness of manufacturing, the conical nozzle (Fig. 4) was widely utilized in early rocket operations. The property that the sidewalls diverge at a fixed angle gives the cone its name. Because it optimizes the axial element of exit velocity and creates a high specific impulse, a narrow-angle generates more force (a measure of rocket efficiency). However, the consequence is a longer, heavier, and more difficult to construct nozzle. A wide nozzle wall angle, on the other hand, reduces the size and weight of the nozzle. However, big angles degrade performance at low altitudes due to rapid expansion and flow separation caused by high ambient pressure.

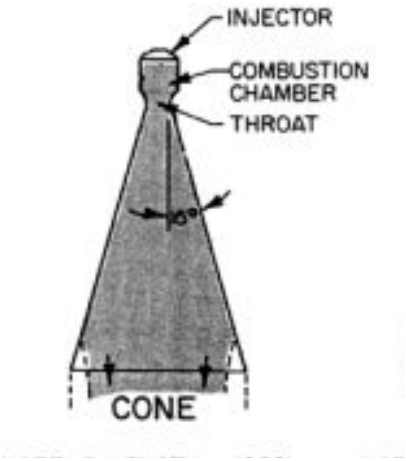

Figure 4 Conical Nozzle [15]

ii. Bell Nozzle:

The bell nozzle, Fig. 5, the most common nozzle shape, has considerable size and productivity benefits over the conical nozzle. The nozzle deviates at a rather wide angle near the throat, while the degree of divergence decreases further downwards. The divergence angle at the nozzle exit is quite modest. The bell is therefore a balance between the two poles of the conical nozzle, as it reduces weight while increasing performance. The most significant aspect of the design is contouring the nozzle to prevent transverse shocks and enhance performance. However, it must be kept in mind that the final bell design will be optimal only at a single height.

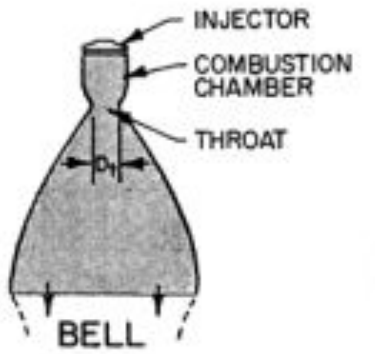

Figure 5 Bell Nozzle [15]

iii. Annular Nozzle:

Due to its increased complexity, the annular nozzle, also known as the plug or "altitude-compensating" nozzle, is the least commonly used of those described. The name "annular" alludes to the concept that combustion takes place around the root of the nozzle in a ring or annulus. The center body that restricts the airflow from what would be the center section of a typical nozzle is referred as the "plug". The term "altitude-compensating" is occasionally used to characterize these nozzles because it is their principal benefit.

- Igniter:

The igniter's primary job is to start the combustion process in a regulated and predictable manner at a predetermined rate [16]. It is necessary to understand the interrelation between the igniter's ignition, flame spreading phenomena and the interior ballistics of the SPRM which will lead to a reliable performance of the igniter [17]. Thus, a mathematical model is usually formed to simulate the ignition process.

- Types of Igniters:

There are basically two types of igniters used in solid propellant rocket motors, i.e., Pyrogen igniters and Pyrotechnic igniters.

- Pyrogen Igniter:

The purpose of a pyrogen igniter, shown in Fig. 6, is to provide a regulated, high-temperature, high-pressure gas to ignite solid propellant particles in a rocket engine. Many inert components make up today's pyrogens. A cap with many integrally molded elements, an ignition pellet retention plate, and a tube with other solidly molded characteristics make up the Standard Molded Pyrogen Igniter (SMPI). An analysis is described that shows the SMPI idea is a realistic method for the design and fabrication of pyrogen igniters for solid propellant rocket motors. Integrating the mechanical and thermal characteristics of molded composites can lead to the production of lighter components at a lower cost in some applications. The displacement compression procedure is used to create high strength, narrow-sided tubes with high length to diameter proportions from the reinforced plastic molding compound [18].

The propulsion systems used in pyrogens must meet the same standards as propellants used in rocket motors. As a result, the evaluation of these propulsion systems is comparable to that of rocket motors. The restrictions on heat release rate and physical qualities of propellants used in pyrogen igniters, on the other hand, are typically less stringent than when propellants are employed in rocket motors. The needed energy flux outputs can be produced over a wide range of burning rates. Pyrogens have smaller propellant webs, thicknesses, and lengths, which means they are less stressed by temperature variation.

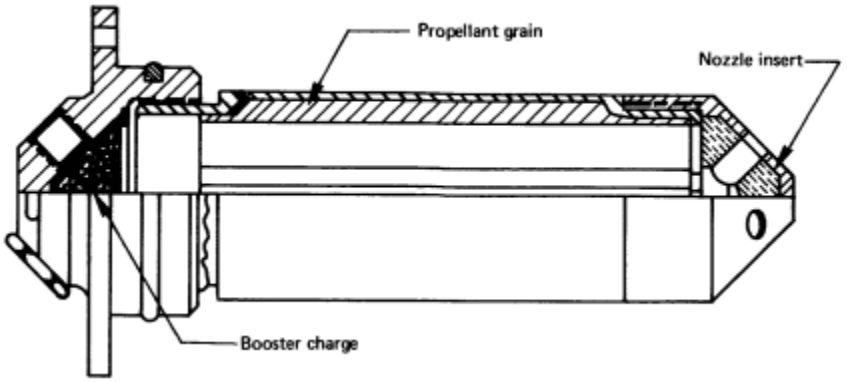

Figure 6 Pyrogen Igniter [18]

- Pyrotechnic Igniter:

A pyrotechnic initiator (also known as an igniter or an initiator), shown in Fig. 7, is a device that contains a pyrotechnic composition that is used to ignite certain, more difficult-to-ignite materials including thermites, gas generators, and solid-fuel rockets. The name is frequently used in the compositions as well. The phrase "heat of explosion" refers to the measurement of available energy created when a certain mass of pyrotechnic is ignited in an inactive environment in order to determine the overall energy generated by the reaction. This number may be easily tested with laboratory equipment and is a decent, if not perfect, an indication of pyrotechnic performance.

However, this statistic does not account for the rate of energy output, which is determined by the rate of combustion. Since pyrotechnics are often utilized in compressed form with a wide range of sizes, press settings, densities, and other factors, there is no universally approved burning-rate test. As a result, the rate of pressurization created by a pelleted pyrotechnics sample is used to determine the rate of burning. Crushing strength is the most typical test for pyrotechnic pellet durability, but resonance, shock, and impact tests are also used to determine fracture toughness. Differential thermal analysis (DTA), ignitability determination, and analysis of the radiated power spectra during pyrotechnic combustion are some of the special testing methods used to analyze new or altered formulations [19].

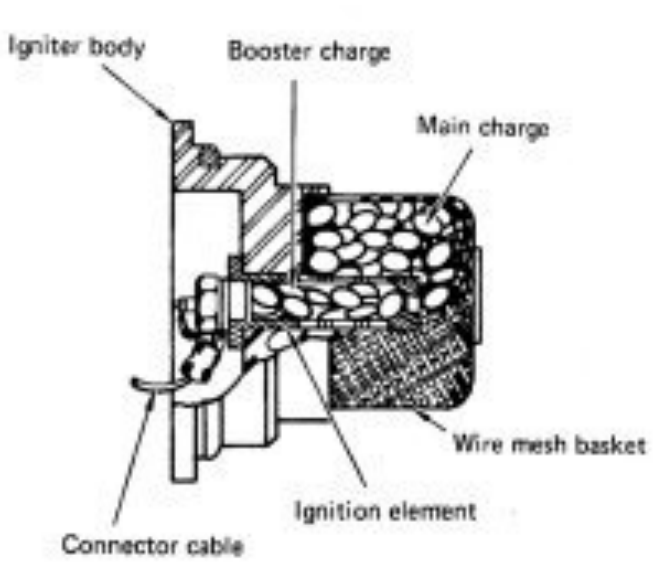

Figure 7 Pyrotechnic igniter [19]

- Insulation:

The flame temperatures produced by solid propellant rockets frequently approach more than 3000 K. The demand for an enhanced thermal protection system (TPS) to shield the rocket's case wall from the extremely high temperatures created grows as the necessity for extended functioning of solid propellant rocket engines grows. Multiple factors could decide on the optimum TPS which are purpose, weight, durability during processing, special properties, and the processing method. For several minutes, the insulation must be able to endure high temperatures. Aside from heat resistance, the insulation must be resistant to erosion, which is a common reaction in combustion products. The fundamental goal of insulation is to keep the rocket motor casing safe. The amount of heat that the motor casing can bear is determined by its material and structural design. The casing temperature should be maintained below 300°C in many instances for the duration of firing [20].

Ablative thermal protection is another form of thermal protection systems in solid propellant rocket motors based on specially designed ablative materials to withstand high temperatures and gradually erode or ablate when exposed to heat. Common ablative materials include carbon phenolic composites, epoxy resins, and other high-temperature polymers. The ablative material is typically applied as a liner or coating on the inner surface of the motor casing. As the solid propellant burns and produces hot gases, the ablative material begins to erode or ablate. This erosion process is intentional and controlled. As the ablative material erodes, it takes away heat with it, effectively cooling the motor casing. The material's erosion rate is carefully calculated and engineered to ensure that the casing remains below its critical temperature [21].

Spray-on foam insulation, as well as other classic insulation materials like cork, will offer thermal protection for all rocket components, big and small.

- Inhibitor:

An inhibitor is a film or coating of a slow-burning or non-burning substance that is placed on a portion of the propellant grain area to avoid it from burning. The early burning area can be decreased and managed by avoiding burning on restricted surfaces. The grain can be held in its shell in one of two ways. The casing is utilized as a mold in case-bonded grains, and the propellant is cast directly into the casing and attached to it. Since freestanding propellant grains are produced independently from the casing (by extrusion or casting into a cylindrical mold or cartridge) and then filled into or compiled into the casing, the structure selected for the grain for this report is the freestanding one, because it often has a lower cost and permits the grain to be split into smaller segments for easy design and construction. In this freestanding type, the inhibitor makes contact with the grain surface of the casing, acting as a cylindrical mold in the casting process as well as heat protection.

After ignition of a solid-propellant rocket, the mixture of oxidizer and fuel within the propellant grain produces a rise in temperature and pressure in the combustion chamber owing to the propellant burning. Because the heat transmission in the combustion chamber might be particularly detrimental to the rocket motor construction as a result of this burning, it is advised that an inhibitor be used [22].

1.2 Burn-back analysis

The design of the propellant grain starts by selecting the grain shape which will deliver the required performance from the rocket motor since each grain configuration has a specific profile, and this topic will be discussed in the next section. Nevertheless, it is required to calculate the burning surface area of the selected propellant grain. The calculation will describe how the burning of the propellant grain progresses during the combustion in the chamber, and this process is called the burn-back analysis. Knowing the burned surface area will contribute into finding the main performance parameters of the rocket motor. This analysis could be done either analytically via the geometry equations or numerically using 3D CAD parametric modeling software like PTC CREO. It will be calculated analytically in this project of two-component propellant grain where the burn-back analysis equations will be defined, and they will be implemented in MATLAB to run the calculations numerically and calculate the burning surface area at different steps.

Grain burn-back analysis determines the change in a solid propellant's burning surface and is split into three types [23]. The first is analytical approaches, which are simple to use and have a quick computation time, therefore they are commonly employed for conceptual or optimal design with several calculations [24]. These approaches, on the other hand, are not suited for difficult-to-formulate complicated 3D setups.

In drawing methods, the other two kinds of techniques are utilized to evaluate 3D configurations, and a CAD application is used to acquire configuration data. A CAD application may be used to construct and change a propellant's configuration in a virtual environment, which has the benefit of validating complicated configuration variations.

The third method of conducting the burnback analysis is using the level-set method which is a numerical technique used in computational fluid dynamics (CFD) and other scientific simulations to track the evolution of interfaces. In grain burnback analysis, the primary focus is on tracking the evolving interface between the burning propellant and the unburned propellant. The level-set method provides a way to describe and track this interface explicitly. The evolution of the level-set function is governed by a partial differential equation (PDE) called the level-set equation. This equation describes how the interface moves over time as a result of various physical processes, such as burning, heat transfer, and fluid flow. In grain burnback analysis, it would include terms related to the propellant regression rate, heat generation, and thermal conduction.

The analytical technique, in which the burning surface or contact is described using mathematical relations, is another way to do burnback analysis. Unlike the drawing approach, the analytical method represents the burning evolution quickly and continuously [25]. The analytical technique has the drawback that the relationships are dedicated to a single grain arrangement, making it difficult to infer the necessary mathematical equations for some complicated configurations.

Burnback analysis is a crucial stage in estimating a solid-propellant rocket motor's ballistic performance. The drafting methodology, in which the modelling of the burning is done by merging basic forms to define the grain starting geometry and the burning surface is considered to propagate normal to itself [26], is the earliest way of doing the burn back analysis. The drawing approach is used in the well-known Solid Performance Program [27]. The primary disadvantages of this approach are that it is explicit, that it involves a lot of human-computer contact, which can lead to mistakes, and that it takes a long time.

1.3 Propellant grains' configurations

As mentioned earlier, the propellant's grain shape can play a vital rule in defining the thrust-pressure curves which provide the type of the mission the rocket motor will provide when the propellant characteristics are set. Then, indeed the grain's shape is selected upon defining the thrust profile as there are multiple burning behaviors can be delivered as shown in Fig. 8. In some applications, it's required to have a progressive burning behavior where the burning surface area progresses starting from a lower burning surface area. In contrast, some applications require a regressive burning behavior. The most common burning over combustion time is the neutral burning where the burning stays constant throughout the combustion process. Other infrequent used shapes are the ones contain two or more burning behaviors like having a dual thrust profile that have a boost phase then a longer sustaining phase. There are some important aspects need to be taken into consideration when designing the propellant grain shape which are the volumetric loading fraction, web fraction and the sliver fraction.

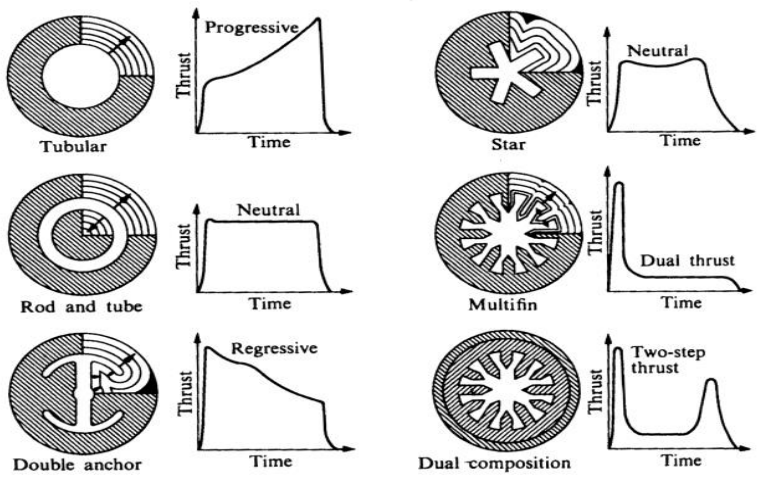

Figure 8 Different thrust profiles in respect with different grain configuration [28]

The volumetric loading fraction, also known as the propellant loading fraction, is an important parameter in the design and analysis of solid propellant rocket motors. It represents the fraction of the motor's total volume that is occupied by the solid propellant Eq. 1. The volumetric loading fraction plays a critical role in determining the motor's performance characteristics, such as thrust and specific impulse. A higher V_1 generally leads to greater propellant mass and, consequently, higher thrust and longer burn times. Achieving an optimal volumetric loading fraction is essential for motor efficiency. An excessively low or high V_1 can result in inefficient use of the motor's internal volume and may lead to suboptimal performance. Thus, high values may lead to more aggressive burn rates and potentially higher internal pressures, requiring stronger motor casings. Conversely, a very low V_1might result in insufficient thrust. The volumetric loading fraction is usually between 0.75 and 0.85 for some tactical missiles [29].

$$V_1 = \frac{V_p}{V_a} \tag{1}$$

whereV_1 is the volumetric loading fraction,V_p is the propellant's grain volume, and V_a is the total available chamber volume.

When the propellant grain reaches the burnout, there could be some propellant left unburned which is called the sliver. Hence, the sliver fraction is known as the ratio of the sliver mass at the end of the combustion to the total mass of the propellant grain [30]. The web thickness of a solid propellant grain is the minimum thickness of from the initial burning surface area to the insulated or inhibited surface area of the grain. In the case of two propellant grains forming one grain inside the case, the web thickness would be the minimum thickness from the burning surface area to the intersection of other propellant's burning surface area. The general form of web thickness of a cylindrical grain with an inhibited outer diameter is as the following:

$$w = \frac{D - d}{2} \tag{2}$$

The web fraction is the ratio of the grain web thickness to the outer radius of the grain Eq. 3, and it contributes into controlling the burning time in a rocket motor.

$$w_f = \frac{2w}{D} \tag{3}$$

where D is the grain outer diameter and d is the grain inner diameter as show in Fig. 9.

Erosive burning is defined as the burning rate being influenced by the cross flow characteristics of the burned products over the burning surface, in addition to the pressure. It is necessary to avoid erosive burning during the propellants combustion or to control it to ensure optimum and successful rocket motor mission. The erosive burning model based on the heat transfer theory was developed Lenoir and Robillard [31].

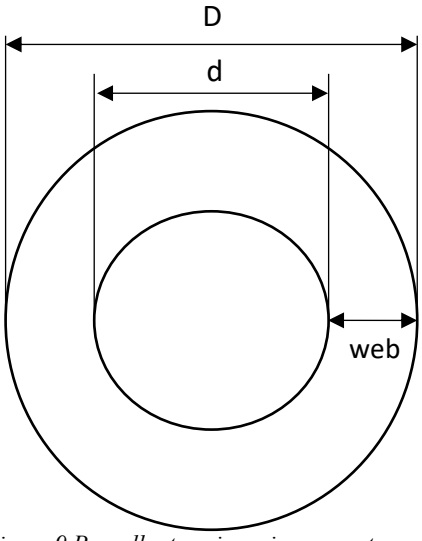

Figure 9 Propellant grain main parameters

As shown in Fig. 8, propellant grains could come in different shapes based on the need and the requirements of the rocket motor performance. It will be discussed briefly the main existing grain configurations which are currently in use.

- Cylindrical/Tubular:

The cylindrical or tubular shape, as the name suggests, is a propellant grain that has a central cavity as shown in Fig. 10. This shape is defined by three variables which are the outer diameter, length and internal diameter. The burning occurs radially starting from the internal cylindrical surface towards the outer diameter if the two front sides are inhibited which results in a progressive profile. The simplicity of manufacturing this grain's shape makes it desirable by rocket motor designers. However, they tend to use two propellant compositions to achieve neutrality which will be the case in this project.

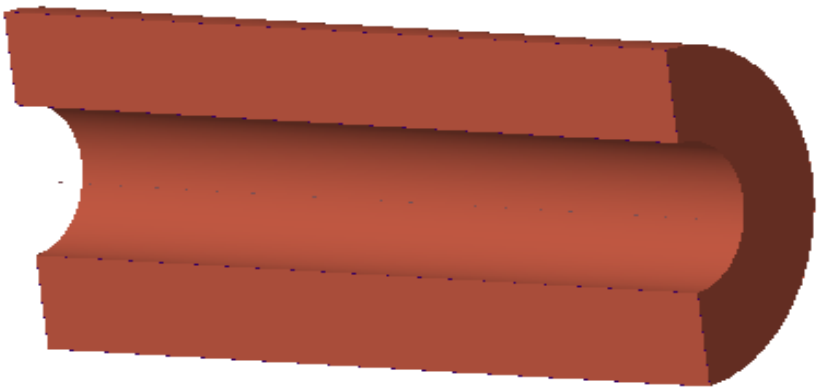

Figure 10 Cylindrical grain shape

- End burner

End burner grains are defined by only two parameters which are the outer diameter and the total length Fig. 11. The burning takes place only at the front side because it is usually inhibited through the rest of the surfaces around. Rocket motors with this propellant grain geometry provide a neutral thrust profile because the burning surface area stays constant throughout the combustion process. Despite of the high volumetric fraction that the end burner grain shape has, but it has low burning surface area which could be considered as a disadvantage because it leads to generating low pressure and thrust profiles. However, it provides long burning duration since it burns only from the end face.

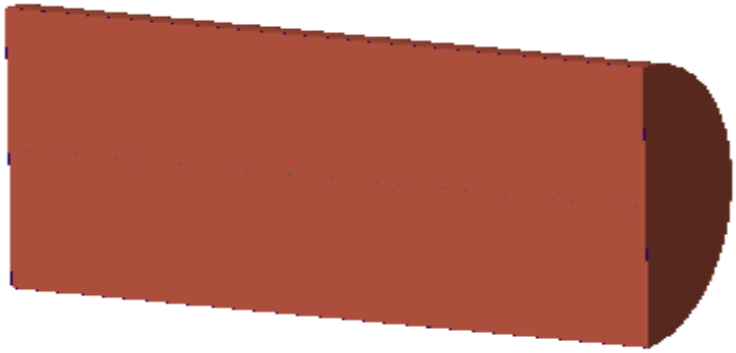

Figure 11 End burner grain shape

- Star

Star shapes are commonly used in the solid propellant rocket motors industry due to the advantages that they have. They could deliver either progressive, neutral, or regressive burning surface area based on the number of the slots of the shape. A star propellant grain is characterized by a central core surrounded by multiple radially arranged burning segments. The resulting shape resembles a star when viewed from the front or back Fig. 12. Star grains provide a significantly larger burning surface area compared to cylindrical grains of the same length and diameter. This increased burning surface allows for higher thrust levels and can result in a shorter burn time, making star grains suitable for applications requiring rapid acceleration. Star grains are usually chosen for their advantage of delivering neutral pressure and thrust profiles. More internal slots mean more burning surface area.

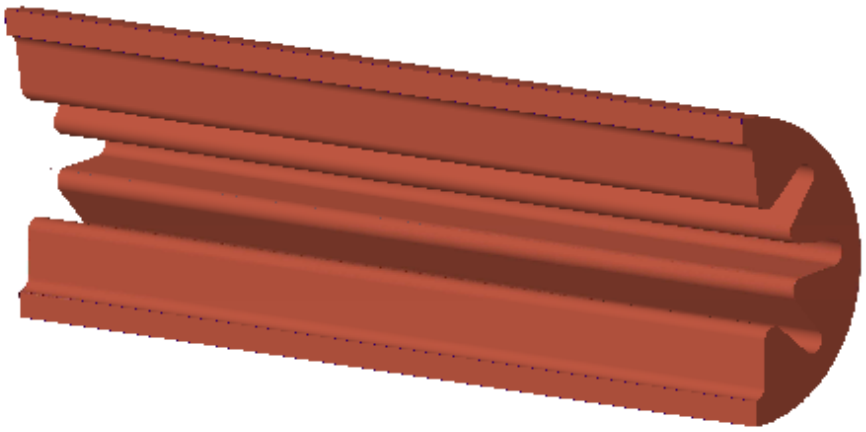

Figure 12 Star grain shape

- Funnel

It was shown that the cylindrical or tubular grain shape would give a progressive burning behavior; thus, it's required sometimes to have a neutral burning surface area profile. Such a thing could be achieved by trimming one of the grains' ends to form a conical shape as shown in Fig. 13. The burning surface area neutrality of this shape is controlled mainly by the slant angle which is the angle that form the cone. A detailed design of a funnel grain was investigated in [32].

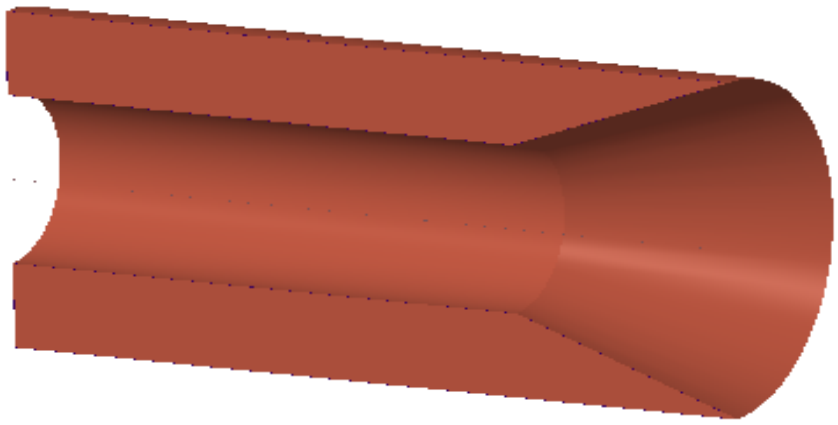

Figure 13 Funnel grain shape

- Dual thrust

Some applications require a dual thrust profile that consist of two phases. The first phase gives a high thrust in the beginning then it drops to a lower thrust which lasts usually longer than the first phase. The second phase provides sustaining conditions to the projectile which makes it reach higher ranges by overcoming the air drag. Such profiles could be achieved by two methods which is using two different propellant compositions, one of them has a low burning rate and the other gives a high burning rate. The second method to achieve this profile is by using a certain grain shape with one propellant composition as shown in Fig. 14. Four parameters define this grain shape which are the outer diameter D, total length L, internal cavity d and internal length l. Defining these parameters shall be looking into carefully as it is essential to define the optimum design. This type of grain shape was studied and analyzed in detail in [33].

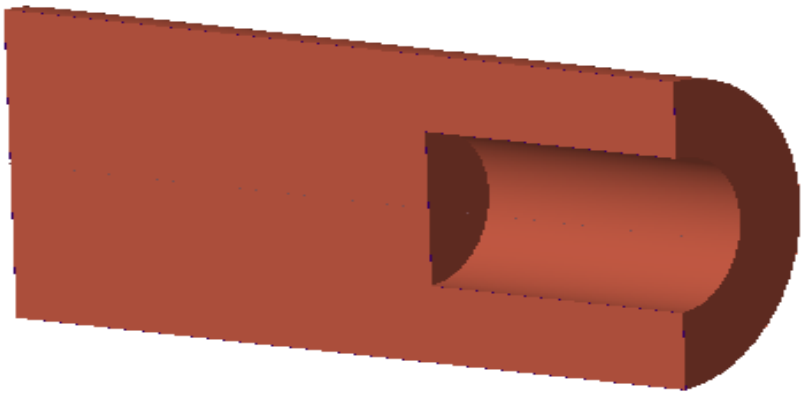

Figure 14 Dual thrust grain shape

- Finocyl

Speaking of dual thrust propellant grains, finocyl grain shapes could deliver such performance. However, they are considered as three-dimensional grain shapes unlike the previous geometries which they are two-dimensional. Finocyl geometries usually consist of two geometries, a star shape with multiple fins at one end then a cylindrical shape. The fins part provide higher burning surface area at the start of the burning when the grain start burning radially. Then, the cylindrical part burns slower to give lower thrust level. The erosive burning is reduced in this shape by the fins at the aft end. The finocyl grain shape is widely used in the rocket motors industry especially for launch vehicles [34]. It is difficult to calculate the burning surface area analytically; therefore, it could be calculated numerically using parametric modelling by 3D CAD software like PTC CREO.

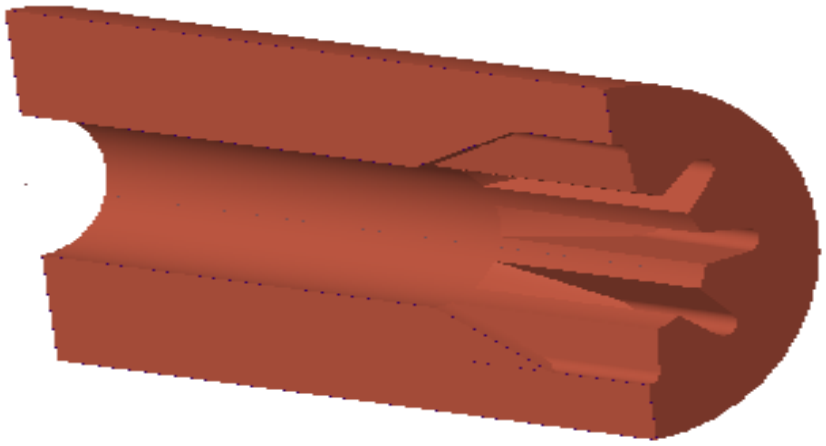

Figure 15 Finocyl grain shape

In summary, there are several main characteristics that should be taken into consideration before choosing the optimum propellant grain design for a certain application as each mission require a specific performance output. Table 1 illustrate the main characteristics of different grain shapes [35].

Table 3 Common grain configurations with their main characteristics

Geometry	Volumetric loading	Web thickness	Burn area neutrality	Sliver fraction	Web fraction
End burner	0.98-1	Very large	Excellent	0	>1
Star	0.75-0.84	Medium	Good	5-10%	0.3-0.6
Finocyl	0.75-0.85	Large	Good	0	3

1.4 Interior ballistics

The internal flow conditions inside the combustion chamber of a SPRM could be known through the interior ballistics parameters which its values reflect on how the motor's operation depends on the combustion chamber characteristics of the propellant (its burning rate, burning surface and grain geometry) and the nozzle design parameters. Thus, it is essential to calculate the interior ballistic parameters in order to predict the rocket motor performance. Multiple models of the interior ballistics were studied and analyzed by different researches [36-38]. One of the objectives of this project is to build a program consist of the interior ballistics equations using the inputs from the burnback analysis formulas. The main parameters are defined and briefly described accordingly.

1.4.1 Burning rate

The burning of the rocket motor propellant grain regresses in a perpendicular way to the surface which characterizes the combustion of the grain. The rate of the burning that it travels at per unit time is the burning rate r.Success in the rocket motor design and development depends significantly on the knowledge of the burning rate behavior of the selected propellant under all motor operating conditions and design limit conditions. Propellant grains of a high burning rate is usually considered for rocket motors, so there are several ways of increasing the propellant's burn rate. It could be done by changing the propellant chemical composition, and aside form that it could by increased by the following:

1. Combustion chamber pressure.
2. Initial temperature of the solid propellant prior to start.
3. Combustion gas temperature.
4. Velocity of the gas flow parallel to the burning surface.

The burning rate as a function of chamber pressure p could be determined for different types of propellants using empirical Saint Robert or Vieille law for a given burning rate coefficient b and pressure exponent nEq. 4. The value of the pressure exponent range between 0.2 and 0.7 for a given propellant with a chamber pressure ranging from 3 to 15 MPa [39].

$$r = bp^n \tag{4}$$

1.4.2 Temperature sensitivity

The ambient temperature of propellant grains has a great influence on the conditions of the propellant by changing the chemical reaction rates of the combustion which results on changing the expected performance obtained from the rocket motor. Therefore, rocket motors shall be stored at a certain temperature as desired for fulfilling the mission requirements and to keep the motor performance characteristics within the specified acceptable limits. An increase of the grain's initial ambient temperature causes an increase of the chamber pressure and shorten the burning time, yet the opposite occurs when the initial temperature goes low as shown in Fig. 16. One important

parameter studies this influence is the burning rate temperature sensitivity σ_p which is the percent change of burning rate per degree change in propellant temperature at a specific chamber pressure.

$$\sigma_p = \left(\frac{\delta lnr}{\delta T}\right)_p = \frac{1}{r}\left(\frac{\delta r}{\delta T}\right)_p \tag{5}$$

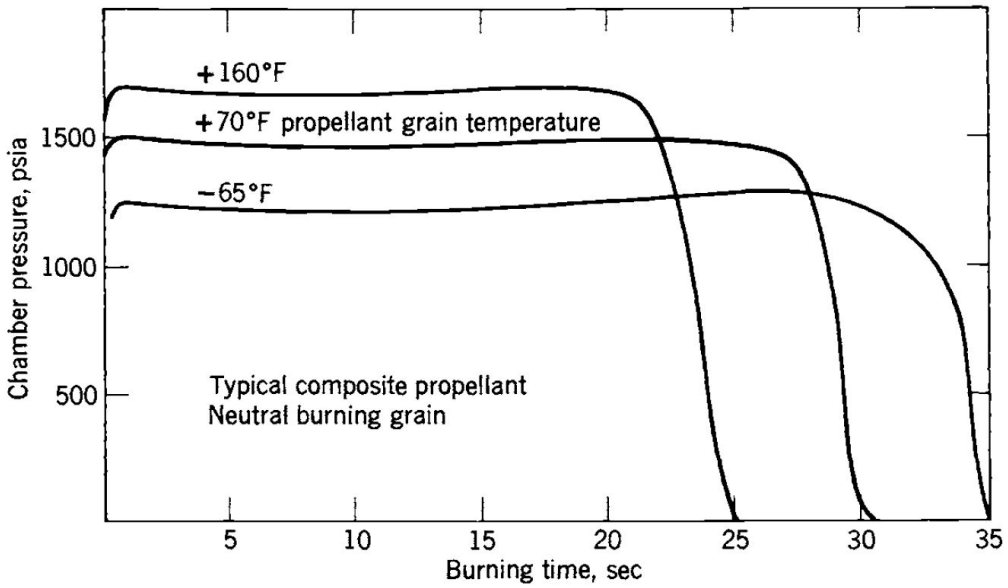

Figure 16 Change in chamber pressure with respect to burning time [28]

1.4.3 Total impulse

The total impulseI_t is an important parameter of rocket motor since its value is used further in the interior ballistics calculations. It is calculated by taking the integral of the thrust force over time which is simply finding the area under the curve of the thrust profile Eq. 6. Generally, big rocket motors have higher total impulse.

$$I_t = \int_o^{t_b} F\,(t)\,dt \tag{6}$$

where t_b is the burning time. An average thrust could be taken to calculate the total impulse assuming that its constant, then I_t could be calculated as the following form:

$$I_t = F\,t_b \tag{7}$$

1.4.4 Specific impulse

Solid propellant rocket motors are usually presented or classified by their value of specific impulseI_s which gives a quick indication of their performance. It is the total impulse per unit mass

of the propellantm_p Eq. 8. The higher specific impulse of a rocket motor, the better performance that it gives.

$$I_s = \frac{I_t}{m_p} \tag{8}$$

In addition, the specific impulse quantifies the effectiveness of a rocket motor in converting propellant mass into thrust. Specific impulse is typically measured in seconds and is a crucial factor in determining a rocket's overall performance. It is defined as the ratio of the thrust generated by the rocket motor to the rate at which the propellant is expelled. Thus, when I_s is high, it means the rocket motor can generate more thrust for a given mass of propellant or, conversely, the same thrust can be achieved with less propellant. It can be calculated using the following formula:

$$I_s = \frac{F}{\dot{m}} \tag{9}$$

1.4.5 Thrust coefficient

The thrust coefficient $c_F$value has a significant influence on the design of the rocket motor nozzle. It is defined as the value of thrust per unit chamber pressure and throat area A_t Eq. 10. If the thrust and pressure values are known from experiments, then c_F could be calculated for a certain throat area.

$$c_F = \frac{F}{A_t\, p} \tag{10}$$

An alternative equation of c_F from the general thrust equation could be expressed [40]:

$$c_F = \sqrt{\frac{2k^2}{k-1}\left(\frac{2}{k+1}\right)^{\frac{k+1}{k-1}}\left[1-\left(\frac{p_e}{p_o}\right)^{\frac{k-1}{k}}\right]} + \frac{p_e - p_a}{p_o}\frac{A_e}{A_t} \tag{11}$$

The ratio of exit area $A_e$to throat area A_t is the nozzle area expansion ratio. The thrust coefficient is a function of gas property k, expansion ratio ϵ, and the pressure ratio across the nozzle $\frac{p_e}{p_o}$. The optimum thrust coefficient is the peak value when the pressure at the nozzle's exit p_e is equal to the atmospheric pressure p_a. Figure 17 shows the variation of c_F for different values of k, ϵ, and pressure ratios where $p_1 = p_o$ and $p_2 = p_e$. When the composition of the propellant and the grain geometry are fixed, the design of the nozzle becomes the dominant factor in achieving optimal rocket performance. It's a dimensionless factor that indicates the extent to which the nozzle amplifies the thrust. The thrust coefficient depends on gas properties, such as the specific heat ratio of the gas, and various thermodynamic parameters. It is also influenced by nozzle geometry, including the expansion ratio and pressure ratio. The thrust coefficient is at its maximum when the nozzle effectively expands the gases down to the ambient pressure at the nozzle exit plane.

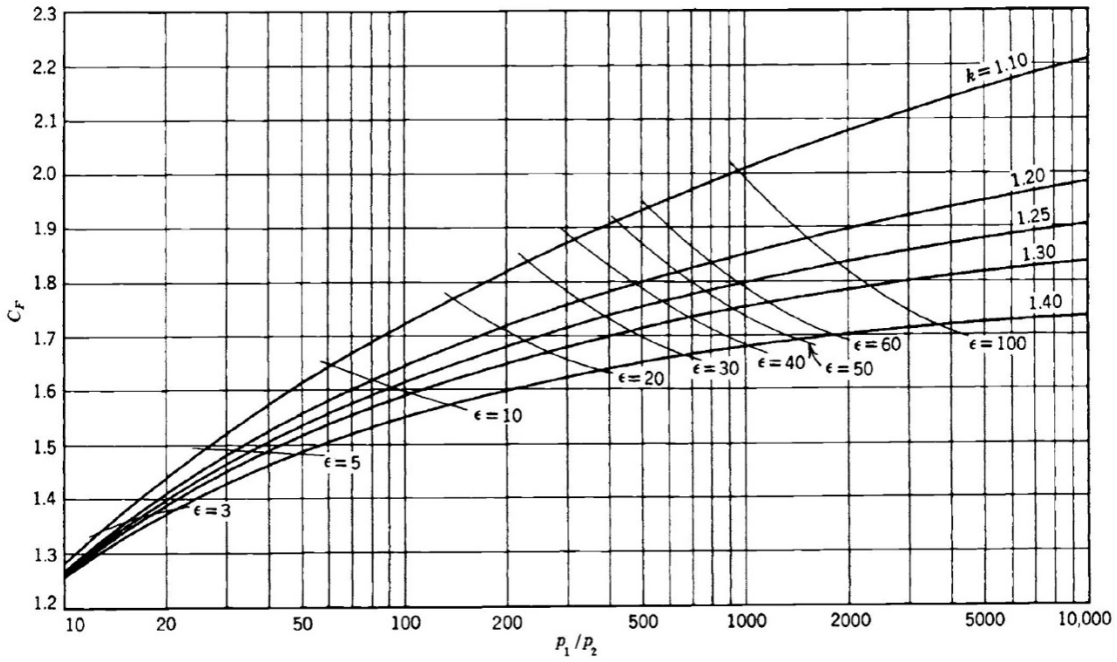

Figure 17 Thrust coefficient versus pressure ratio for different values of k and ϵ[I28]

1.4.6 Nozzle throat and expansion ratio

The throat area of a nozzle in a rocket motor is the smallest cross-sectional area where the exhaust flow gets choked and Mach number becomes 1.0. The ratio of the nozzle exit area A_e to the throat area A_t is called the nozzle area expansion ratio ϵ,

$$\epsilon = \frac{A_e}{A_t} \tag{12}$$

Another expression for the expansion ratio could be derived,

$$\epsilon = \left(\frac{2}{k+1}\right)^{\frac{1}{k-1}} \sqrt{\frac{k-1}{k+1}} \left(\frac{p_o}{p_e}\right)^{\frac{1}{k}} \frac{1}{\sqrt{1-\left(\frac{p_e}{p_o}\right)^{\frac{k-1}{k}}}} \tag{13}$$

The expansion ratio is an important parameter for designing the nozzle. For an ideal nozzle, the exit pressure p_e could be assumed to be equal to the atmospheric pressure $p_a (p_a = 101325 \text{ Pa} \approx 1 \text{ bar}$ at the sea level), so the expansion ratio could be found. The optimum value of the expansion ratio is the one that gives the highest total impulse of the motor. If $p_e > p_a$, the nozzle is under-expanded. However, it's over-expanded if $p_e < p_a$ as shown in Fig. 18 along with the other conditions. Therefore, a nozzle is designed for the altitude at which it has to operate.

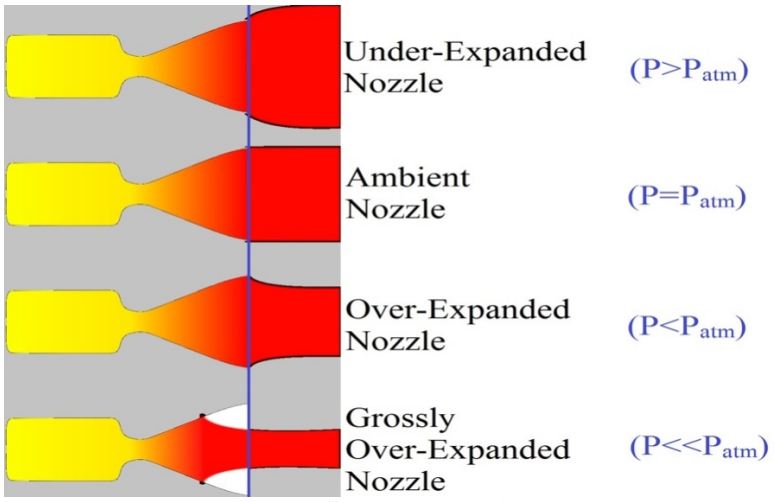

Figure 18 Different nozzle conditions [41]

1.4.7 Characteristic velocity

The characteristic velocity c^* is a function of the propellant characteristics and combustion chamber design, and it is essentially independent of the nozzle characteristics. It is defined as the product of chamber pressure and nozzle throat area divided by the propellant mass flow rate $\dot{m}$.

$$c^* = \frac{p_o A_t}{\dot{m}} \tag{14}$$

The characteristic velocity could be calculated theoretically based on the gas properties:

$$c^* = \frac{I_s}{c_F} = \frac{\sqrt{kRT_o}}{k\sqrt{\left[\frac{2}{k+1}\right]^{\frac{k+1}{k-1}}}} \tag{15}$$

1.4.8 Mass flow rate

In general terms of physics, the mass flow rate $\dot{m}$of a substance is its mass per unit time. It could be calculated using the following equation, which is the product of burning surface area$A$, propellant densityρ_p and burning rate:

$$\dot{m} = A\rho_p r \tag{16}$$

Due to the conservation of mass principle in rocket motors, the mass flow rate of generated gas gets to be balanced by the mass flow rate of the same gas through the nozzle and it is represented by the following formula:

$$\dot{m} = A_{nozzle}\rho_g v_g \tag{17}$$

1.4.9 Chamber pressure

As seen in the previous equations of interior ballistics, the chamber pressure has a strong influence on the propellant burn rate, thermodynamic efficiency, and the overall performance of the rocket motor. Therefore, it is necessary to ensure that the pressure generated inside the combustion chamber meets the requirements to have a successful rocket motor operation. The chamber pressure versus time curve is one of the main outputs of every SPRM interior ballistics model where its profile splits into three main phases as shown in Fig. 19. The start-up phase is basically representing the ignition of the propellant grain which is the time and energy needed to build up the required temperature and pressure inside the chamber to start the burning of the grain. The tail-off is the end of the grain's combustion when the burning surface area is significantly decreasing. The steady state phase is when the mass of the propellant grain varies with time due to combustion and recession of the burning surface area with time [42].

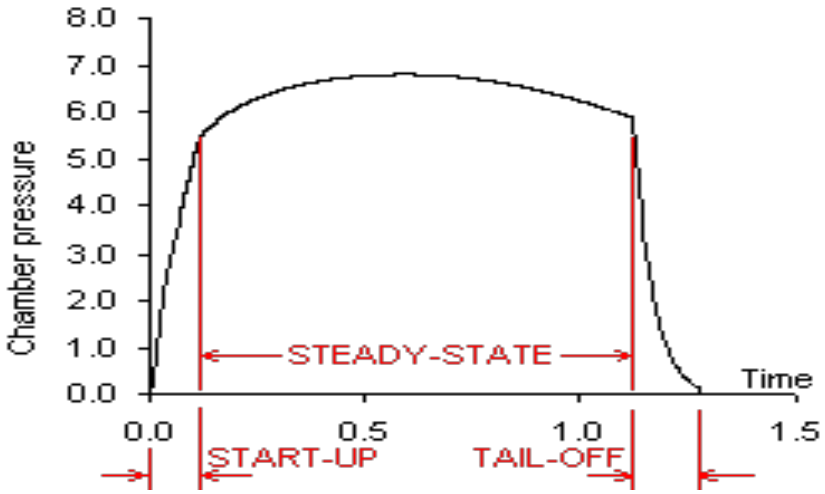

Figure 19 Chamber pressure versus time profile illustrating the three combustion phases [43]

The rocket motor shall be designed in a way that its mass flow rate generated from the combustion chamber equals to the mass flow rate through the nozzle, so the equilibrium chamber pressure could be calculated by balancing equations 14 and 16:

$$A\rho_p r = \frac{p_o A_t}{c^*} \tag{18}$$

Solving Eq. 18 for p_o, it will give the following equation to calculate the chamber pressure when there is only one propellant burning:

$$p_0 = \left(b\rho_p c^* \frac{A}{A_t}\right)^{\frac{1}{1-n}} \tag{19}$$

The previous equation is not applicable to calculate the chamber pressure when the two propellants are burning simultaneously because the total mass flow rate at the nozzle is the sum of the generated mass flow rate of both propellants:

$$\dot{m} = \dot{m}_f + \dot{m}_s \tag{20}$$

Which is equivalent to the following form to calculate the equilibrium chamber pressure numerically knowing the burning surface areas, burning rates, nozzle throat area and the average characteristic velocity of the mixture of combustion products $\bar{c}^*$:

$$\frac{p\dot{A}_t}{\bar{c}^*} = \rho_f A_f b_f p^{n_f} + \rho_s A_s b_s p^{n_s} \tag{21}$$

1.4.10 Thrust

The final and most important parameter of interior ballistics to be discussed is the thrust F that moves the rocket motor, which is the force generated by expelling the hot gasses through the nozzle. In the interior ballistics model of this project, the thrust is calculated by taking the multiplication of the specific impulse and mass flow rate:

$$\mathrm{F} = I_s \dot{m} \tag{22}$$

1.5 Motivations

The journey of learning about propulsion systems had begun during my undergraduate studies of aerospace engineering when I took propulsion as a concentration in the studies program. It has been always an area of interest to explore and get myself acquainted with. The first spark was firstly initiated when I attended and witnessed the launch of a couple of space vehicles from Cape Canaveral, Florida which was an hour away from Embry-Riddle Aeronautical University. Watching the flames exiting the nozzle during the launch while the rocket making its way to the sky made me wonder how such systems work and what are the scientific principles behind them.

The quest for pushing the limits of rocket propulsion and contributing to the evolution of defense technology has been a driving force in my academic and professional journey. I am dedicated to advancing the field of solid rocket motor design and bringing innovative solutions to the challenges that lie ahead. Getting all the knowledge in propulsion made it easier to have a contribution in this field through the research work that have been done throughout the studies period and work. Thus, it was decided to advance my research in this discipline after the completion of the master's degree, and multiple publications were submitted in conferences and a journal.

The main initiative of this work was to explore the two-component propellant grains which have a simple shape as a whole yet a complex interior geometry. A certain shape was selected for this project as a problem to start with. Thus, a solution had to be provided and an optimization of that solution. One of the main motivations to work on this project was to develop a code that is

capable to predict the performance of a solid propellant rocket motor with a complex propellant grain shape. This code is supposed to perform all the necessary calculation starting from calculating the burnback analysis to solving the deferential equations of interior ballistics. Once that is done, an optimization model shall be proposed which could simplify the design in terms of calculations and a possible simpler production process while delivering the same or enhanced performance of the original propellant grain.

1.6 Methodology

As stated in the PhD proposal submitted for the dissertation, this project will engage several research and design methods to achieve the objectives set such as intensive research of certain subjects in rocket propulsion, analytical mathematical modeling of the grain shape and experimental work. The developed work was expected to have the following scientific contribution:

- Developing a tool for designing and optimizing the SPRM: The tool shall provide a comprehensive computational simulation for the purposes of designing SPRM that is capable of receiving certain input data and deliver graphical output of the results along with the performance analysis.
- Possibilities of using two-component grain: Several grain configurations will be analyzed in the project in order to collect rich data to study the influence of the grain's shape on the performance of the SPRM and some of those configurations will be complex like two-component grain.
- Insightful comparison of the research methods: Exploration of the different research methods to gain an insight of the correlation between those methods.
- Practical significance: The obtained results will be checked against the hypothesis if they are practically significant and find their practical importance.

Consequently, the workflow of the design process went thought the steps shown in Fig. 20. The propellant's composition of both propellants was defined upon defining the SPRM performance requirement. A conical shape nozzle was selected for this project and nozzle parameters were defined. The cylindrical grain shape that consisting of two propellants was chosen to achieve the neutrality profile. The grain shape was defined, and the analytical burn-back analysis was performed. Multiple iterations were conducted to reach the optimized model of the grain shape. The results from the static test showed the need of obtaining an optimized grain shape. The design cycle led to developing an accurate program that could imitate the data obtained from static test bench. Thus, the design methodology used in this project could be used in designing other propellant grain shapes.

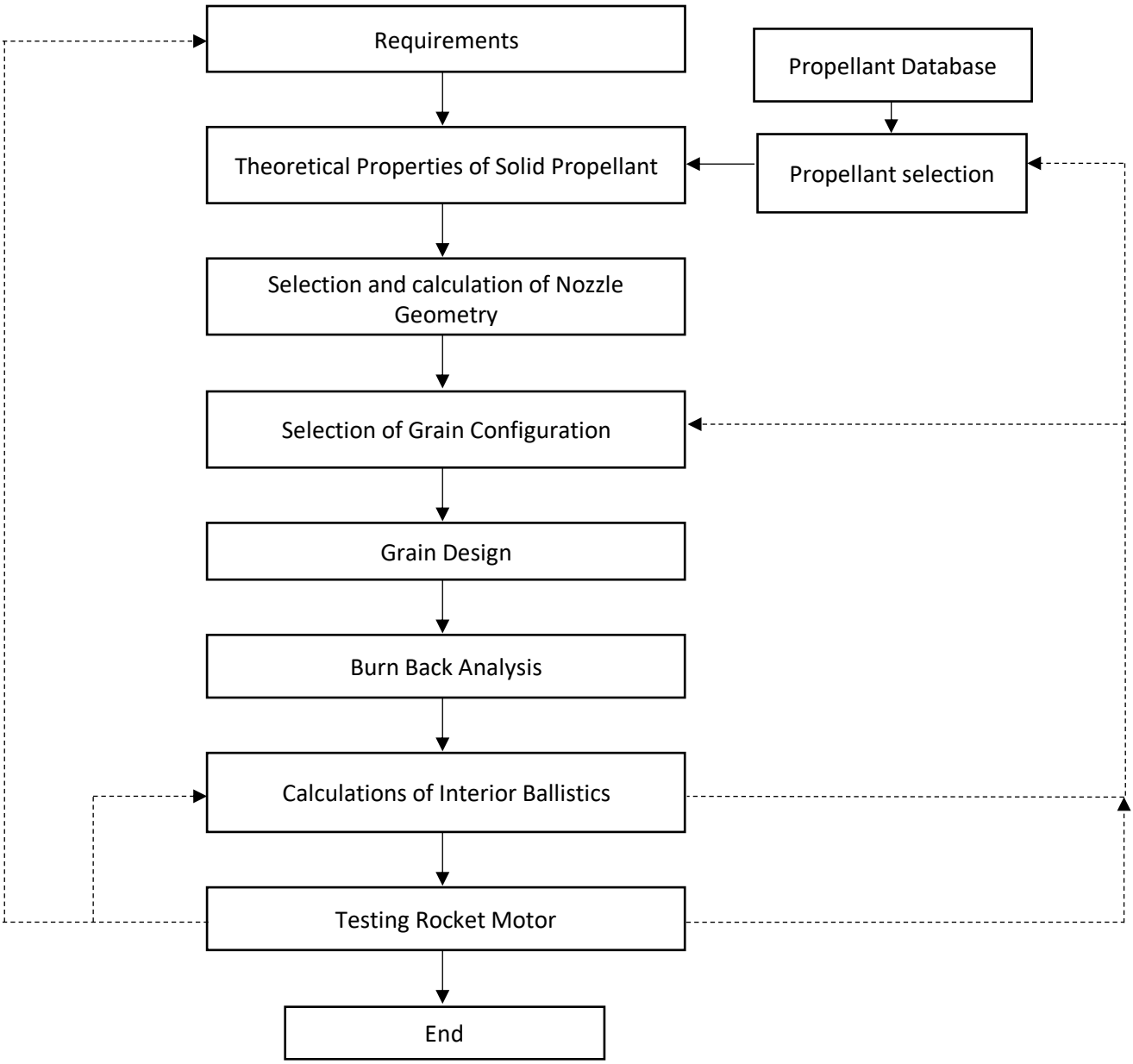

Figure 20 Flow diagram of the design process

2. Burnback Analysis

The burnback analysis definition was briefly explained in section 1.2, and it was stated that an analytical model will be developed to calculate the burning surface area of propellant grain shapes of this project. Not all the grain shapes have their mathematical models of burnback available; however, there are bunch of researchers in this field who tried to present their work for different grain shapes [44-45]. This project's burnback analysis model will consist of mainly the two equations of the tubular grain shape which are the core or internal cavity surface areaA_c Eq. 23, and the surface area of one of the front endsA_l Eq. 24. Those equations will be rearranged and solved numerically based on the boundary conditions of each step.

$$A_c = \pi\, L\, D \tag{23}$$

$$A_l = \frac{\pi}{4}(D^2 - d^2) \tag{24}$$

where A is the bunring surface area, L is the grain's length, D is the grain's outer diameter and d is the grain's inner diameter.

2.1 Original model

The original propellant grain has a unique shape as shown in Fig. 21. Due to the neutrality requirements and technological manufacturing limitations, such a shape was designed. This grain's design introduces the possibility of including two propellants with a certain way of contact surface. The propellants have multiple steps that introduce the way they are separated. The burnback analysis model will be developed in a way that describes the progression of the burning inside the grain and the right frontal end. The outer cylindrical surface and left frontal surface will be inhibited. The total burning surface area will be the sum of the burned surface areas of the fast and slow propellants.

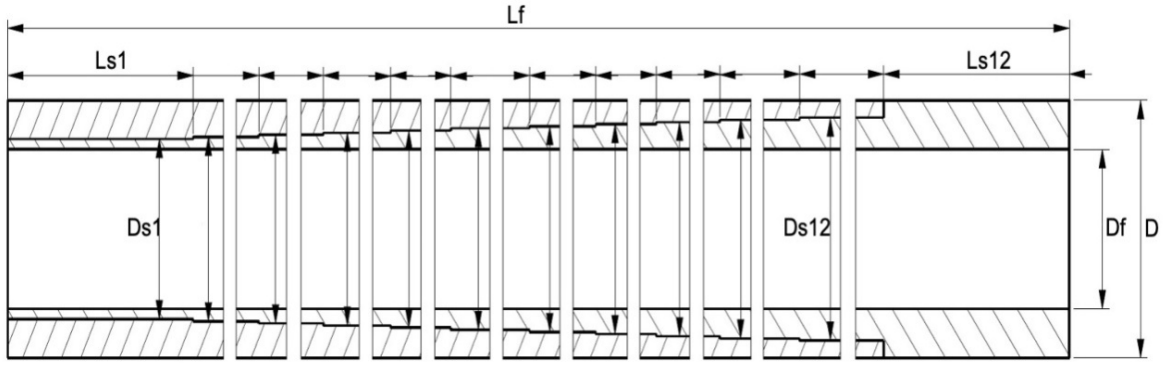

Figure 21 Original propellant grain geometry

2.1.1 First step

The first set of the burning surface area calculations will be only for the fast burning propellant which will be denoted as propellant f, and it will be included as an index for each

parameter of this propellant. Figure 21 indicates the first surfaces that will be burned which are defined by the grain's total length L_f, outer diameter of the grain D, and the inner diameter D_f. The boundary conditions for this step are set to start from D_f to D_{s1} where the second step starts. The web thickness w is defined by the internal cavity of the cylindrical grain D_f and the outer diameter D. As stated in equations 23 and 24, the burning surface area of the fast burning propellant grain A_f will be the sum of the burned web at the inner diameter and right front end, and the burning surface area of the slow propellant grain A_s is going to be zero. The burning surface area relations of the first step are as the following:

$$A_f = \pi L_f D_f + \frac{\pi}{4}(D^2 - {D_f}^2) \tag{25}$$

$$L_f = L_f - w \tag{26}$$

$$D_f = D_f + 2w \tag{27}$$

$$A_s = 0 \tag{28}$$

$$\mathrm{A} = A_f + A_s \tag{29}$$

2.1.2 Second step

In this step, the combustion of the second propellant which has slower burning rate will begin, and it will be referred to as propellant s. Thus, the total burning surface area formulas will be the sum of A_f and A_s. The initial conditions of this segment start when the previous segment reaches its end, so the new dimensions will be the original grain total surface area minus the burned area.

$$A_f = \pi L_{f1} D_{f1} + \frac{\pi}{4}(D^2 - {D_{f1}}^2) \tag{30}$$

$$L_{f2} = L_{f1} - w \tag{31}$$

$$D_{f2} = D_{f1} + 2w \tag{32}$$

$$A_s = \pi\, L_{s1} D_{s1} + A_{s1e} \tag{33}$$

$$A_{s1e} = \pi(D_{f1} + D_{s1})\frac{e_1}{2} \tag{34}$$

$$\mathrm{A} = A_f + A_s \tag{35}$$

A new convex slope shape is formed when the burning front reaches a new step due to the burning rate differences of the two propellants. This new step will be formed at the edge of each slow burning grain step. The burning of this step will be spreading in axial and radial directions, which defines the newly formed slope and calculating this new step via A_{s1e} which will increase the burnback analysis model accuracy. The burning surface area relations of the slope shape are based on Fig.22 and the following relations:

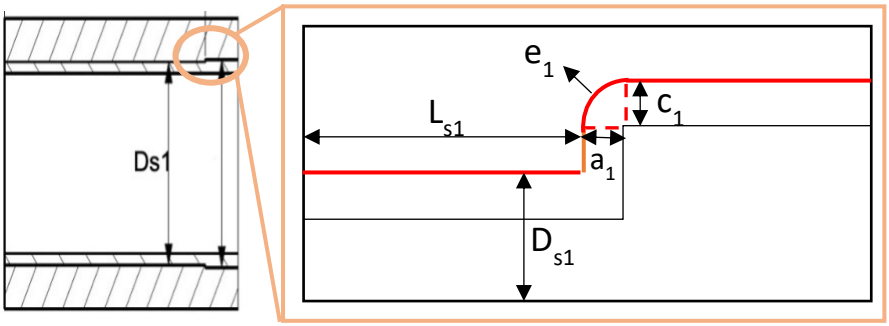

Figure 22 Illustration of the new formed step

$$D_{s2} = D_{s1} + 2w\frac{r_2}{r_1} \tag{36}$$

$$a_1 = a_1 + w\frac{r_2}{r_1} \tag{37}$$

$$c_1 = c_1 + w \tag{38}$$

$$e_1 = \sqrt{{a_1}^2 + (c_1 - a_1)^2} \tag{39}$$

$$L_{s1} = L_{s1} - a_1 \tag{40}$$

where e is the length of the slope which is calculated based on the axial length of the edge of the step a and the radial length c.

2.1.3 Third step

The third step will be a continuation from the previous step, but for the third segment with its boundary conditions will be starting from Ds_2. Thus, the burning surface area will be calculated in a similar way to the next segment defined by the diameter D_{s3}.

$$A_f = \pi L_{f1} D_{f1} + \frac{\pi}{4}(D^2 - {D_{f1}}^2) \tag{41}$$

$$L_{f2} = L_{f1} - w \tag{42}$$

$$D_{f2} = D_{f1} + 2w \tag{43}$$

$$A_s = \pi\, L_{s1} D_{s1} + A_{s1e} \tag{44}$$

$$A_{s1e} = \pi(D_{f1} + D_{s1})\frac{e_1}{2} \tag{45}$$

$$D_{s2} = D_{s1} + 2w\frac{r_2}{r_1} \tag{46}$$

$$a_1 = a_1 + w\frac{r_2}{r_1} \tag{47}$$

$$c_1 = c_1 + w \tag{48}$$

$$e_1 = \sqrt{{a_1}^2 + (c_1 - a_1)^2} \tag{49}$$

$$L_{s1} = L_{s1} - a_1 \tag{50}$$

$$\mathrm{A} = A_f + A_s \tag{51}$$

2.1.4 General step

Taking the previous steps as a reference, a general form of equations could be derived to calculate the burning surface area at each step for the remaining parts of the propellant grain where Eqs. [52-54] are devoted to calculating A_f and Eqs. [55-61] are set to calculate A_s with the step formed at each iteration.

$$A_f = \pi L_{f(k)} D_{f(k)} + \frac{\pi}{4}\left(D^2 - {D_{f(k)}}^2\right) + \sum \pi L_{f(i)(k)} D_{f(i)(k)} \tag{52}$$

$$L_{f(i)(k+1)} = L_{f(i)(k)} - w \tag{53}$$

$$D_{f(k+1)} = D_{f(k)} + 2w \tag{54}$$

$$A_s = \pi\, L_{s1} D_{s1} + A_{s1e} \tag{55}$$

$$A_{s1e} = \pi(D_{f(k)} + D_{s1(k)})\frac{e_1}{2} \tag{56}$$

$$D_{s1(k+1)} = D_{s1(k)} + 2w\frac{r_2}{r_1} \tag{57}$$

$$a_{1(k+1)} = a_{1(k)} + w\frac{r_2}{r_1} \tag{58}$$

$$c_{1(k+1)} = c_{1(k)} + w \tag{59}$$

$$e_{1(k+1)} = \sqrt{{a_{1(k+1)}}^2 + (c_{1(k+1)} - a_{1(k+1)})^2} \tag{60}$$

$$L_{s1(k+1)} = L_{s1(k)} - a_{1(k+1)} \tag{61}$$

$$\mathrm{A} = A_f + A_s \tag{62}$$

As part of the general form simplification, the number of each step or segment is defined by index *"i"*, *k* will represent the currently running iteration in the analytical model in MATLAB, and the upcoming next iteration is marked with *k+1*.

2.1.5 Last step

At a certain point during the burning process, the fast-burning propellant will be burned out before the slower burning propellant, which leads to burning only the slower burning propellant. Therefore, the burning surface area relations will calculate the remaining-disappearing steps in the following form so A_s could be calculated.

$$A_f = 0 \tag{63}$$

$$A_s = \pi\, L_{s1} D_{s1} + A_{s1e} \tag{64}$$

$$A_{s1e} = \pi (D_{f(k)} + D_{s1(k)}) \frac{e_1}{2} \tag{65}$$

$$D_{s1(k+1)} = D_{s1(k)} + 2w \frac{r_2}{r_1} \tag{66}$$

$$a_{1(k+1)} = a_{1(k)} + w \frac{r_2}{r_1} \tag{67}$$

$$c_{1(k+1)} = c_{1(k)} + w \tag{68}$$

$$e_{1(k+1)} = \sqrt{a_{1(k+1)}{}^2 + (c_{1(k+1)} - a_{1(k+1)})^2} \tag{69}$$

$$L_{s1(k+1)} = L_{s1(k)} - a_{1(k+1)} \tag{70}$$

$$\mathrm{A} = A_f + A_s \tag{71}$$

2.2 Optimized model

It was complicated finding the total burning surface area of the previous model. Thus, an optimized grain configuration was developed to simplify the calculations and reduce the oscillations which were caused by the shape of the segments. Unlike the original grain geometry, the optimized shape consists of fewer parameters that define the configuration which is another reason for being simpler. Total length area L_f, inner diameter D_f, and outer diameter D are similar for both grains as well as the dimensions of the first and last steps. In this grain configuration, a slope line will be replacing the segments, which makes the burning process splits into five main phases as described below (Fig. 23). The outer diameter and the left front end are inhibited.

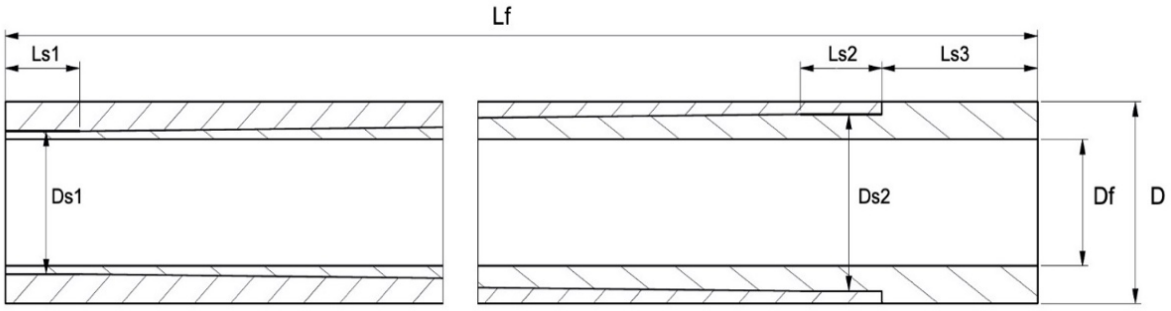

Figure 23 Optimized geometry model

2.2.1 First phase

In this phase, the propellant's burning will evolve in similar way to the original grain first phase that it will progress only through the fast burning propellant as indicated in Fig. 24 with its equations accordingly. The fast burning propellant of the first phase has boundary conditions from D_f to D_{s1} and from L_{f0} to L_{f1}.

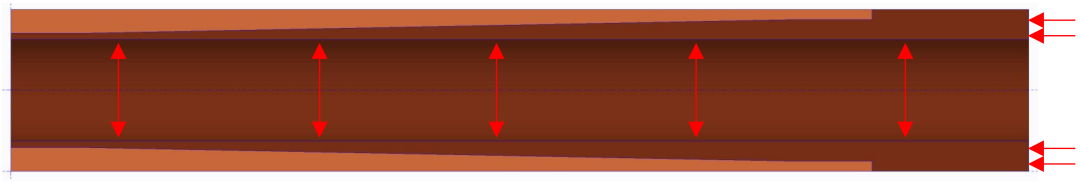

Figure 24 Indication of the burning surfaces during phase 1

$$A_f = \pi L_f D_f + \frac{\pi}{4}(D^2 - {D_f}^2) \tag{72}$$

$$L_f = L_f - w \tag{73}$$

$$D_f = D_f + 2w \tag{74}$$

$$A_s = 0 \tag{75}$$

$$A_{phase\ 1} = A_f + A_s \tag{76}$$

2.2.2 Second phase

The second phase of the burning is going to include the burning of both propellants. The fast burning propellant is going to have similar way to calculate the burned surface area, but the boundary condition is up to D_{s2}. On the other hand, the burning of the slow propellant grain will be the sum of the burned surface area at the step from D_{s1} to D_{s2} and the burning of the slope newly formed which is defined by e_s as shown in Fig. 25.

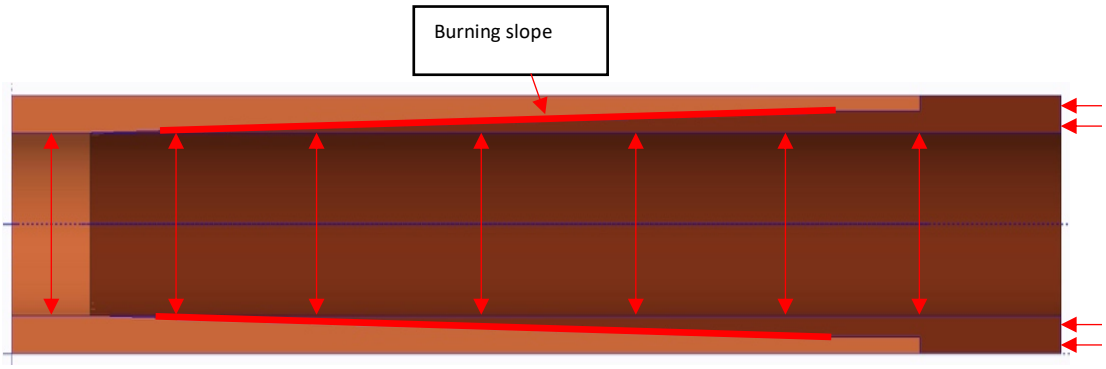

Figure 25 Indication of the burning surfaces during phase 2

$$A_f = \pi L_f D_f + \frac{\pi}{4}(D^2 - {D_f}^2) \tag{77}$$

$$L_f = L_f - w \tag{78}$$

$$D_f = D_f + 2w \tag{79}$$

$$A_s = \pi L_{s1(k)} D_{s1(k)} + \pi (D_{f(k)} + D_{s1(k)}) \frac{e_{s(k)}}{2} \tag{80}$$

$$e_{s(k+1)} = \sqrt{\left(L_{slope(k)}\right)^2 + \left(\frac{D_{f(k)}}{2} - \frac{D_{s1(k)}}{2}\right)^2} \quad (81)$$

$$L_{slope(k+1)} = L_{slope(k)} + L_{s3(k)} d_x + w\frac{r_2}{r_1} \quad (82)$$

$$L_{s1(k+1)} = L_{s1(k)} - w\frac{r_2}{r_1} \quad (83)$$

$$L_{f(k+1)} = L_{f(k)} - w - L_{s3(k)} w \quad (84)$$

$$D_{f(k+1)} = D_{f(k)} + 2w \quad (85)$$

$$D_{s1(k+1)} = D_{s1(k)} + 2w\frac{r_2}{r_1} \quad (86)$$

$$A_{phase\ 2} = A_f + A_s \quad (87)$$

2.2.3 Third phase

At the start of this phase, the fast burning propellant will be already burned out from the radial burning direction, and the front end part will be only burning at the area defined by L_{s3} as shown in Fig. 26. The slower burning propellant will carry on the same burning behavior throughout the slope and the two steps from each side of the grain which are defined by L_{s1} and L_{s2}. In this phase, the burning surface area equation of the slow burning propellant will include e_f which is the burning slope of the fast burning propellant.

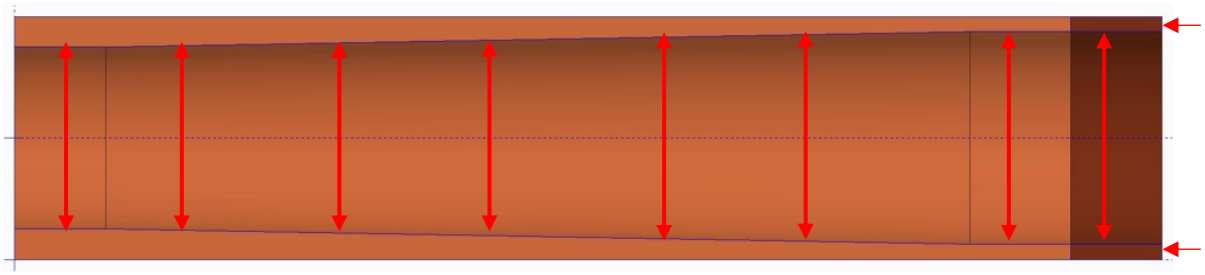

Figure 26 Indication of the burning surfaces during phase 3

$$A_s = \pi L_{s1(k)} D_{s1(k)} + \left(\pi(D_{s2(k)} + D_{s1(k)})\frac{e_{s(k)}}{2}\right) + \pi L_{s2(k)} D_{s2(k)} + \pi(D_{f(k)} + D_{s2(k)})\frac{e_{f(k)}}{2} \quad (88)$$

$$e_{s(k+1)} = \sqrt{\left(L_{slope(k)}\right)^2 + \left(\frac{D_{s2(k)}}{2} - \frac{D_{s1(k)}}{2}\right)^2} \quad (89)$$

$$L_{slope(k+1)} = L_{slope(k)} + L_{s3(k)} w + w\frac{r_2}{r_1} \quad (90)$$

$$L_{s1(k+1)} = L_{s1(k)} - w\frac{r_2}{r_1} \quad (91)$$

$$L_{f(k+1)} = L_{f(k)} - w \tag{92}$$

$$D_{f(k+1)} = D_{f(k)} + 2w \tag{93}$$

$$D_{s1(k+1)} = D_{s1(k)} + 2w\frac{r_2}{r_1} \tag{94}$$

$$D_{s2(k+1)} = D_{s2(k)} + 2w\frac{r_2}{r_1} \tag{95}$$

$$e_{f(k+1)} = a_{(k)}{}^2 + \sqrt{\left(c_{(k)} - a_{(k)}\right)^2} \tag{96}$$

$$a_{(k+1)} = a_{(k)} + w\frac{r_2}{r_1} \tag{97}$$

$$c_{(k+1)} = c_{(k+1)} + w \tag{98}$$

$$A_{phase\ 3} = A_f + A_s \tag{99}$$

2.2.4 Fourth phase

As the grain progresses to burn, the last two main phases of the burnback analysis will be evolving only around the slow burning propellant that the grain defined by D_{s2} and L_{s2} will start disappearing since its web thickness is less than the area defined by the slope and L_{s1} Fig. 27.

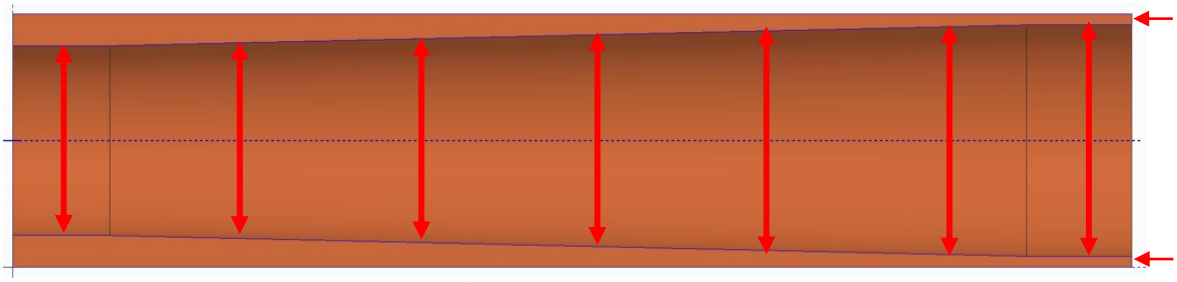

Figure 27 Indication of the burning surfaces during phase 4

$$A_f = 0 \tag{100}$$

$$A_s = \pi L_{s1(k)} D_{s1(k)} + \left(\pi(D_{s2(k)} + D_{s1(k)})\frac{e_{s(k)}}{2}\right) + \pi L_{s2(k)} D_{s2(k)} + \pi(D_{f(k)} + D_{s2(k)})\frac{e_{f(k)}}{2} \tag{101}$$

$$L_{s1(k+1)} = L_{s1(k)} - w \tag{102}$$

$$e_{s(k+1)} = \sqrt{\left(L_{slope(k)}\right)^2 + \left(\frac{D_{s2(k)}}{2} - \frac{D_{s1(k)}}{2}\right)^2} \tag{103}$$

$$e_{f(k+1)} = a_{(k)}{}^2 + \sqrt{\left(c_{(k)} - a_{(k)}\right)^2} \tag{104}$$

$$c_{(k+1)} = c_{(k)} - w \tag{105}$$

$$a_{(k+1)} = a_{(k)} + w \tag{106}$$

$$D_{s1(k+1)} = D_{s1(k)} + w \tag{107}$$

$$D_{s2(k+1)} = D_{s2(k)} + w \tag{108}$$

$$A_{phase\ 4} = A_f + A_s \tag{109}$$

2.2.5 Fifth phase

As discussed previously, A_f is set to be zero as it is fully burned up; therefore, the total burning surface area will consist of the reaming unburned area which is illustrated in Fig. 28 as the area from D_{s1} to D and the area formed by the slope e_s.

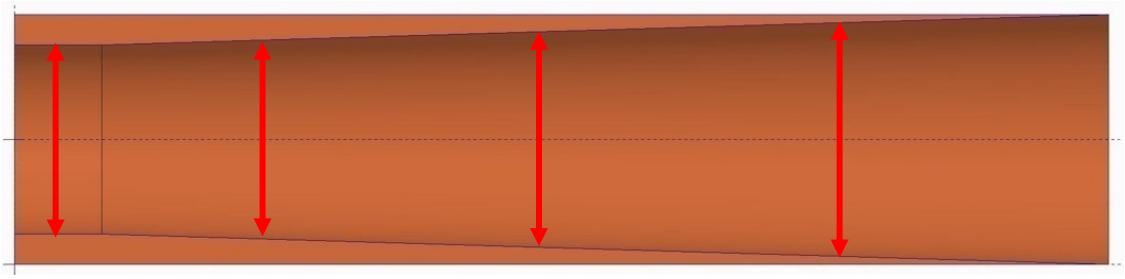

Figure 28 Indication of the burning surfaces during phase 5

$$A_s = \pi L_{s1(k)} D_{s1(k)} + \left(\pi (D_{f(k)} + D_{s1(k)}) \frac{e_s}{2}\right) \tag{110}$$

$$e_{s(k+1)} = \sqrt{\left(L_{slope(k)}\right)^2 + \left(\frac{D}{2} - \frac{D_{s1(k)}}{2}\right)^2} \tag{111}$$

$$L_{s1(k+1)} = L_{s1(k)} - w \tag{112}$$

$$L_{slope(k+1)} = L_{slope(k)} - kw \tag{113}$$

$$D_{f(k+1)} = D_{f(k)} + 2w \tag{114}$$

$$D_{s1(k+1)} = D_{s1(k)} + 2w \tag{115}$$

$$A_{phase\ 5} = A_s \tag{116}$$

3. Propellants compositions

Propellant is a chemical mixture made up of a fuel and an oxidizer that is burned to generate a propulsive force in rockets. For propulsion, a fuel is a substance that burns when coupled with oxygen-producing gas. An oxidizer is a substance that releases oxygen when mixed with a fuel. The mixture ratio is the proportion of oxidizer to fuel. The condition of a propellant is classified as liquid, solid, or hybrid. The propellant's composition is a very important thing when it comes to designing solid propellant rocket motors; therefore, its selection is very crucial for the success of the design.

As discussed under the interior ballistics' equations that specific impulse, measured in Ns/kg, is used to define the efficiency of rocket propellants. One kilogram of propellant consumed in one second produces a certain amount of thrust. The exact value of specific impulse varies to some extent depending on the design of the rocket engine and operating conditions [46].

Therefore, two most important theoretical aspects in rocket propellant efficiency are thrust produced by a specific type of propellant and the specific impulse. These two are the defining factors in the propellant selection.

These two factors will always be compared when selecting a propellant. The selection of propellant is from the available options. There are different types of propellants used in a rocket for example liquid propellants, solid propellants and hybrid propellants. In this section solid propellants will be discussed.

3.1 Solid propellants overview

Solid propellants are mostly employed in the propulsion of classical projectiles and rockets. They have a lot of energy and emit high-temperature gaseous products when they burn. Solid propellants have a high material density, which necessitates a high energy density to generate the requisite propulsive force. To provide appropriate thrust, propellants in onboard rockets are burned in a regulated manner.

An oxidizer, fuel, binder, plasticizer, curing agent, stabilizer, and cross-linking agent are just a few of the chemical components in a solid propellant. The required combustion characteristics determine the chemical composition for each mission. Solid propellants are frequently customized and classified for specific applications, including space launches, rockets, and weapons. The chemical substances used, and their amounts affect physical and chemical features, combustion characteristics, and performance [47].

Any solid rocket motor design begins with the selection of propellant type. Like any other product, factors such as ignition properties, high density, ease of production, cheap cost, and acceptable aging characteristics are all desirable features for a solid propellant. They key differences that stand out in the selection of solid propellant are high specific impulse and thrust produced. Added green energy revolution effects desire propellants should produce low-smoke exhaust and be resistant to combustion instability from a safety standpoint.

There are different types of chemical ingredients present in a solid propellant. Each of them has a unique feature or purpose, making them an integral part of the propellant composition. The chemical ingredients of a solid propellant are as follows:

- Oxidizer
- Metal Fuel
- Binder / Fuel
- Catalyst
- Plasticizer
- Curing Agent
- Additive

The propellants can be further classified as homogenous and heterogeneous. Homogenous propellants can be single- and double-based, whereas heterogeneous propellants are composite. The chemical ingredients present in a propellant depend on what type of propellant it is. Single, double-based, or composite propellants have different chemical ingredients compositions.

3.1.1 Single base propellants

As the name suggests, there is only a single base in this type of propellant. Single-base propellants are a type of energetic material used in small-caliber to large-caliber ammunition. Nitrocellulose is used to make these propellants. A single base propellant comprises a single chemical with both oxidation and reduction capabilities and does not have two different bases for two different purposes. Its single base and the material and composition of that base are self-sufficient to serve a purpose for the propellant completely.

3.1.2 Double base propellants

These propellants are arguably the oldest. Their key feature is their stealth advantage because they produce no smoke or fumes while propelling to the target. Nitrocellulose and nitroglycerine, along with a plasticizer, are the most common ingredients in double base propellants. Under typical circumstances, homogeneous propellants have specific impulses of around 2100 Ns/kg. They are often employed in tactical weapons since they do not emit identifiable odors.

Fuel and oxidizer are molecularly combined in double-base propellants. Most propellants comprise nitrocellulose gun powder dissolved in nitroglycerine, along with minor additions. These fundamental constituents are explosives with a molecular structure containing fuel and an oxidizer [48].

The main difference between simple and double base propellants is the need for an extra base. However, it produces no smoke or fumes; therefore, it is used for stealth military warfare. Small guns, cannons, mortars, and rockets all employ double-based fuel/propellants.

3.1.3 Composite propellants

This type of propellant has higher specific impulse and burn rate than the other types of propellants. The main applications of composite propellants are used in rocket motors of sophisticated missiles and launch vehicles. These are heterogeneous propellants and are made of a chemical mixture that contains four components which are fuel, oxidizer, binder, and other additives. The fuel component in composite solid propellants is typically a hydrocarbon material, and powdered aluminum or other metals. These fuels provide the energy necessary for combustion. The oxidizer component is responsible for providing the oxygen required for the combustion of the fuel. Common oxidizers include ammonium perchlorate (AP), ammonium nitrate (AN), and others. The binder acts as the matrix that holds the fuel and oxidizer particles together. It ensures that the propellant maintains its solid form and provides structural integrity. Binders are often based on synthetic rubber or plastic materials. Various additives can be incorporated into composite propellants to enhance their performance. These may include plasticizers, curing agents, burn rate modifiers, stabilizers, and reinforcing agents. Generally, the oxidizer has the highest proportion in the mixture by almost 70 percent [47].

3.2 Composite propellants

3.2.1 Ammonium perchlorate composite propellants

When ammonium perchlorate (AP)-based composite propellants burn, they commonly emit white smoke. This is because one of the combustion products, HCl, causes moisture to condense in the atmosphere, resulting in fog or mist. When AN is used, no smoke is created, but the performance is reduced owing to a reduction in the particular impulse. A major disadvantage of this propellant is that one of the combustion products is HCl which is very toxic and can lead to acid rain. Therefore, chlorine-free propellants are now looked upon to avoid this.

3.2.2 Ammonium nitrate based composite propellants

Ammonium nitrate propellants are a perfect fit to produce the chlorine-free emission solution. They provide desired properties and a non-hazardous exhaust. This serves as the biggest advantage to the ammonium nitrate-based propellants. Although the advantage of the non-hazardous exhaust is achieved via AN-based propellants, this brings some disadvantages like low burn rate, low specific impulse, and crack formations in the grains.

3.2.3 Nitramine composite propellants

These types of propellants are very similar to AP composite propellants; however, they serve the advantage of minimal infrared emissions due to a very low proportion of emissions such as CO_2 and H_2O.

3.2.4 Minimum-signature (smokeless) composite propellants

In the 21st century, the era of green energy, the propellant research on these types of propellants is the most active. The new propellant has been designed and tested with great success. The propellant is non-polluting, containing no acid, solid particles, or lead. It is also smokeless, with only a tiny shock diamond pattern visible through the otherwise clear exhaust. These smokeless propellants decrease the risk of exposing positions from where the missiles are fired by eliminating the brilliant flame and voluminous smoke trail created by burning aluminized propellants. The advantages of this propellant are a clear victory in forms of high detonation, shock insensitive and smokeless, but the extremely high cost is still a big disadvantage.

3.3 Selected propellant compositions

As mentioned in the previous chapter, two propellant compositions form the grain in which one of them has a higher burning rate than the other. They are considered to be thermoplastic composite propellant manufactured based on the free standing grain (cartridges). Each propellant has different flame temperature and burning rate characteristics. The propellant composition characteristics are illustrated in Table 4. A thermochemical analysis is crucial to be performed to evaluate the theoretical performance of solid propellants. In this project, the analysis is carried out via a thermochemical computer code EXPLO5 [49] which has the capabilities of predicting the energetic properties of single compounds or mixtures. The program inputs for the analysis are the propellant formula and the combustion pressure. The program output includes the expansion ratio, specific impulse, characteristic velocity, thrust coefficient and some other thermodynamic parameters.

Table 4 Propellant composition characteristics

Parameter	Fast Burning Propellant	Slow Burning Propellant
Adiabatic constant [-]	1.25	1.25
Density [kg/m^3]	1715	1705
Burn rate exponent *n* [-]	0.48	0.47
Burn rate coefficient [ms^{-1}Pa^{-n}]	0.0000101	0.00000855
Burning temperature [K]	2599.2	2744.6

4. Experimental work

The objective of the experimental work of this project was to determine the rocket motor performance by conducting a static test. The importance of performing static tests relies on confirming the rocket motor design parameters by checking them against the test outputs. That will ensure the required performance was met before going for the flight test [50]. It is also important to check the SPRM physical characteristics through some nondestructive testing methods to ensure there are not any defects in it [51]. A system that is built to measure the thrust and pressure must be composed of three main components which are test stand, pressure transducer, load cell and data acquisition system [52]. Generally, there are certain outputs expected as a result from the test, which are thrust, pressure and temperature. In this project, the static test is focused solely on the measurement of the pressure and thrust parameters for the original grain shape configuration.

A lot of past research papers and documents illustrated various methodologies related to the experimental work of solid propellant rocket motors and the methodologies used for the thrust and pressure measurements [53-55]. The most common testing methodology of SPRM is done through the L-block test stand as shown in Fig. 29.

Figure 29 Solid propellant rocket motors L-block test stand [56]

4.1 Test equipment

The test stand used in this project carries the same methodology of the L-block test stands where it consists of the following parts:

- Test stand: It is a structure that is used to mount the rocket motor on [57]. There are two jigs fixed on a thick horizontal steel plate where the rocket motor will be placed as shown in Fig. 29. It incorporates the load cell and pressure transducer.
- Data acquisition system: The data acquisition system consists of measurement and recording devices in order to read and store the test results [58]. Multiple parameters, including pressure, thrust, temperature, and time, can be read by the data acquisition system. The main function of its components is to transform the analog signals received from the static test stand to digital values for processing.

- Load cell: It is basically one of the transducer types that its main function to turn the measured thrust to an electrical signal which could be extracted from the data acquisition system for further analysis. The structure of a typical load cell is illustrated in Fig. 30 where it shows the main component of it which is the strain gauge. The load cell used in the test is based on strain gauge usage and transformation of elastic body deformation into force.

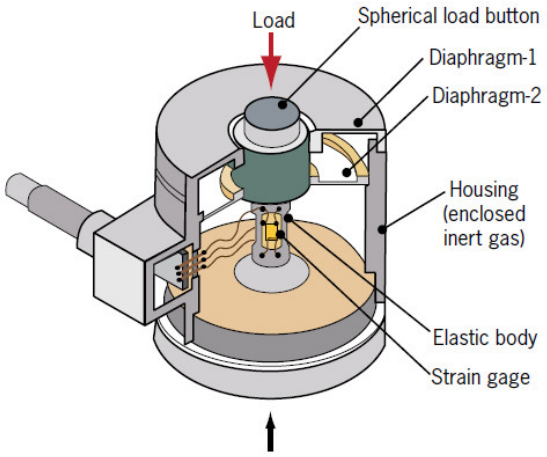

Figure 30 An illustration of a typical load cell [59]

- Pressure transducer: It is a transducer used to measure the built-up pressure inside the motor in order to monitor the pressure growth and make sure it is within the safe region. Working principle is based on piezoelectric effect of a quartz crystal.

4.2 Test preparation

The free-standing propellant grain was produced based on the defined original grain configuration with two propellants. The grain is inhibited from outside and one of the frontal sides where the side at the nozzle uninhibited. The cross section of the propellant grain is shown in Fig. 31, while Fig. 32 shows a closer look to the grain forms, where it shows the two propellants. The case was made of steel, and it was designed in a way that it could withstand the operating pressure. The nozzle used for this rocket motor is a conical nozzle consists of convergent, divergent and throat parts. The preparation of the static test starts by assembling the produced components of SPRM (Fig. 33).

Figure 31 Propellant grain cross section

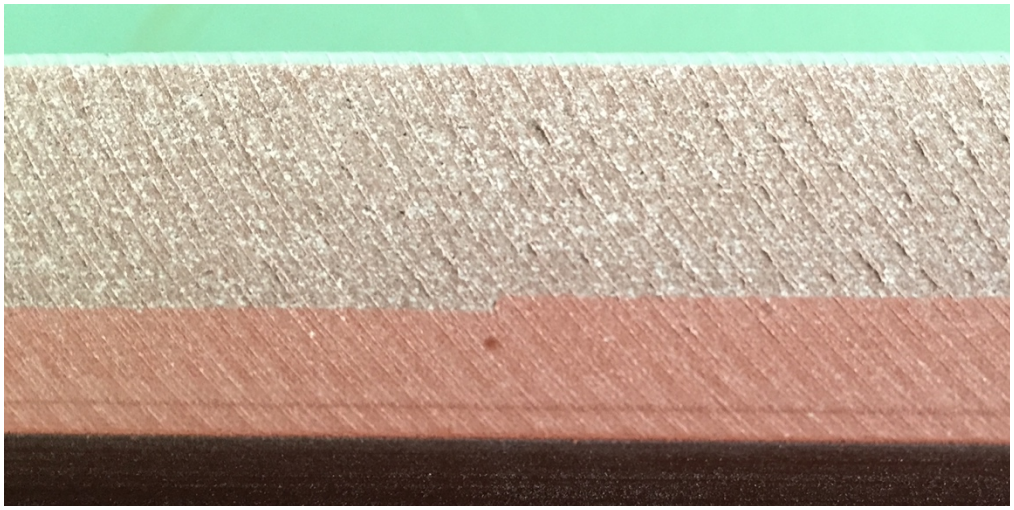

Figure 32 Propellant grains closer look clearly showing two propellants

After assembling the rocket motor, a quality check shall be carried out before placing it on the rocket motor stand as the following steps:

- Detailed visual inspection to insure a proper assembly of the components.
- Checking the physical characteristics by weighing the full assembly and measuring the total length.
- Measuring the final center of gravity (CG) location to ensure that the CG after assembly complies with the design CG location.

Figure 33 Assembly procedure of the rocketmotor

Most of the times, the static test is conducted at ambient temperatures; however, it could be performed at high and low temperatures to study the influence of the temperature on the performance of the rocket motor. Heating and cooling chambers are used to alter the rocket motor temperature prior the test where it could be placed in the chamber over the prescribed period to gain the final desired temperature. After completing the quality check and confirming the temperature which the test will be performed at, the rocket motor was mounted on the test stand as shown in Fig. 34.

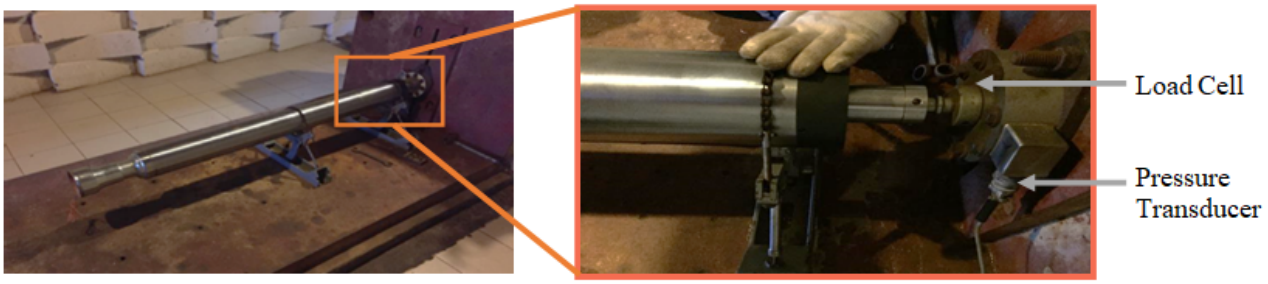

Figure 34 Rocket mounting on test stand

4.3 Test procedure and data acquisition

It is essential to adhere to all the proper procedures and protocols before starting the static test in order to ensure the safety of the personnel and achieve a successful test. After the test completion, a detailed visual inspection was carried out again on each component after disassembling the rocket motor in order to ensure the test went out successfully. Figure 35 shows the rocket components after disassembling the subsystem. Finally, the recorded data was retrieved from the data acquisition system in order to be used for further analysis which will be discussed in chapter 5.

Figure 35 Rocket Components after disassembly

5. Results and Analysis

The program results will be presented in this chapter, and they will be discussed and analyzed accordingly. They will be split in different sections based on the output parameter. The diagrams will be used to compare the outputs of each model by plotting the curves in the same diagram. The propellant's grain temperature sensitivity will be evaluated by running the program at three different temperatures which are ambient, hot and cold. The program's thrust and pressure profiles are checked against the experimental results that were obtained from the static test.

5.1 Program input

An input file has to be formulated with the values of the parameters that will be used to run the program. In order to run the MATLAB program, the dimensions of the propellant grain and its propellants' composition characteristics are required. It is necessary to set the initial conditions for the analysis. The influence of the grain's temperature will be studied by altering the input of the temperature at the beginning of each iteration, as discussed in the temperature sensitivity section. The propellant's grain dimensions are shown in Table 5. The original model dimensions represent the real grains' dimensions, which was tested in the static test bench. The optimized model dimensions were defined after multiple iterations of finding the optimum values that would deliver similar burning surface area profile. It was required to keep the outer diameter D, inner diameter D_f and total length L_f the same for both propellants that the configuration of the contact surfaces between the two propellants were modified. On the other hand, it could be stated that an assumption was taking into consideration which is the thrust coefficient with the value of 1.5. The propellants' composition characteristics are given in table 4, and it could be seen that the adiabatic constant for both propellants is 1.25.

Table 5 Propellant grain dimensions

Dimension	Original model	Optimized model
D [mm]	120	120
D_f[mm]	74.5	74.5
D_{s1}[mm]	81	81
D_{s2} [mm]	83	104
L_f[mm]	1260	1260
L_s[mm]	105	-
L_{s1} [mm]	105	50
L_{s2} [mm]	105	55
L_{s3} [mm]	105	105

5.2 Program outputs

The results generated from the program will be illustrated under this section and discussed accordingly. The parameters that will be shown are burning surface area for each propellant and the total burning surface area of the grain. The other parameters are mass flow rate, burn rate, pressure, and thrust which all of them are plotted versus the burning time. The thrust and pressure

profiles from the mathematical models of both grains will be checked against the pressure and thrust profiles from the experimental static tests of the rocket motor.

5.2.1 Burning surface area

The developed analytical models of burnback analysis of the original and optimized propellant grains will calculate the burning surface area precisely at each step of the combustion process. The burning surface area of each propellant will be compared against each other for the different grain shapes. Then, the total burning surface area will be shown, and there will be three iterations at three different temperatures.

5.2.1.1 At ambient temperature

The program is set to be run at an ambient temperature condition of 15 ºC for the first iteration. As discussed in the burnback analysis chapter, the first step of burning will evolve only around propellant f which its burning will be from t_b equals 0 until the burning time reaches 0.2 s for the original and optimized models which A_s remains zero. After the first step, each grain configuration starts to burn differently. The original model starts forming the new slope at the step between the two propellants due to the difference of the burning rates and the grain's shape. The newly formed slopes create the steps as shown in Fig. 36. The optimized model makes a smoother curve. It can be seen that propellant f will finish burning when t_b reaches 0.9 s. On the other hand, propellant s starts burning after the first step when t_b is 0.2 s and it lasts to grain's burn off which is in this case 1.4 s.

The result and sum of propellant f and s gives the grain's burning surface area as illustrated in Fig. 37. A comparison between the two grain shapes is shown where the optimized model has a smoother line as mentioned over the original grain shape. The burning surface area curve for both grain shapes models show identical results until the fast burning propellant is about to burn out after 0.6 s when the slower burning propellant reaches its highest burning surface values. The tail off starts when the slower burning propellant start disappearing when the burning time is close to 1 s. Overall, both mathematical models showed consistency.

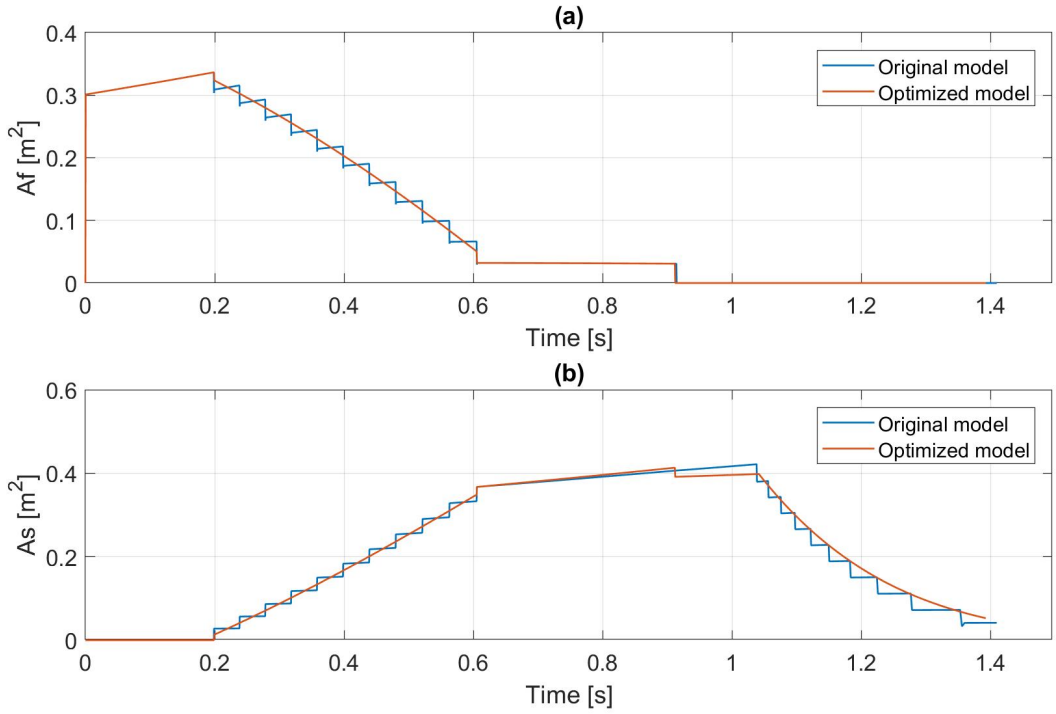

Figure 36 Burning surface area vs. time for the original and optimized grain shapes a) fast burning propellant, b) slow burning propellant

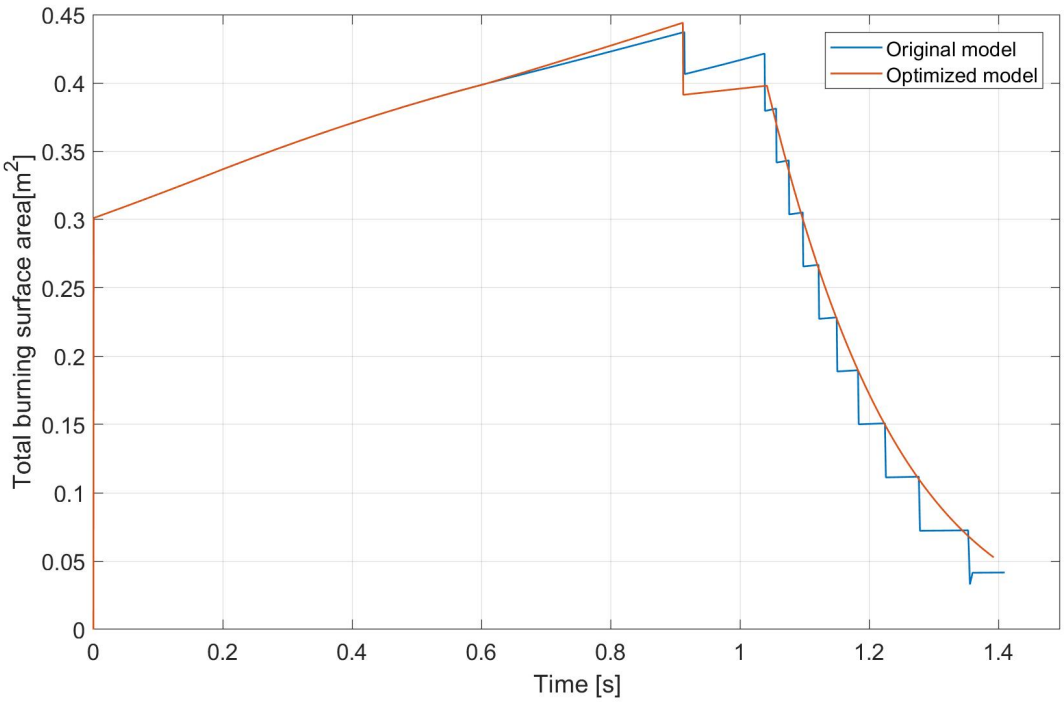

Figure 37 Total burning surface area vs. time for the original and optimized grain shapes

5.2.1.2 At cold temperature

This iteration of the burnback analysis was carried out for the cold temperature condition, which was done by setting the propellant grain initial temperature in the MATLAB code to be -40°C. The influence of propellant grain initial temperature on its burning rate was studied theoretically and experientially by Condon, Renie and Osborn [60]. It could be seen from Fig. 38 and Fig. 39 that the burning surface area profiles in this case are similar to the previous case; nevertheless, the burning time is different. The cold temperature conditions cause a longer burning time based on the temperature sensitivity equation while having the total impulse very close to the other temperature conditions.

From Fig. 39, one can observe that the burning time of the first stage ends at 0.25 s comparing to the ambient temperature burning surface area from Fig. 36. Thus, the whole propellant grain progression will be influenced accordingly.

The total burning surface area in Fig. 39 shows a longer burning time which lasts to 1.6 s comparing to the ambient temperature. Indeed, all the three temperature cases will have the same total burning surface area; however, each case will reach the highest total burned surface area at different times. In the ambient temperature, it reached the maximum A at a burning time of 0.9 s, but it reached the same at t_b equals 1.2 s when the propellant grain is in the cold condition. Overall, both analytical models showed similarity in burning behavior until the slope from the optimized model starts showing a smoother curve comparing to the serrated curve.

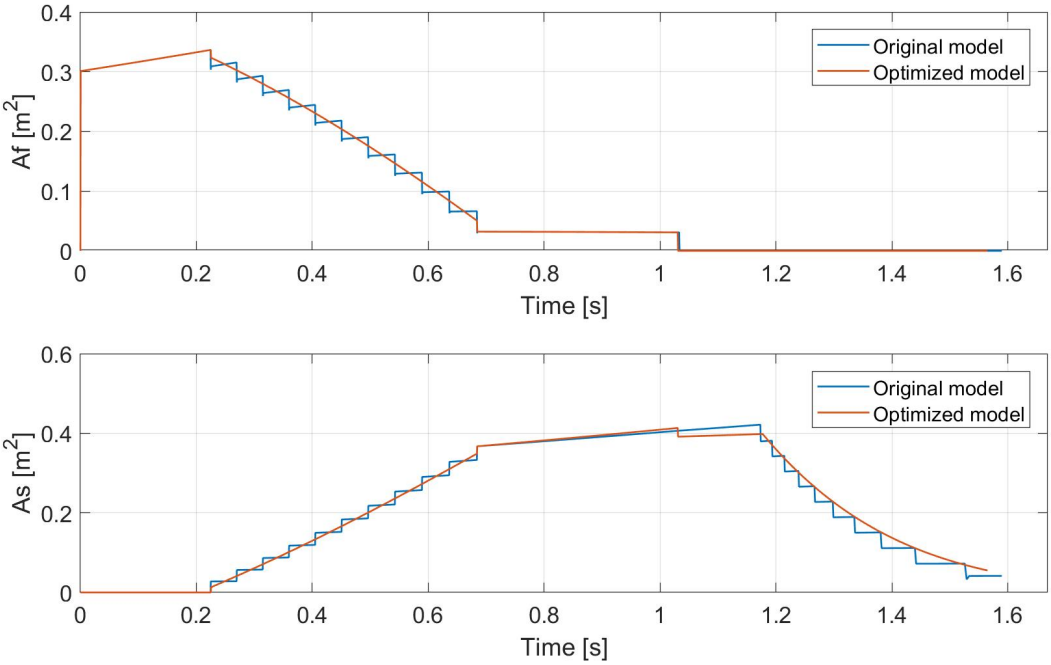

Figure 38 Burning surface area vs. time for the original and optimized grain shapes at cold temperature a) fast burning propellant, b) slow burning propellant

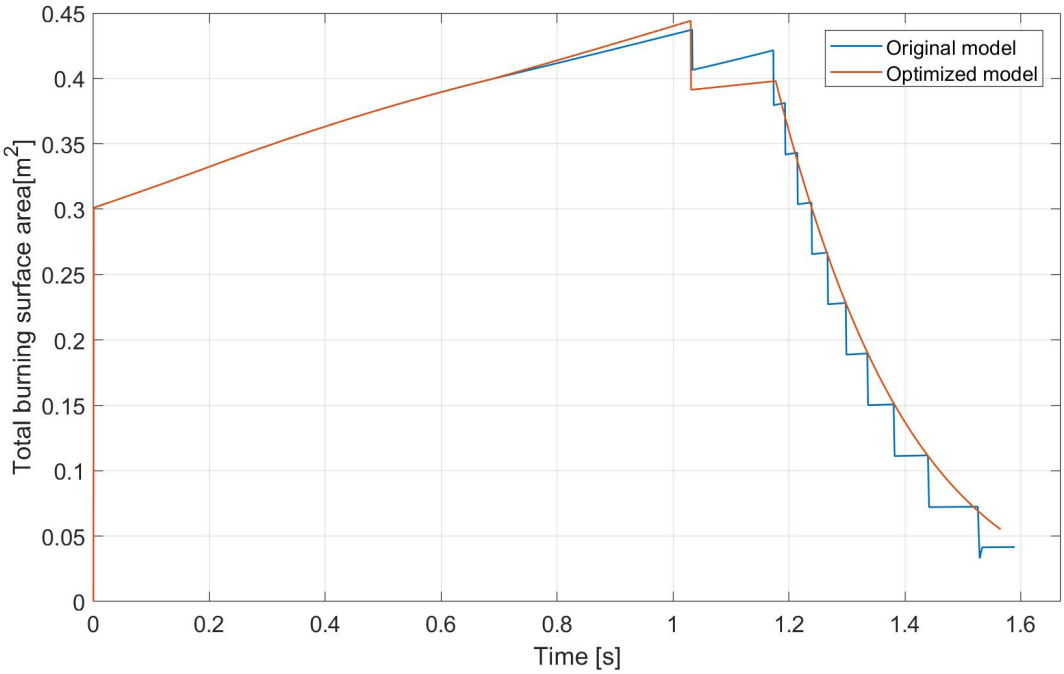

Figure 39 Total burning surface area vs. time for the original and optimized grain shapes at cold temperature

5.2.1.3 At hot temperature

In the last case of the burning surface area iterations, the initial temperature was set to be 50 ºC to study the propellant grain predicted performance at hot temperatures. It is noticeable from Fig. 40 that the burning surface area profiles of both propellants demonstrate similar burning behavior. The only difference is the burning time which the grain burns faster with a burning time of around 1.4 s. The total burning surface area profile shown in Fig. 41is in agreement with the profiles from the previous cases, but with a shorter burning time.

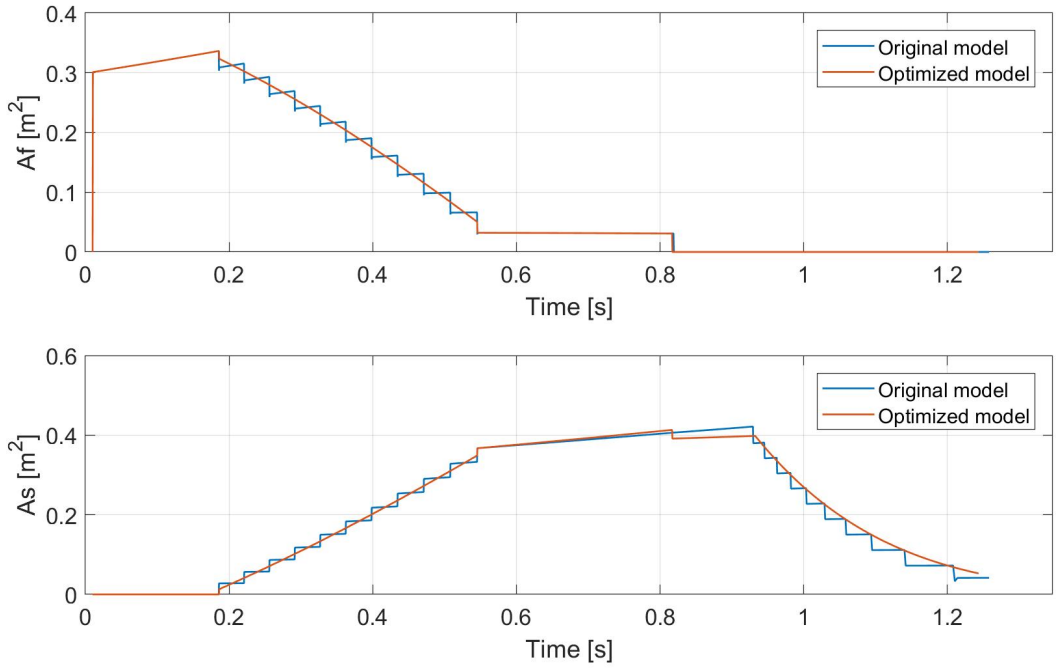

Figure 40 Burning surface area vs. time for the original and optimized grain shapes at hot temperature a) fast burning propellant, b) slow burning propellant

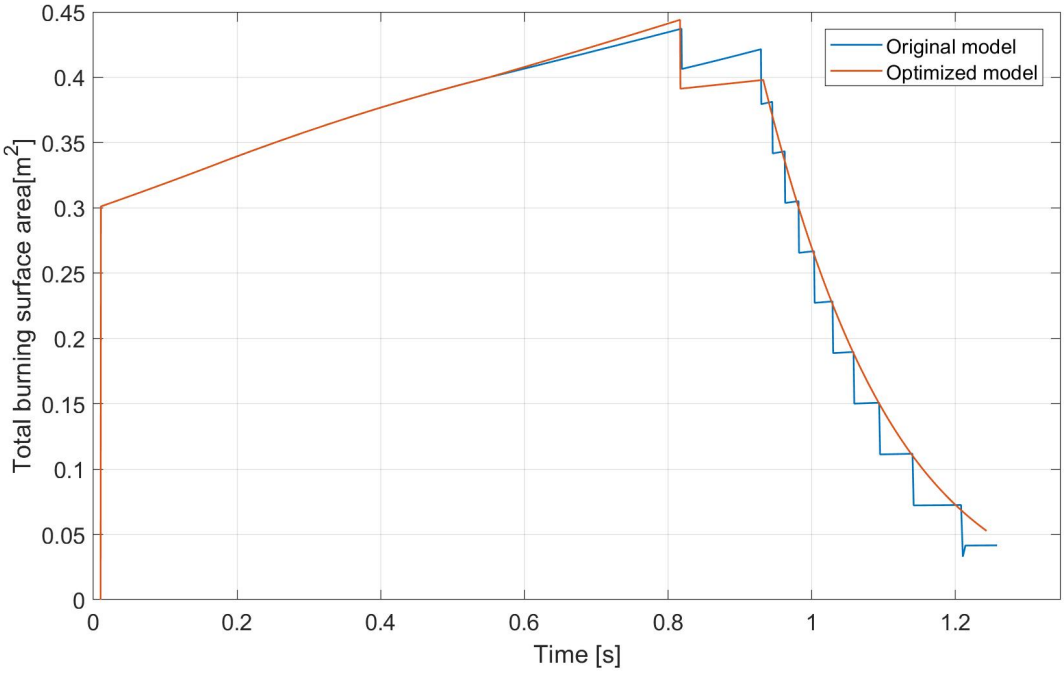

Figure 41 Total burning surface area vs. time for the original and optimized grain shapes at hot temperature

5.2.2 Mass flow rate

The mass flow rate was calculated using Eq.16 for each propellant, and then the sum of both mass flow rates was taken to have the total mass flow rate $\dot{m}$ of the propellant grain. A comparison of the mass flow rate outputs for the original and optimized models from the program will be discussed. In addition, three simulations will be presented for different temperatures of the propellant grain, which are ambient, cold and hot.

5.2.2.1 At ambient temperature

The original and optimized grains show consistency in the value of $\dot{m}$ until 0.2 s of the burning time due to the similarity of the burned surface area at that time interval. After the 0.2 s, the original model starts to have a serrated line compared to the optimized model, which has a smoother line as shown in Fig. 42. The second phase of burning will now start from 0.2 s to 0.6 s where it would include the burning of the steps in the original model and the slope in the optimized model. It can be seen that the optimized model enhanced the profile by getting rid of the serrated line. The mass flow starts to increase after 0.6 s from 12 kg/s to 14 kg/s at 0.9 s with a little of decrease in the original model. During the fourth phase of burning and tail off, the mass flow rate starts to decrease; however, the original model has a high value of $\dot{m}$ between 0.9 s and 1.05 s. In totality, these two models show consistency at the ambient temperature.

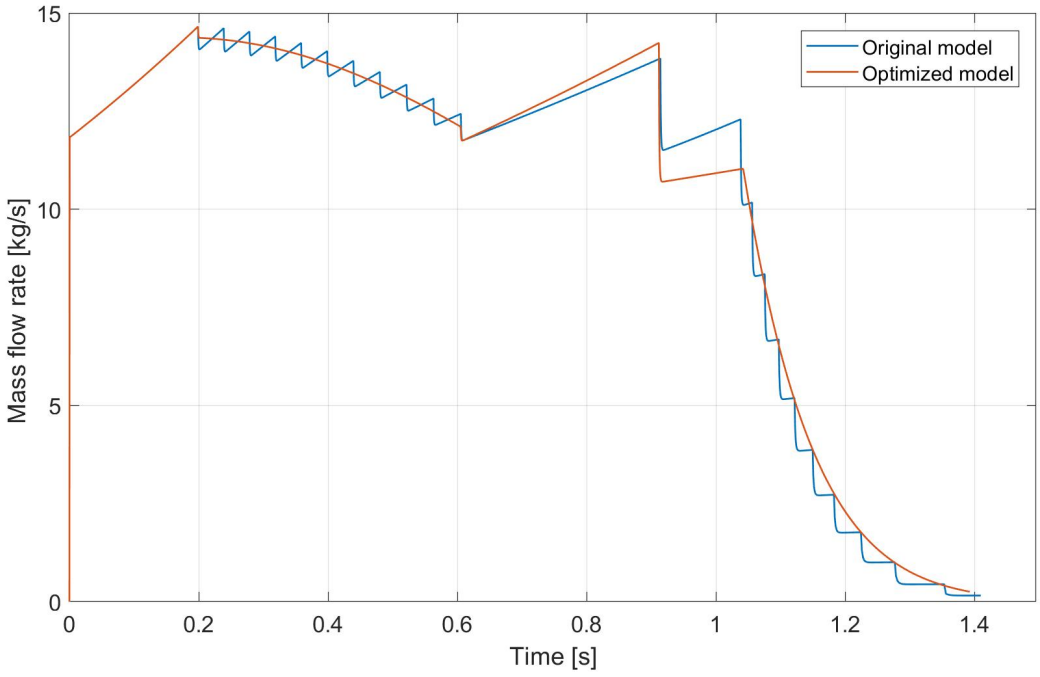

Figure 42 Mass flow rate vs. time for the original and optimized grain shapes at ambient temperature

5.2.2.2 At cold temperature

Due to the temperature sensitivity phenomena, the decrease of the mass flow rate values could be noticed in Fig. 43. However, the mass flow rate vs. time curve illustrates a similar behavior to the ambient temperature simulation. In this case, the mass flow rate starts with a value of 11 kg/s which is around 9 percent less than the previous case. The original and optimized models' profiles are the same until 0.22 s which indicates that the first phase duration of the burned surface area takes longer in colder temperatures. It could be seen that the total burning time is longer which is up to 1.6 s compared to the 1.4 s in the ambient temperature iteration. As seen in Fig. 43, the mass flow rate reaches the highest level to approximately 13 kg/s at two stages during the combustion. The first one is at the end of the first phase of the burned surface area, and the second one is at the end of the fast burning propellant burn out which is around 1.02 s. Similar to the other profiles, the optimized model curve show a smoother line compared to the serrated curve of the original model.

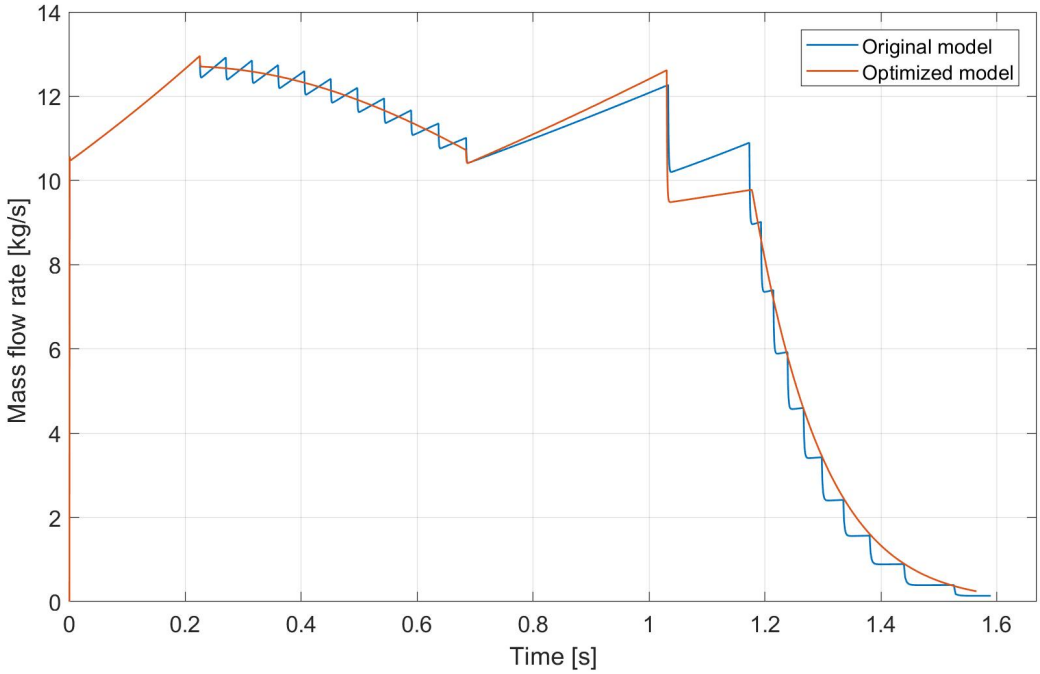

Figure 43 Mass flow rate vs. time for the original and optimized grain shapes at cold temperature

5.2.2.3 At hot temperature

When running the MATLAB program for the third time at the hot temperature condition of 51 ºC, the $\dot{m}$ values are the highest comparing to the ambient and cold temperatures. In addition, the burning time is the shortest in this case with a total t_b of 1.2 s. In this case, the highest mass flow rate value is 16.05 kg/s at 0.19 s and 0.81 s. Overall, the behavior of the original and optimized model is similar in all the three different temperature iterations.

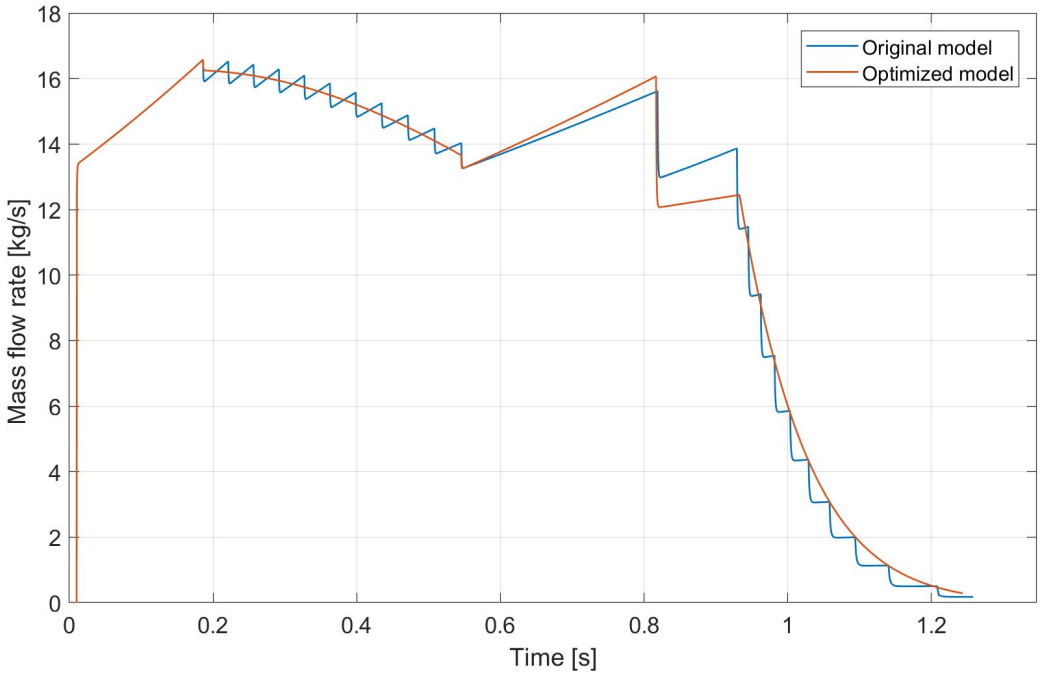

Figure 44 Mass flow rate vs. time for the original and optimized grain shapes at hot temperature

5.2.3 Burning rate

Understanding the burning rates of both propellants is essential to predict the main performance parameters of the rocket motor. In this section, the burning rate outputs from the program of both the original as well as optimized propellant grains will be discussed. The burning rate will be calculated by taking into consideration the temperature sensitivity. Thus, both r_f and r_s will be illustrated at ambient, hot and cold temperatures.

5.2.3.1 At ambient temperature

Initially, the original and the optimized model are set to run at ambient temperature, which is also the first iteration. In the fast burning propellant as shown on the top figure of Fig. 45, both the original as well as optimized model start with a burning rate of more than 20 mm/s. Both models show similar behavior until the burning time reaches 0.2 s, after which the original model shows a serrated line until 0.6 s due to the steps in the original model, compared to the smoother curve seen in the optimized model. Then both models show the same behavior until the end burning of the fast burning propellant. On the other hand, the burning of the slow burning propellant starts at 0.2 s as illustrated on the bottom figure of Fig. 45 which gives a value of 18 mm/s for both models. However, similar to the fast burning propellant, both the models show a similar behavior in the slow burning propellant until 0.2 s. In this case, the last stage cool off starts after 1 s where the original model shows a serrated line compared to the smoother curve seen in optimized model. It can be seen that the propellant will finish burning at 1.4 s in the slow burning propellant compared to 0.9 s in fast burning propellant.

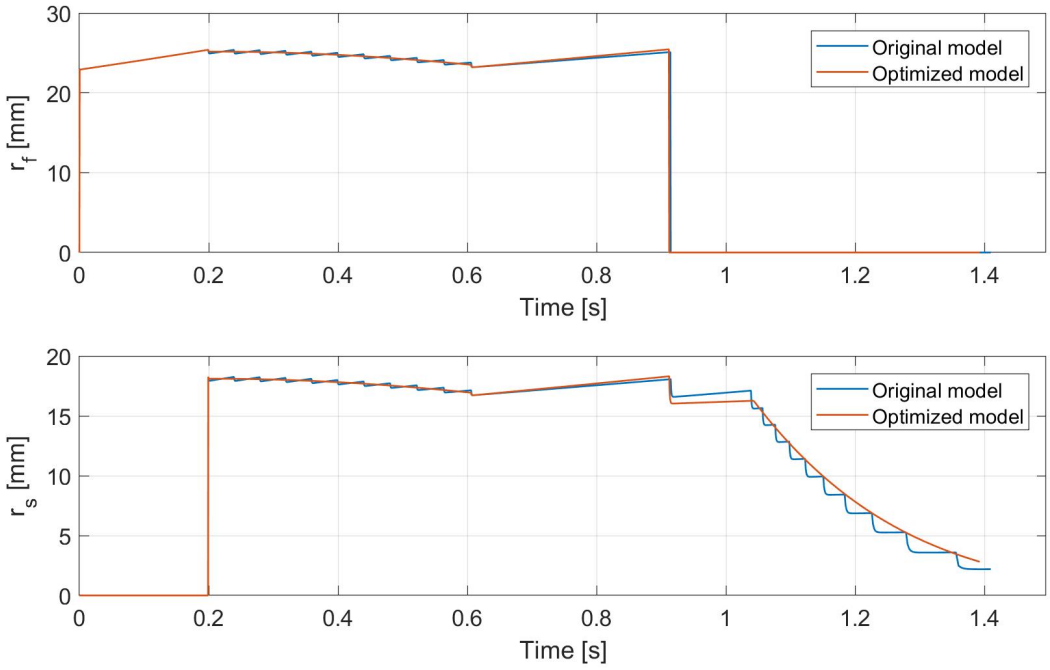

Figure 45 Burn rate vs. time for the original and optimized grain shapes at ambient temperature a) fast burning propellant, b) slow burning propellant

5.2.3.2 At cold temperature

After the ambient temperature iteration, the burning rate analysis was carried out for the cold temperature condition. The burn rate calculations from the program are illustrated in Fig. 46 which shows lower values of r than the ambient condition results. In this case, the burning rate of propellant f starts off with 20 mm/s and it has a natural line until it burn off. On the other hand, propellant s has a lower burning rate value which starts at 16 mm/s. Overall, both Fig. 45 and Fig. 46 show an agreement in the burning behavior for the original and optimized models.

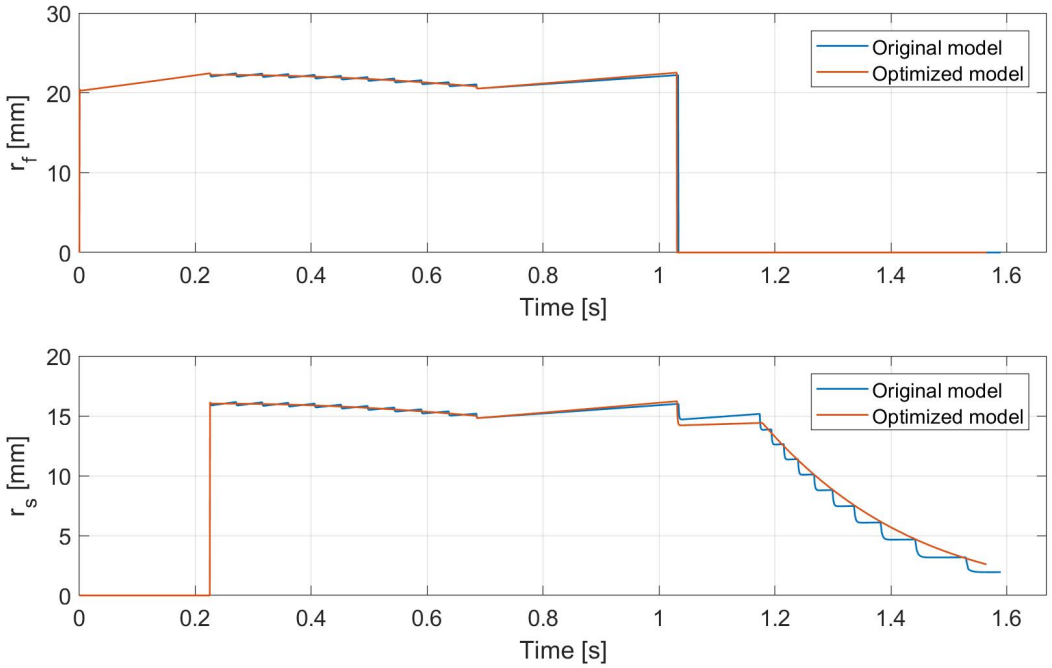

Figure 46 Burn rate vs. time for the original and optimized grain shapes at cold temperature a) fast burning propellant, b) slow burning propellant

5.2.3.3 At hot temperature

The temperature was set to be 50 ºC for this case to study how hot temperatures could influence the burning rate of propellant grains. That could be shown in Fig. 47 where the values of r are the highest comparing to the previous two cases. The fast burning propellant has an average burning rate of 26 mm/s throughout its burning time until it burns off at around 0.8 s which is the fastest in all three temperature cases. The slow burning propellant has an average burning rate value of 20 mm/s until the start if the tail off.

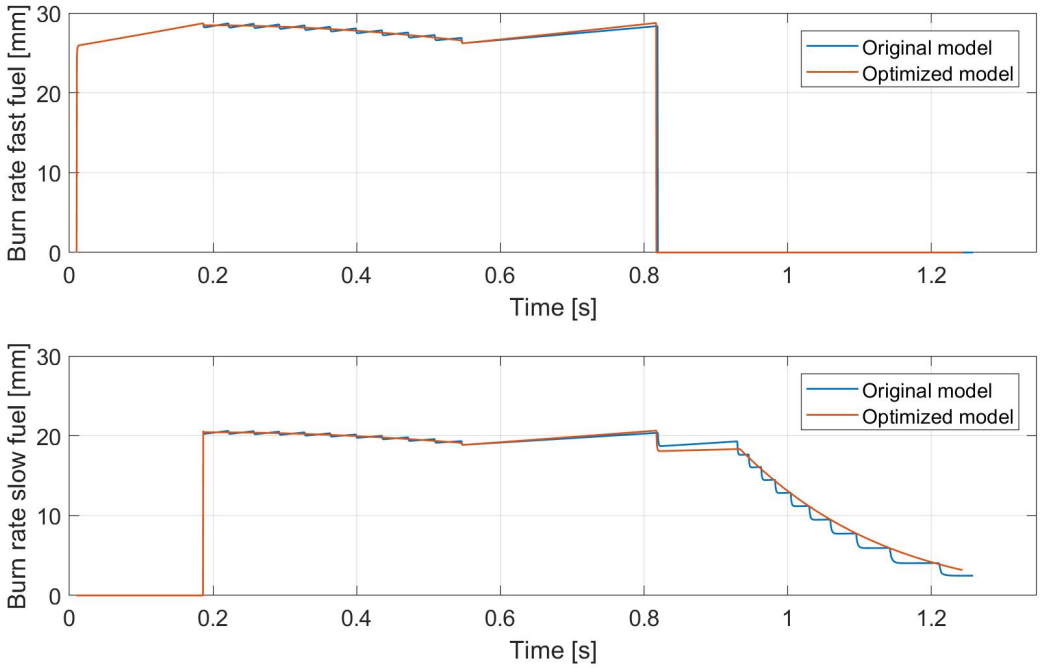

Figure 47 Burn rate vs. time for the original and optimized grain shapes at hot temperature a) fast burning propellant, b) slow burning propellant

5.2.4 Pressure

The combustion chamber pressure is solved numerically via Eq. 19 after calculating the mass flow rate. Three pressure curves will be compared to each other which two of them obtained from the MATLAB program for the original and optimized models and the third one illustrates the measured pressure profile from the static test. Similarly, the pressure profiles will be demonstrated for three different temperatures which are ambient, hot and cold.

5.2.4.1 At ambient temperature

In the first iteration, as seen in Fig. 48 at the ambient temperature of 21 ^{o}C, the original model and the experimental results show a similar behavior at start. However, the original model has a serrated curve. Notably, all three of these, original model, optimized model, and experimental results reaches the highest pressure of a little more than 12 MPa at around 1 s. After reaching the highest-pressure level, the tail off starts, where the original model shows a serrated line compared to the smoother curve seen in the optimized model and experimental results. The three curves have a little drop of pressure to 11 MPa at 0.6 s. As seen in Fig. 48, the original and optimized models start the tail off at around 1.1 s a bit earlier than the experimental curve.

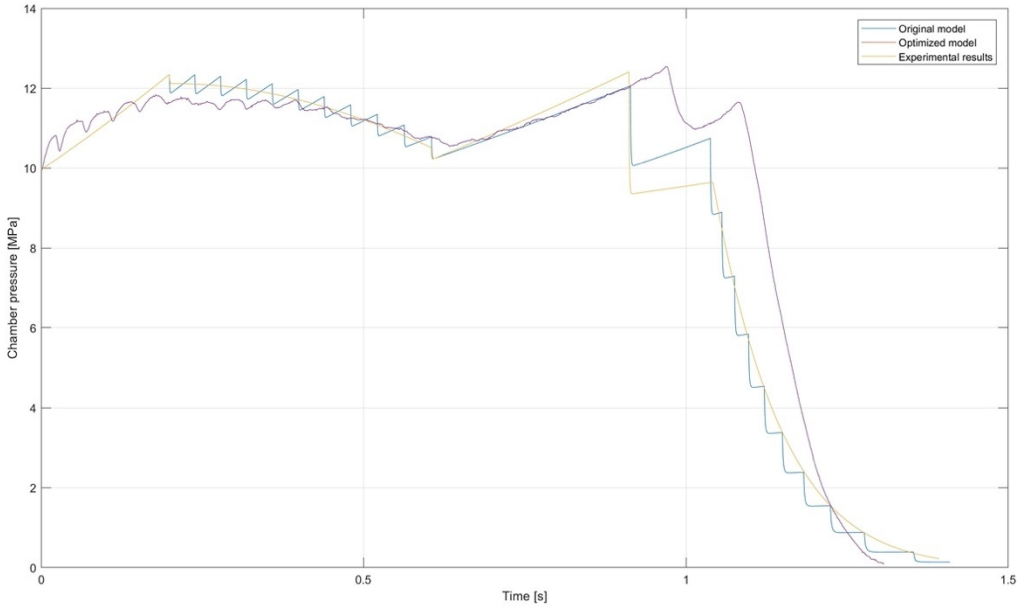

Figure 48 Pressure vs. time for the experimental results, original and optimized grain models at ambient temperature

5.2.4.2 At cold temperature

As seen in Fig. 49, both the original model and optimized model show a similar behavior from t_b equals 0 s to 0.2 s. However, when compared to the ambient temperature iteration, the experimental results in this situation shows a serrated line compared to a straight line in ambient temperature. Moreover, as opposed to the highest pressure of 12 MPa in ambient temperature, the highest pressure in the cold temperature iteration is around 11 MPa for all three, original model, optimized model, and experimental, which is reached after a little more than 1 s. After reaching the highest point, the cool off starts as seen in Fig 49. The optimized and the original model reach 0 pressure at 1.6 s, compared to 1.4 s for experimental results.

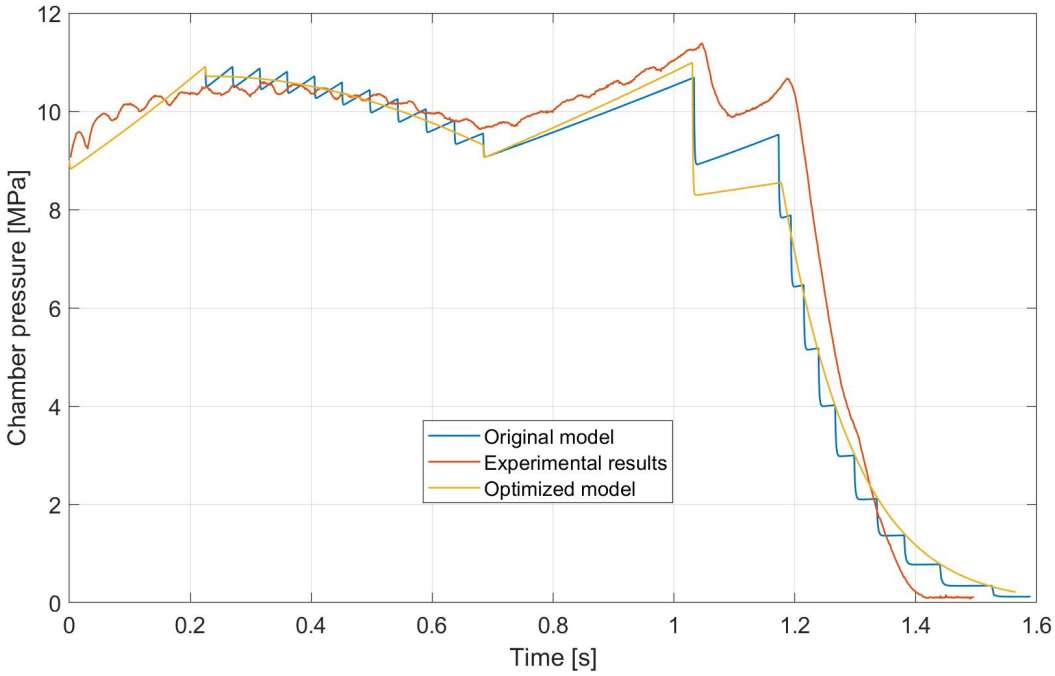

Figure 49 Pressure vs. time for the experimental results, original and optimized grain models at cold temperature

5.2.4.3 At hot temperature

In the hot temperature iteration, chamber pressure shows a similar behavior as that of the cold temperature iteration. However, compared to the highest pressure of around 11 MPa in cold temperature iteration, the highest pressure recorded in the hot temperature situation is 14 MPa, which is also the highest among all three iterations. Moreover, unlike the other two iterations, the original model, optimized model, and experimental results reached 0 chamber pressure at the same time, which is 1.2 s, as seen in Fig 50.

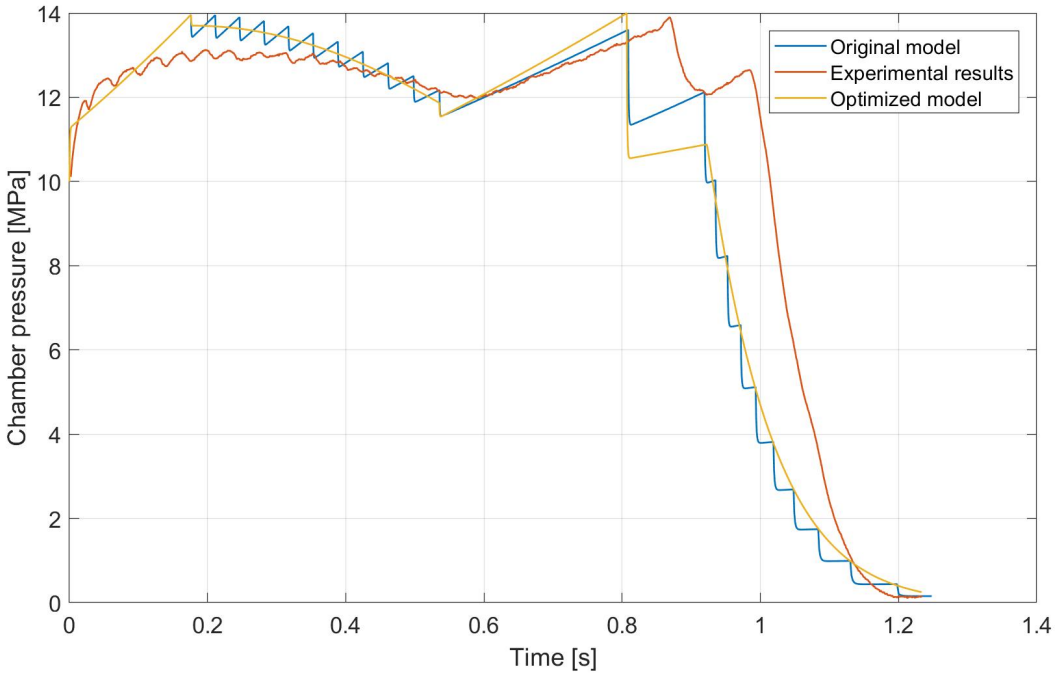

Figure 50 Pressure vs. time for the experimental results, original and optimized grain models at hot temperature

5.2.5 Thrust

Using Eqn. 22 to calculate the thrust and results in obtaining figures 51, 52 and 53. Those figures will compare the thrust profiles of the optimized and original models and the experimental results. In addition, the experimental results at the ambient, hot, and cold temperatures will be checked against the calculated original and optimized models. The three curves for the three different temperatures shall be fairly similar to meet the objective of developing the MATLAB program for this dissertation project.

5.2.5.1 At ambient temperature

Since the ignition phase is neglected, it can be seen in Fig. 51 that all the thrust curves start at 25 kN. The thrust starts increasing until the burning time reaches 0.2 s, and then starts decreasing until 0.6 s. Then, the thrust starts increasing again until it reaches its maximum for the original and optimized models before the curve obtained from the static test bench. The original and optimized models' profiles start tailing off at 1 s when the thrust is around 27 kN for the original model and 25 kN for the optimized model. However, the experimental thrust curve starts to decrease at 1.13 s after reaching its maximum of 32 kN. Overall, all three curves showed close thrust values throughout the burning time. It is noticeable that the optimized model has a smoother curve compared to the sawtooth curve of the original model.

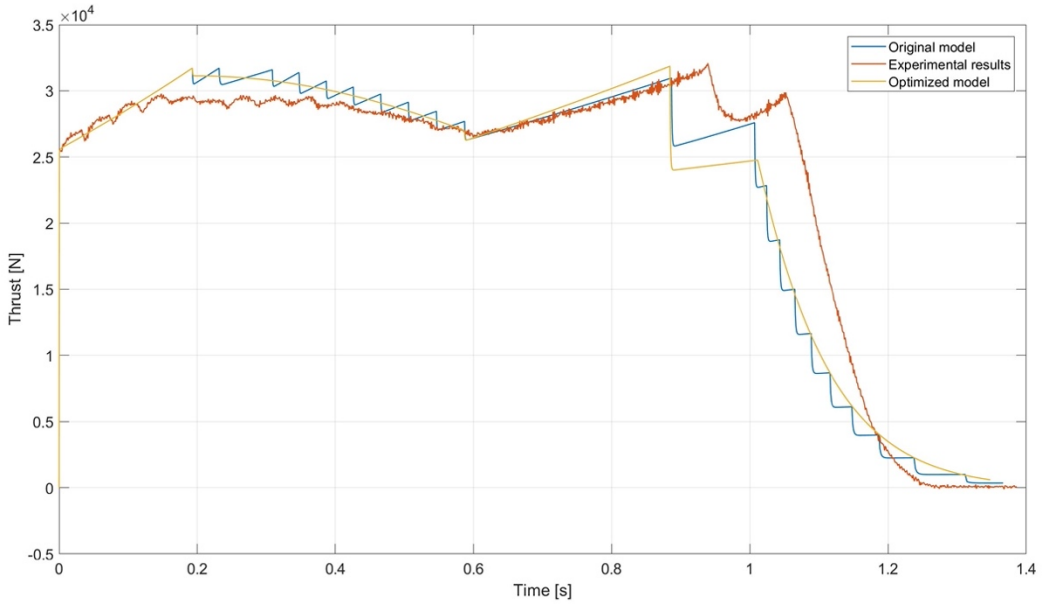

Figure 51 Thrust vs. time for the experimental results, original and optimized grain models at ambient temperature

5.2.5.2 At cold temperature

In the cold temperature iteration, as seen in Fig. 52, all the three curves show an agreement until 0.6 s when the curve from the static test start to have higher thrust values. The highest thrust values were 29 kN at 1.05 s, 26.5 kN at 1.05 s and 26 kN at 1.05 s for the experimental results, optimized model, and original model respectively. Comparing Fig 52 to Fig 51, the thrust values are lower in the cold temperature conditions with higher burning time. The average thrust value is 25 kN for this case and the burning time is 1.4 s. In addition, the optimized model profile shows similarity to the experimental curve unlike the original model curve which has the serrated profile.

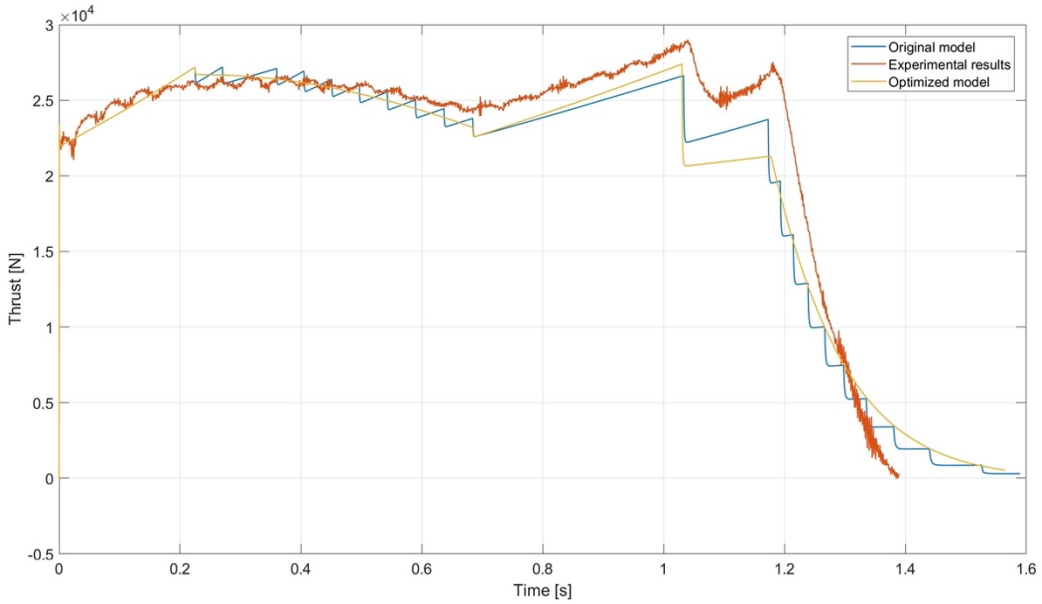

Figure 52 Thrust vs. time for the experimental results, original and optimized grain models at cold temperature

5.2.5.3 At hot temperature

The last case to be evaluated is for the hot temperature at 51 ºC. In the hot temperature iteration, as seen in Fig. 53, the behavior of the original model, optimized model, and experimental results, is the same when compared to the cold temperature and ambient temperature iterations. All the three curves have close thrust values one to the other until the burning time reaches 0.8 s where the original and optimized models start decreasing but not the experimental curve. Figure 53 illustrates how the temperature sensitivity of burning rate influence the solid propellant rocket motor performance where the thrust values are the highest in this temperature's condition and the shortest burning time compared to the ambient and cold temperatures. The average thrust is 3300 daN, yet the maximum thrust value is 35 kN for the three curves and the burning time is 1.2 s.

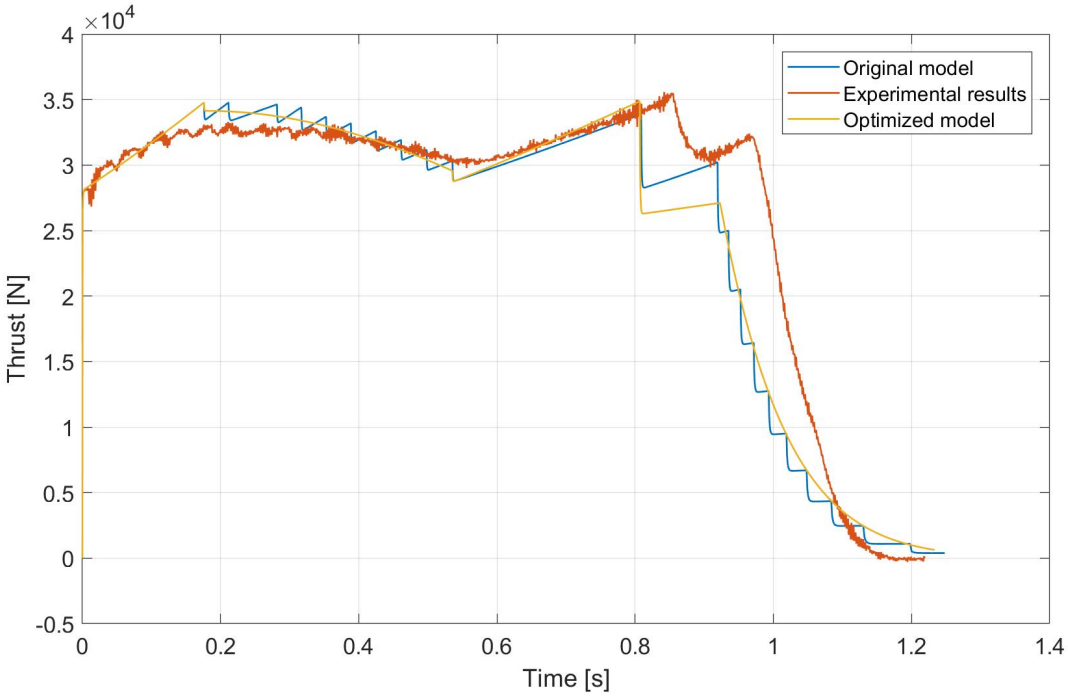

Figure 53 Thrust vs. time for the experimental results, original and optimized grain models at hot temperature

6. Conclusion

A MATLAB code was developed to give an accurate performance prediction of a two-propellant grain. The theoretical results were checked against the experimental results from the static test in order to verify the code. The code comprised the burnback analysis equations and the internal ballistics equations. The mathematical model of the burn back analysis was derived using geometrical relations that represent the burned surface area at each interval of the web. The original model consisted of 21steps to deliver an accurate model where each phase consisted of the burning surface of the fast and slow propellant grains and their sum gave the total burning surface area. The mathematical burn back analysis of the optimized model consisted of only five phases to deliver similar values to the original model. The program's final outputs showed the thrust and pressure profiles versus time along with the other figures of the burning surface area, burning rate and mass flow rate.

The major effort of this project was to develop an accurate burnback analysis model depending on the geometrical shapes of the propellant grain. The first model was created for a two-component propellant grain Fig. 21 which is an existing propellant grain that has been tested and qualified. It has a tubular shape from the outside and inner cavity. Yet, it compromises two different propellants. The two propellants were segregated by steps as a ladder shape to split the combustion into different phases so it can deliver approximately neutral burning behavior. One of the objectives of this project was to find an alternative-simpler grain shape that can deliver the same performance. Thus, the grain's shape as shown in Fig. 23 was founded as an optimized solution that would involve less geometrical equations. The new shape replaced the steps with a slope that separates the two propellants. It was found out that the burnback analysis model was shortened as discussed in chapter two. The geometrical equations were solved numerically at each segment of geometric change in the combustion process.

The fifth chapter of this dissertation illustrated the final outputs which showed a comparison between the optimized and original models for the burning surface area, mass flow rate and burning rate. An agreement on the results was illustrated in all the results figures which could approve the feasibility of the optimized model. The second part of the results demonstrated the pressure and thrust profiles versus time where the original and optimized models were compared against the curves from the static test. Those figures showed an agreement among them, which was a great validation that the developed mathematical models could predict the rocket motors performance. All the cases were run for ambient, hot, and cold temperatures.

The recommended future work of this project summarizes in a few major points as described in the following. First, to develop a general algorithm that solves two-component propellant grains and give an optimum solution of the internal grain dimensions which are the length and diameter of each segment. In other words, using machine learning capabilities like the genetic algorithm to predict the propellant's grain configuration by only given the rocket motor performance requirements. That will be enabled through introducing multiple case studies to train the software so it can give the optimum solution. Second, this code was developed based on a 128 mm rocket motor as a given case to enable running the program while having available experimental results, yet the input file to the program could be altered with another rocket motor dimensions to ensure the functionality of the program. The third-potential idea of a future work is to manufacture the

optimized propellant grain and conduct a firing test to validate the optimized mathematical model experimentally. Generally, the main goal is optimizing the program in a way to maximize the performance of rocket motors for a given requirements. One of the things that could be done in the future work is to calculate the burning surface area through a level set method model and compare the results of the two methods in terms of accuracy.

References

[1] Alemayehu, A. Y. and Solomon, L. G. (2020) "Design of a Solid Rocket Propulsion System," *International Journal of Aeronautics Aerospace Research*, 7(2), pp. 224–229. doi: 10.19070/2470-4415-2000027

[2] Skrishnan, 2022: SKRISHNAN. 2022. *Classification of Propulsion Systems* [Online]. Available: https://propulsion-skrishnan.com/pdf/Classification%20of%20Propulsion%20Systems.pdf [Accessed May 23 2022].

[3] Kabe, A. M. and Sako, B. H. (2020) "Forced vibration of multi-degree-of-freedom systems," *Structural Dynamics Fundamentals and Advanced Applications*, pp. 437–609.

[4] Stausland, C. (2019) "Liquid Propellants," *NAROM*. Available at: http://www.narom.no/undervisningsressurser/sarepta/rocket-theory/rocket-propellants-2/liquid-propellants/ (Accessed: June 12, 2021).

[5] Maxwell, W. R. and Young, G. H. S. (1961) "Solid propellant rocket motors," *Journal of the Royal Aeronautical Society*, 65(604), pp. 252–262. doi: 10.1017/s0368393100089872.

[6] Surmacz, P. and Rarata, G. (2009) "Hybrid rocket propulsion development and application," *Progress in Astronautics*, *1*, pp.13-25

[7] Rice, J. (2013) "Introduction to rocketry 1 June rocket concepts Newton's laws of motion thrust drag stability moments of inertia parachutes rocket construction," *Slideplayer.com*. Available at: https://slideplayer.com/slide/9131863/ (Accessed: May 15, 2022).

[8] Zandbergen, B.T.C. (2013) "Some typical solid propellant rocket motors," *Delft University of Technology, Faculty of Aerospace Engineering, Memorandum M-712 (Version 2.0)*.

[9] Tshokotsha, M. H. (2016) *Internal ballistic modelling of solid rocket motors using level set methods for simulating grain burnback.* Doctoral Dissertation. Stellenbosch: Stellenbosch University.

[10] Wicaksono, B. *et al.* (2020) "Analytical calculation, numerical and hydrostatic test as a validation of material strength of the new RX-450 rocket motor tube," *Proceedings of the 6th International Conference and Exhibition on Sustainable Energy and Advanced Materials*. Singapore: Springer, pp. 827–838.

[11] Hartfield et al., 2003: HARTFIELD, R., JENKINS, R., BURKHALTER, J. & FOSTER, W. A review of analytical methods for solid rocket motor grain analysis. 39th AIAA/ASME/SAE/ASEE Joint Propulsion Conference and Exhibit, 2003. 4506

[12] Rajesh et al., 2017): RAJESH, S., SURESH, G. & MOHAN, R. C. 2017. A review on material selection and fabrication of composite solid rocket motor (SRM) casing. Int. J Mech. Solid, 9, 125-138.

[13] Peters, 2011: PETERS, S. T. 2011. *Composite filament winding*, ASM International.

[14] Wikipedia contributors. (2021) "*de Laval nozzle*," *Wikipedia, The Free Encyclopedia*. Available at: http://en.wikipedia.org/w/index.php?title=De_Laval_nozzle&oldid=1062746288 (Accessed: May 15, 2022).

[15] Aerospaceweb, 2022: AEROSPACEWEB. 2022. *Rocket Nozzle Shapes* [Online]. Available: http://www.aerospaceweb.org/design/aerospike/shapes.shtml#:~:text=To%20date%20three%20major%20types,or%20plug%2C%20have%20been%20employed. [Accessed May 20 2022].

[16] Barrett, D. H. (1971) *Solid Rocket Motor Igniters*. Springfield: National Aeronautics And Space Administration.
[17] Foster, W. A., Jr and Sforzini, R. H. (1982) "Optimization of solid rocket motor igniter performance requirements," *Engineering optimization*, 6(1), pp. 31–38. doi: 10.1080/03052158208902452.
[18] NASA TECHNICAL REPORTS SERVER. 2022. Standard Molded Composite Rocket Pyrogen Igniter - A progress report [Online]. Available: https://ntrs.nasa.gov/citations/19780047566 [Accessed May 20 2022].
[19] NTRS. 1971. SOLID ROCKET MOTOR IGNITERS [Online]. Available: https://core.ac.uk/download/pdf/80651664.pdf [Accessed May 20 2022].
[20] ROGOWSKI, G. S., DAVIDSON, T. F. & LUDLOW, T. 1990. Insulating liner for solid rocket motor containing vulcanizable elastomer and a bond promoter which is a novolac epoxy or a resole treated cellulose. Google Patents.
[21] Mohan Kumar, L., Usha, K. and Chakravarthy, P. (2018). Advanced Ablative composites for Aerospace applications. *IOP Conference Series: Materials Science and Engineering*, 360, p.012036. doi:https://doi.org/10.1088/1757-899x/360/1/012036.

[22] OKNINSKI, A. 2021. Solid rocket propulsion technology for de-orbiting spacecraft. Chinese Journal of Aeronautics.
[23] ATA, Y. 2015. Numerical burnback analysis of three dimensional solid propellant grains. Middle East Technical University.
[24] OH, S.-H., KIM, Y.-C., CHA, S.-W. & ROH, T.-S. 2017. Study of Hybrid Optimization Technique for Grain Optimum Design. International Journal of Aeronautical and Space Sciences, 18, 780-787.
[25] TOLA, C. & NIKBAY, M. 2019. Internal ballistic modeling of a solid rocket motor by analytical burnback analysis. Journal of Spacecraft and Rockets, 56, 498-516.
[26] BARRERE, M. 1960. Rocket Propulsion Elsevier Publishing Company. New York.
[27] BARRON, J. Generalized coordinate grain design and internal ballistics evaluation program. 3rd Solid propulsion conference, 1968. 490.
[28] Ward, T.A. (2010) *Aerospace propulsion systems*. John Wiley & Sons.
[29] Sutton. G. P., "Rocket Propulsion Elements", NEW York, 1992
[30] Subramaniam, K. and Jeenu, R. (2020) "*Introduction*," Chemical Rockets. Cham: Springer International Publishing, pp. 195–204.
[31] Lenoir, J. M. and Robillard, G. (1957) "A mathematical model to predict the effects of erosive burning of solid propellant rockets," *Proceedings of the sixth international symposium on combustion*, pp. 663–672.
[32] Shekhar, H. (2009) "Design of funnel port tubular propellant grain for neutral burning profile in rockets," *Defence science journal*, 59(5), pp. 494–498. doi: 10.14429/dsj.59.1550.
[33] Alazeezi, M. and Elek, P. (2018) "Analytical and numerical burnback analysis of end burner grain with cylindrical cavity," *8th International Scientific Conference on Defensive Technologies-OTEH*
[34] AGARD. (1988) "Design Methods in Solid Rocket Motors," AGARD Lecture Series No: 150.
[35] Zarchan, P., Jensen, G. E. and Netzer, D. W. (1996) *Tactical Missile Propulsion*. Virginia: American Institute of Aeronautics and Astronautics.

[36] Tola, C. and Nikbay, M. (2019) "Internal ballistic modeling of a solid rocket motor by analytical burnback analysis," *Journal of spacecraft and rockets*, 56(2), pp. 498–516. doi: 10.2514/1.a34065.
[37] Willcox, M. A. *et al.* (2007) "Solid rocket motor internal ballistics simulation using three-dimensional grain burnback," *Journal of propulsion and power*, 23(3), pp. 575–584. doi: 10.2514/1.22971.
[38] Račkauskas, S., Fedaravičius, A. and Survila, A. (2019) "Numerical study on internal ballistics characteristics of a solid propellant rocket motor," *Mechanika*, 25(3), pp. 187–196.
[39] Gossant, B. (1993) "REMOVED: Solid propellant combustion and internal ballistics of motors," in *Solid Rocket Propulsion Technology*. Elsevier, pp. 111–191.
[40] Seitzman, J. M. (2005) "Thrust coefficient, characterictic velocity and ideal nozzle expansion," *https://seitzman.gatech.edu/.* Available at: http://soliton.ae.gatech.edu/people/jseitzma/classes/ae4451/thrust_coefficient2.pdf (Accessed: May 15, 2022).
[41] Sharma, V. (2017) "How does a de Laval (convergent-divergent) nozzle work?,"*https://www.quora.com/*. Available at:https://www.quora.com/How-does-a-de-Laval-convergent-divergent-nozzle-work(Accessed: May 15, 2022).
[42] Cavallini, E., 2010. *Modeling and numerical simulation of solid rocket motors internal ballistics*. Dissertation. Rome: Sapienza University of Rome.
[43] Nakka, R. (2001) "Solid Rocket Motor Theory-Chamber Pressure,"https://www.nakka-rocketry.net/. Available at: https://www.nakka-rocketry.net/th_pres.htm(Accessed: May 15, 2022).
[44] Püskülcü, G. and Ulas, A. (2008a) "3-D grain burnback analysis of solid propellant rocket motors: Part 1-ballistic motor tests," *Aerospace Science and Technology*, 12(8), pp. 579–584.
[45] Püskülcü, G. and Ulas, A. (2008) "3-D grain burnback analysis of solid propellant rocket motors: Part 2-modeling and simulations," *Aerospace Science and Technology*, 12(8), pp. 585–591.
[46] Braeunig.us. 2022. Basics of Space Flight: Rocket Propellants. [online] Available at: http://www.braeunig.us/space/propel.htm
[47] Chaturvedi, S. and Dave, P.N. (2019). Solid propellants: AP/HTPB composite propellants. *Arabian Journal of Chemistry*, 12(8), pp.2061–2068. doi:https://doi.org/10.1016/j.arabjc.2014.12.033.

[48] Braeunig, R.A. (n.d.). *Basics of Space Flight: Rocket Propellants*. [online] www.braeunig.us. Available at: http://www.braeunig.us/space/propel.htm#:~:text=Basics%20of%20Space%20Flight%3A%20Rocket%20Propellants&text=Propellant%20is%20the%20chemical%20mixture [Accessed 14 Nov. 2023].

[49] Thermochemical Computer Code EXPLO5. (n.d.). *Thermochemical Computer Code EXPLO5*. [online] Available at: https://www.ozm.cz/explosives-performance-tests/thermochemical-computer-code-explo5/ [Accessed 5 Nov. 2023].

[50] Babayomi, O. O. *et al.* (2013) "Low cost ground test equipment for atmospheric rocket flights using embedded systems," in *2013 IEEE International Conference on Emerging &*

Sustainable Technologies for Power & ICT in a Developing Society (NIGERCON). IEEE, pp. 26–29.
[51] Fan, J. W. and Tan, F. T. (2013) "Analysis of major defects and nondestructive testing methods for solid rocket motor," in *Applied Mechanics and Materials*. Trans Tech Publications Ltd, pp. 618–622.
[52] Soares, D. M. (2018) "Development of a Vertical Static Test Bench for Amateur Rocket Engines," *International Journal of Advanced Scientific and Technical Research*, 5, pp. 45–49.
[53] Fedaravičius, A. *et al.* (2015) "Design of the testing system for solid propellant rocket motor thrust measurements using mathematical modelling techniques," *Journal of Measurements in Engineering*, 3(4), pp. 123–131.
[54] Singh, S. (2013) "Solid rocket motor for experimental sounding rockets," *Advances in Aerospace Science and Applications*, 3(3), pp. 199–208.
[55] Suksila, T. (2018) "Experimental investigation of solid rocket motors for small sounding rockets," in *IOP Conference Series: Materials Science and Engineering*. IOP Publishing.
[56] Ziraksaz, M. H. (2009) "How to Design, Build and Test Small Solid Propellant Rocket Motor (Part One)," in *45th AIAA/ASME/SAE/ASEE Joint Propulsion Conference & Exhibit*.
[57] Kumar, A. and Anjaneyulu, L. (2015) "Emerging Trends in Instrumentation in Rocket Motor Testing Over Three Decades," *Defence Science Journal*, (1).
[58] Tekscan. (2014)"Load cell vs. Force sensor," Available at: https://www.tekscan.com/resources/ebook/load-cell-vs-force-sensor (Accessed: June 03, 2021).
[59] Chandru, R. A. *et al.* (2018) "Additive manufacturing of solid rocket propellant grains," *Journal of Propulsion and Power*, 34(4), pp. 1090–1093.
[60] Condon, J. A., Renie, J. P. and Osborn, J. R. (1977) "Temperature sensitivity of propellant burning rates," *Combustion and flame*, 30, pp. 267–276. doi: 10.1016/0010-2180(77)90075-x.

7. Appendices

7.1 Program inputs script

```
k = ; %adiabatic constant
Gama = (k^0.5)*((2/(k+1))^((k+1)/(2*(k-1))));
Toc = ; %initial grain temperature [∞C]
Too = Toc+273.15; %initial grain temperature [K]

%Fast burning fuel
rho1 = 1715; %Density [kg/m^2]
b1 = ; %burn rate coeficient
n1 = ; %pressure exponent
Sigmap1 = 0.0016; %temperature sensitivity
Tc1 = 2599.2; %burning temperature
Rg1 = 326.1; %approximate gas constant (326.1-360)
cstar1 = ((Rg1*Tc1)^0.5)/Gama; %c* - characteristic velocity

%Slow burning fuel
rho2 = 1705; %Density [kg/m^2]
b2 = ; %burn rate coeficient
n2 = ; %pressure exponent
Sigmap2 = 0.0016; %temperature sensitivity
Tc2 = 2744.6; %burning temperature
Rg2 = 332.7; %gas constant
cstar2 = ((Rg2*Tc2)^0.5)/Gama; %c* - characteristic velocity

%General characteristics
D = 0.1189; %Outer grain diameter [m]
dkr = 0.046; %critical nozzle diameter [m]
Akr = (dkr^2)*pie/4; %critical area [m^2]
pc = 100*10^5; %initial chamber pressure

cf=1.5; %thrust coefficient

x = 0; %burned length
dx = 0.00001; %burn step [m]
r1 = 0; %burn rate of fast propellant
r2 = 0; %burn rate if slow propellant
Isp1=0; %fast propellant specific impulse
Isp2=0; %slow propellant specific impulse
t = 0; %time
mdot = 0; %mass flow
Af = 0; %burning surface area of fast propellant
As = 0; %burning surface area of slow propellant
Atotal = 0; %total burning surface area
f = 0; %thrust

%matrix
T = []; %time
PC = []; %chamber pressure
F = []; %Thrust
Mdot = []; %mass flux
A1 = []; %fast fuel burn area
A2 = []; %slow fuel burn area
A = []; %total burn area
R1 = []; %fast burn rate
R2 = []; %slow burn rate
DS1 = [];  %step diameter
```

7.2 Original model script

```
%% BURNING PROCESS

if var <= 1

   %ORIGINAL DESIGN

   Lf = ; %inital grain length
   Df0 = ; %initial grain diameter
   Df = Df0;
   step = 1;
   Vctotal = Lf*D*pie;
   Vc = Lf*Df*pie;

   %STEP 1 (only fast propellant)
   while Df < 0.084

      T = [T t]; %time
      PC = [PC pc]; %pressure
      F = [F f]; %thrust
      Mdot = [Mdot mdot]; %mass flow rate
      R1 = [R1 r1]; %fast burn rate
      R2 = [R2 r2]; %slow burn rate
      A1 = [A1 Af]; %fast fuel burn area
      A2 = [A2 As]; %slow fuel burn area
      A = [A Atotal]; %total burn area

      Af = Lf*Df*pie+((D^2)-(Df^2))*pie/4; %burning surface area of fast propellant
      As = 0;
      Atotal = Af+As; %total burning surface area

      r1 = (b1*(pc^n1))*(exp(Sigmap1*(Too-288.15))); %fast burn rate
      r2 = 0; %slow burn rate (no burning at this step)
      mdot1 = Af*rho1*r1; %mass flow rate
      mdot2 = 0;
      mdot = mdot1+mdot2;
      pc = mdot1*((Rg1*Tc1)^0.5)/(Gama*Akr); %chamber pressure pc=pc(mdot)
      Isp1 = cstar1*cf;
      Isp2 = cstar2*cf;
      f = Isp1*mdot1+Isp2*mdot2;

      Lf = Lf-dx;
      Df = Df+2*dx; %inner diameter
      t = t + dx/r1; %time
      x = x+dx;
   end
```

```
%STEP 2
Lf = Lf-0.105;
Af = Lf*Df*pie;
Ds0 = Df;
Ds1 = Ds0;
Ls = 0.105;
Ls1 = Ls;
x = 0;
a1 = 0; %axial edge burning of slow fuel
c1 = 0; %radial edge burning of slow fuel
e1 = 0; %length of edge
As1e = 0; %burning area of edge
As1 = Ls1*Ds1*pie + As1e;
As = As1;
step = step+1;

while Df < 0.086

    T = [T t];
    PC = [PC pc];
    F = [F f];
    Mdot = [Mdot mdot];
    R1 = [R1 r1]; %fast burn rate
    R2 = [R2 r2]; %slow burn rate
    A1 = [A1 Af]; %fast fuel burn area
    A2 = [A2 As]; %slow fuel burn area
    A = [A Atotal]; %total burn area

    Af = Lf*Df*pie+((D^2)-(Df^2))*pie/4; %Burning surface area of fast propellant
    As1e = pie*(Df+Ds1)*e1/2; %edge burning area

    As1 = Ls1*Ds1*pie + As1e;
    As = As1; %burning surface area of slow propellant
    Atotal = Af + As; %total burning surface area

    r1 = (b1*(pc^n1))*(exp(Sigmap1*(Too-288.15))); %fast burn rate
    r2 = (b2*(pc^n2))*(exp(Sigmap2*(Too-288.15))); %slow burn rate (no burning at this time)
    mdot1 = Af*rho1*r1; %mass flow
    mdot2 = As*rho2*r2;
    mdot = mdot1+mdot2;
    pc = mdot1*((Rg1*Tc1)^0.5)/(Gama*Akr)+mdot2*((Rg2*Tc2)^0.5)/(Gama*Akr); %chamber pressure pc=pc(mdot)
    Isp1 = cstar1*cf;
    Isp2 = cstar2*cf;
    f = Isp1*mdot1+Isp2*mdot2;

    Df = Df+2*dx; %inner diameter

    %step 1 (new step)
    Ds1 = Ds1+2*dx*(r2/r1);
    a1 = a1+dx*(r2/r1); %axial edge burning of slow fuel
    c1 = c1+dx; %radial edge burning of slow fuel
    e1 = ((a1^2)+((c1-a1)^2))^0.5;
    Ls1 = Ls-a1;

    Lf = Lf-dx;
    t = t + dx/r1; %time
    x = x+dx;

end
```

```
%STEP 3
Lf = Lf-0.105;
Af = Lf*Df*pie;
Ds0 = Df;
Ds2 = Ds0;
Ls = 0.105;
Ls2 = Ls;
x= 0;
a2 = 0; %axial edge burning of slow fuel
c2 = 0; %radial edge burning of slow fuel
e2 = 0; %length of edge
As2e = 0;
As2 = Ls2*Ds2*pie + As2e;
As = As+As2;
step = step+1;

while Df < 0.088
   T = [T t];
   PC = [PC pc];
   F = [F f];
   Mdot = [Mdot mdot];
   R1 = [R1 r1]; %fast burn rate
   R2 = [R2 r2]; %slow burn rate
   A1 = [A1 Af]; %fast propellant burn area
   A2 = [A2 As]; %slow propellant burn area
   A = [A Atotal]; %total burn area

   Af = Lf*Df*pie+((D^2)-(Df^2))*pie/4; %burning surface area of fast propellant
   As1e = pie*(Ds1+Ds2)*e1/2; %edge burning area
   As2e = pie*(Df+Ds2)*e2/2;
   As1 = Ls1*Ds1*pie + As1e;
   As2 = Ls2*Ds2*pie + As2e;
   As = As1+As2; %burning surface area of slow propellant
   Atotal = Af + As;

   r1 = (b1*(pc^n1))*(exp(Sigmap1*(Too-288.15))); %fast burn rate
   r2 = (b2*(pc^n2))*(exp(Sigmap2*(Too-288.15))); %slow burn rate
   mdot1 = Af*rho1*r1; %mass flow rate
   mdot2 = As*rho2*r2;
   mdot = mdot1+mdot2;
   pc = mdot1*((Rg1*Tc1)^0.5)/(Gama*Akr)+mdot2*((Rg2*Tc2)^0.5)/(Gama*Akr); %chamber pressure pc=pc(mdot)
   Isp1 = cstar1*cf;
   Isp2 = cstar2*cf;
   f = Isp1*mdot1+Isp2*mdot2;

   Df = Df+2*dx; %inner diameter

   %Slow burn
   Ds1 = Ds1+2*dx*(r2/r1);
   a1 = a1+dx*(r2/r1);
   Ls1 = Ls-a1;
   %new step
   Ds2 = Ds2+2*dx*(r2/r1);
   a2 = a2+dx*(r2/r1); %axial edge burning of slow fuel
   c2 = c2+dx; %radial edge burning of slow fuel
   e2 = ((a2^2)+((c2-a2)^2))^0.5;

   Lf = Lf-dx;
   t = t + dx/r1; %time
   x = x+dx;
end
```

```
%STEP 21

while Ds1< D

    T = [T t];
    PC = [PC pc];
     F = [F f];
    Mdot = [Mdot mdot];
    R1 = [R1 r1]; %fast burn rate
    R2 = [R2 r2]; %slow burn rate
    A1 = [A1 Af]; %fast propellant burn area
    A2 = [A2 As]; %slow propellant burn area
    A = [A Atotal]; %total burn area

    Af = 0; %burning surface area of fast propellant
    As1e = pie*(Ds1+D)*e1/2;

    As1 = Ls1*Ds1*pie + As1e;
    As = As1; %burning surface area of slow propellant

    Atotal = Af + As;

    r1 = 0; %fast burn rate
    r2 = (b2*(pc^n2))*(exp(Sigmap2*(Too-288.15))); %slow burn rate
    mdot1 = 0; %mass flow
    mdot2 = As*rho2*r2;
    mdot = mdot1+mdot2;
    pc = mdot2*((Rg2*Tc2)^0.5)/(Gama*Akr); %chamber pressure pc=pc(mdot)
    Isp1 = cstar1*cf;
    Isp2 = cstar2*cf;
    f = Isp1*mdot1+Isp2*mdot2;

    Df = D; %inner diameter

    %Disappearing step
    Ds1 = Ds1+2*dx;
    a1 = a1+dx;
    Ls1 = Ls-a1;
    Ds1 = Ds1+2*dx;
    c1 = c1-dx; %radial edge burning of slow propellant
    e1 = ((a1^2)+((c1-a1)^2))^0.5;

    t = t + dx/r2; %time
    x = x+dx;

end
```

7.3 Optimized model script

```
%PHASE 1 (fast burning only)

while Df < Ds1

    T = [T t];
    PC = [PC pc];
    F = [F f];
    Mdot = [Mdot mdot];
    R1 = [R1 r1]; %fast burn rate
    R2 = [R2 r2]; %slow burn rate
    A1 = [A1 Af]; %fast propellant burn area
    A2 = [A2 As]; %slow propellant burn area
    A = [A Atotal]; %total burn area
    DS1 =[DS1 Ds1];
    LSLOPE = [LSLOPE Lslope];

    Af = Lf*Df*pie+((D^2)-(Df^2))*pie/4;
    As = 0;

    Atotal = Af+As;

    r1 = (b1*(pc^n1))*(exp(Sigmap1*(Too-288.15)));
    r2 = 0;
    mdot1 = Af*rho1*r1; %mass flow
    mdot2 = As*rho2*r2;
    mdot = mdot1+mdot2;

    pc = mdot1*((Rg1*Tc1)^0.5)/(Gama*Akr)+mdot2*((Rg2*Tc2)^0.5)/(Gama*Akr);

    Isp1 = cstar1*cf;
    Isp2 = cstar2*cf;
    f = Isp1*mdot1+Isp2*mdot2;

    Lf = (Lf-dx);
    Df = Df+2*dx;

    t = t + dx/r1;
    x = x+dx;

end
```

```
%PHASE 2 (slope)

while Df < Ds2

  T = [T t];
    PC = [PC pc];
    F = [F f];
    Mdot = [Mdot mdot];
    R1 = [R1 r1]; %fast burn rate
    R2 = [R2 r2]; %slow burn rate
    A1 = [A1 Af]; %fast fuel burn area
    A2 = [A2 As]; %slow fuel burn area
    A = [A Atotal]; %total burn area
    DS1 =[DS1 Ds1];
    LSLOPE = [LSLOPE Lslope];

    Af = Lf*Df*pie+((D^2)-(Df^2))*pie/4;
    As = (Ds1*Ls1*pie+(pie*(Df+Ds1)*es/2));
    Atotal = Af+As;

    r1 = (b1*(pc^n1))*(exp(Sigmap1*(Too-288.15)));
    r2 = (b2*(pc^n2))*(exp(Sigmap2*(Too-288.15)));
    mdot1 = Af*rho1*r1; %mass flow
    mdot2 = As*rho2*r2;
    mdot = mdot1+mdot2;
    pc = mdot1*((Rg1*Tc1)^0.5)/(Gama*Akr)+mdot2*((Rg2*Tc2)^0.5)/(Gama*Akr);
    Isp1 = cstar1*cf;
    Isp2 = cstar2*cf;
    f = Isp1*mdot1+Isp2*mdot2;

    Lf = Lf-dx- dx*105;
    Ls1 = (Ls1-dx*r2/r1);
    Lslope = Lslope + dx*105 + dx*r2/r1;
    es = (((Lslope)^2)+((Df/2-Ds1/2)^2))^0.5;
    Df = Df+2*dx;
    Ds1 = Ds1+2*dx*(r2/r1);

    t = t + dx/r1;
    x = x+dx;
end
```

```
    %PHASE 3

while Df < D

  T = [T t];
    PC = [PC pc];
    F = [F f];
    Mdot = [Mdot mdot];
    R1 = [R1 r1]; %fast burn rate
    R2 = [R2 r2]; %slow burn rate
    A1 = [A1 Af]; %fast fuel burn area
    A2 = [A2 As]; %slow fuel burn area
    A = [A Atotal]; %total burn area
    DS1 =[DS1 Ds1];
    LSLOPE = [LSLOPE Lslope];

    Af = Lf*Df*pie+((D^2)-(Df^2))*pie/4;
    As = (Ds1*Ls1*pie+(pie*(Df+Ds1)*es/2)+pie*(Ds2+Df)*ef/2)+Ds2*Ls2*pie;
    Atotal = Af+As;

    r1 = (b1*(pc^n1))*(exp(Sigmap1*(Too-288.15)));
    r2 = (b2*(pc^n2))*(exp(Sigmap2*(Too-288.15)));
    mdot1 = Af*rho1*r1; %mass flow
    mdot2 = As*rho2*r2;
    mdot = mdot1+mdot2;
    pc = mdot1*((Rg1*Tc1)^0.5)/(Gama*Akr)+mdot2*((Rg2*Tc2)^0.5)/(Gama*Akr);
    Isp1 = cstar1*cf;
    Isp2 = cstar2*cf;
    f = Isp1*mdot1+Isp2*mdot2;

    Lf = Lf-dx;
    Ls1 = (Ls1-dx*r2/r1);
    es = (((Lslope)^2)+((Ds2/2-Ds1/2)^2))^0.5;
    Df = Df+2*dx;
    Ds1 = (Ds1+2*dx*r2/r1);
    Ds2 = Ds2+2*dx*r2/r1;
    a1 = (a1+dx*r2/r1);
    c1 = (c1+dx);
    ef = ((a1^2)+((c1-a1)^2))^0.5;

    t = t + dx/r1;
    x = x+dx;
end
```

```
    %PHASE 4 (slow burning only)

while Ds2 < D

  T = [T t];
    PC = [PC pc];
    F = [F f];
    Mdot = [Mdot mdot];
    R1 = [R1 r1]; %fast burn rate
    R2 = [R2 r2]; %slow burn rate
    A1 = [A1 Af]; %fast fuel burn area
    A2 = [A2 As]; %slow fuel burn area
    A = [A Atotal]; %total burn area
    DS1 =[DS1 Ds1];
    LSLOPE = [LSLOPE Lslope];

    Af = 0;
    As = (Ds1*Ls1*pie+(pie*(D+Ds1)*es/2));
    Atotal = Af+As;

    r1 = 0;
    r2 = (b2*(pc^n2))*(exp(Sigmap2*(Too-288.15)));
    mdot1 = Af*rho1*r1; %mass flow
    mdot2 = As*rho2*r2;
    mdot = mdot1+mdot2;
    pc = mdot1*((Rg1*Tc1)^0.5)/(Gama*Akr)+mdot2*((Rg2*Tc2)^0.5)/(Gama*Akr);
    Isp1 = cstar1*cf;
    Isp2 = cstar2*cf;
    f = Isp1*mdot1+Isp2*mdot2;

    Lf = 0;
    Ls1 = (Ls1-dx);
    es = (((Lslope)^2)+((D/2-Ds1/2)^2))^0.5;
    Df = D;
    Ds1 = (Ds1+2*dx);
    Ds2 = Ds2 + 2*dx;

    t = t + dx/r2;
    x = x+dx;
end
```

```
    %PHASE 5

while Ds1 < D

    T = [T t];
    PC = [PC pc];
    F = [F f];
    Mdot = [Mdot mdot];
    R1 = [R1 r1]; %fast burn rate
    R2 = [R2 r2]; %slow burn rate
    A1 = [A1 Af]; %fast fuel burn area
    A2 = [A2 As]; %slow fuel burn area
    A = [A Atotal]; %total burn area
    DS1 =[DS1 Ds1];
    LSLOPE = [LSLOPE Lslope];

    Af = 0;
    As = (Ds1*Ls1*pie+(pie*(Df+Ds1)*es/2));
    Atotal = Af+As;

    r1 = 0;
    r2 = (b2*(pc^n2))*(exp(Sigmap2*(Too-288.15)));
    mdot1 = Af*rho1*r1; %mass flow
    mdot2 = As*rho2*r2;
    mdot = mdot1+mdot2;
    pc = mdot1*((Rg1*Tc1)^0.5)/(Gama*Akr)+mdot2*((Rg2*Tc2)^0.5)/(Gama*Akr);
    Isp1 = cstar1*cf;
    Isp2 = cstar2*cf;
    f = Isp1*mdot1+Isp2*mdot2;

    Lf = 0;
    Ls1 = (Ls1-dx);
    Lslope = Lslope-340*dx;
    es = (((Lslope)^2)+((D/2-Ds1/2)^2))^0.5;
    Df = D;
    Ds1 = (Ds1+2*dx);

    t = t + dx/r2;
    x = x+dx;
end
```

Biography

Mohammed Alazeezi, 33 years old, was born and raised in Al Ain, United Arab Emirates. He has been very passionate about space and aviation, and his ambition devoted him to pursue studies that can lead him to a career in the aerospace industry. Upon the completion of high school and after a competitive selection for a scholarship, he was awarded a full scholarship from the Ministry of Presidential Affairs in the UAE to pursue the bachelor's degree in Aerospace Engineering.

He started the bachelor's degree studies on 2010 and graduated on 2014 from Embry-Riddle Aeronautical University, Daytona Beach, FL, USA. The major was Aerospace Engineering with a sub-plan of propulsion. Throughout those four years, he gained the basic knowledge of aerospace and mechanics that qualified him to start a career on such a field. The senior's year graduation project was to design a nuclear fusion propulsion system in a team of four students.

A couple of months after graduation, he started a job as a Propulsion Engineer at Emirates Advanced Research & Technology Company (EARTH) where he worked on several projects before getting the opportunity to pursue a master's degree at the Faculty of Mechanical Engineering – Weapons Systems department, University of Belgrade. The program assisted him to raise his knowledge on the weapons systems mainly missiles. The master's thesis topic was "Design of dual thrust rocket motors". A MATLAB program was developed to perform all the necessary calculations to satisfy the given requirements of the motor's caliber and thrust profile. The master's thesis work and the proposed ideas for future work had the potential to be continued to the PhD level. Therefore, he started the PhD program on 2017 in the field of Rocket Propulsion.

He is currently holding the position of a Department Manager of Propulsion at HALCON, Abu Dhabi which is a company specializes in developing and manufacturing precision guided systems. This rule in the company focuses on building the rocket motors development capabilities in terms of fostering skilled manpower and establishing manufacturing and testing infrastructure, which both can serve the demand and need of solid rocket motors in the UAE's defense market and worldwide.

Bibliography:

1. Alazeezi, M., Elek, P.: Analytical and Numerical Burnback Analysis of End Burner Grain with Cylindrical Cavity, 8th International Scientific Conference on Defensive Technologies – OTEH 2018, October 2018, Belgrade, Serbia.
2. Alazeezi, M., Elek, P. (2020). Nozzle Optimization of Dual Thrust Rocket Motors. In: Karabegović, I. (eds) New Technologies, Development and Application II. NT 2019. Lecture Notes in Networks and Systems, vol 76. Springer, Cham. https://doi.org/10.1007/978-3-030-18072-0_54
3. Alazeezi, M., Popović, N., P. Elek: "Two-Component Propellant Grain for Rocket Motor: Combustion Analysis and Geometric Optimization." Thermal Science, vol. 26, no. 2 Part B, 2022, pp. 1567–1578, 10.2298/tsci210604290a.

Биографија

Мохамед Алазези (Mohammed Alazeezi, 1990), рођен је и одрастао у Ал Аину, Уједињени Арапски Емирати (УАЕ). Био је веома заинтересован за космос и ваздухопловство, и његова амбиција га је довела до студија које омогућавају каријеру у ваздухопловној индустрији. По завршетку средње школе и након селекције добио је пуну стипендију Министарства председничких послова УАЕ за основне студије ваздухопловног инжењерства.

На Аеронаутички универзитет Ембри-Ридле (Embry-Riddle Aeronautical University) са седиштем у Дејтона Бичу на Флориди уписао се 2010. године, а четворогодишње основне академске студије је завршио 2014. године. Изабрао је усмерење Аерокосмотехника (Aerospace Engineering), са ужом облашћу Погон летелица. У току четири године школовања, стекао је фундаментална знања из домена механике и аерокосмотехнике која су га квалификовала да започне каријеру у овој области. Дипломски пројекат у завршној години студија радио је у области погонског система на принципима нуклеране фузије у тиму од четири студента.

Неколико месеци после дипломирања, Мохамед Алазизи запошљава се као инжењер у области пропулзије у компанији Emirates Advanced Research & Technology (EARTH) у Абу Дабију (Abu Dhabi), УАЕ. После ангажовања на више пројеката, 2015. године добија прилику да настави усавршавање кроз мастер студије на Универзитету у Београду – Машинском факултету. На модулу за Системе наоружања успешно дипломира 2017. године са средњом оценом 9.45. Савладани програм му је помогао да зачајно унапреди знање у домену система наоружања, посебно вођених ракета. Тема мастер рада је била "Пројектовање ракетних мотора са двостепеном кривом потиска" ("Design of dual thrust rocket motors"). Рад је резултирао развојем комплексног програма за одређивање свих неопходних параметара мотора специфичне конфигурације, тако да буду задовољени постављени захтеви у погледу калибра и профила потиска.

Ангажовање на мастер раду, сагледавање могућности за унапређење добијених резултата, као и подршка компаније, допринели су одлуци да настави усавршавање на докторским студијама. На докторске студије на Машинском факултету у Београду се уписује 2017. године и дефинише програм студија који у фокусу поново има погон ракета са применама у системима наоружања. У току студија учествовао је на више пројеката и објавио је два рада на међународним конференцијама.

Тренутно је на позицији менаџера одељења за погон у компанији Halcon, Абу Даби, која је специјализована за развој и производњу прецизних вођених система. Компанија је фокусирана на развој и производњу ракетних мотора, кроз подстицање квалификоване радне снаге и успостављања инфраструктуре за производњу и тестирање, у циљу задовољавања потражње за ракетним моторима на одбрамбеном тржишту УАЕ и широм света.

Библиографија:

4. Alazeezi, M., Elek, P.: Analytical and Numerical Burnback Analysis of End Burner Grain with Cylindrical Cavity, 8th International Scientific Conference on Defensive Technologies – OTEH 2018, October 2018, Belgrade, Serbia.
5. Alazeezi, M., Elek, P. (2020). Nozzle Optimization of Dual Thrust Rocket Motors. In: Karabegović, I. (eds) New Technologies, Development and Application II. NT 2019. Lecture Notes in Networks and Systems, vol 76. Springer, Cham. https://doi.org/10.1007/978-3-030-18072-0_54
6. Alazeezi, M., Popović, N., P. Elek: "Two-Component Propellant Grain for Rocket Motor: Combustion Analysis and Geometric Optimization." Thermal Science, vol. 26, no. 2 Part B, 2022, pp. 1567–1578, 10.2298/tsci210604290a.

Прилог 1.

Изјава о ауторству

Потписани-а **Mohammed Alazeezi**

број индекса **Д25/2017**

Изјављујем

да је докторска дисертација под насловом

Design and Optimization of Dual-Propellant Grains of Solid Propellant Rocket Motors

(Пројектовање и оптимизација двокомпонентних погонских пуњења ракетних мотора са чврстом погонском материјом)

- резултат сопственог истраживачког рада,
- да предложена дисертација у целини ни у деловима није била предложена за добијање било које дипломе према студијским програмима других високошколских установа,
- да су резултати коректно наведени и
- да нисам кршио/ла ауторска права и користио интелектуалну својину других лица.

Потпис докторанда

У Београду, 29.01.2024.

Прилог 2.

Изјава о истоветности штампане и електронске верзије докторског рада

Име и презиме аутора	**Mohammed Alazeezi**
Број индекса	**Д25/2017**
Студијски програм	**Докторске студије**
Наслов рада	**Design and Optimization of Dual-Propellant Grains of Solid Propellant Rocket Motors**
	(Пројектовање и оптимизација двокомпонентних погонских пуњења ракетних мотора са чврстом погонском материјом)
Ментор	**Предраг Елек**
Потписани/а	**Mohammed Alazeezi**

Изјављујем да је штампана верзија мог докторског рада истоветна електронској верзији коју сам предао/ла за објављивање на порталу **Дигиталног репозиторијума Универзитета у Београду.**

Дозвољавам да се објаве моји лични подаци везани за добијање академског звања доктора наука, као што су име и презиме, година и место рођења и датум одбране рада.

Ови лични подаци могу се објавити на мрежним страницама дигиталне библиотеке, у електронском каталогу и у публикацијама Универзитета у Београду.

Потпис докторанда

У Београду, 29.01.2024.

Прилог 3.

Изјава о коришћењу

Овлашћујем Универзитетску библиотеку „Светозар Марковић“ да у Дигитални репозиторијум Универзитета у Београду унесе моју докторску дисертацију под насловом:

Design and Optimization of Dual-Propellant Grains of Solid Propellant Rocket Motors

(Пројектовање и оптимизација двокомпонентних погонских пуњења ракетних мотора са чврстом погонском материјом)

која је моје ауторско дело.

Дисертацију са свим прилозима предао/ла сам у електронском формату погодном за трајно архивирање.

Моју докторску дисертацију похрањену у Дигитални репозиторијум Универзитета у Београду могу да користе сви који поштују одредбе садржане у одабраном типу лиценце Креативне заједнице (Creative Commons) за коју сам се одлучио/ла.

(1.) **Ауторство**

2. Ауторство - некомерцијално

3. Ауторство – некомерцијално – без прераде

4. Ауторство – некомерцијално – делити под истим условима

5. Ауторство – без прераде

6. Ауторство – делити под истим условима

(Молимо да заокружите само једну од шест понуђених лиценци, кратак опис лиценци дат је на полеђини листа).

Потпис докторанда

У Београду, 29.01.2024.

1. Ауторство - Дозвољавате умножавање, дистрибуцију и јавно саопштавање дела, и прераде, ако се наведе име аутора на начин одређен од стране аутора или даваоца лиценце, чак и у комерцијалне сврхе. Ово је најслободнија од свих лиценци.

2. Ауторство – некомерцијално. Дозвољавате умножавање, дистрибуцију и јавно саопштавање дела, и прераде, ако се наведе име аутора на начин одређен од стране аутора или даваоца лиценце. Ова лиценца не дозвољава комерцијалну употребу дела.

3. Ауторство - некомерцијално – без прераде. Дозвољавате умножавање, дистрибуцију и јавно саопштавање дела, без промена, преобликовања или употребе дела у свом делу, ако се наведе име аутора на начин одређен од стране аутора или даваоца лиценце. Ова лиценца не дозвољава комерцијалну употребу дела. У односу на све остале лиценце, овом лиценцом се ограничава највећи обим права коришћења дела.

4. Ауторство - некомерцијално – делити под истим условима. Дозвољавате умножавање, дистрибуцију и јавно саопштавање дела, и прераде, ако се наведе име аутора на начин одређен од стране аутора или даваоца лиценце и ако се прерада дистрибуира под истом или сличном лиценцом. Ова лиценца не дозвољава комерцијалну употребу дела и прерада.

5. Ауторство – без прераде. Дозвољавате умножавање, дистрибуцију и јавно саопштавање дела, без промена, преобликовања или употребе дела у свом делу, ако се наведе име аутора на начин одређен од стране аутора или даваоца лиценце. Ова лиценца дозвољава комерцијалну употребу дела.

6. Ауторство - делити под истим условима. Дозвољавате умножавање, дистрибуцију и јавно саопштавање дела, и прераде, ако се наведе име аутора на начин одређен од стране аутора или даваоца лиценце и ако се прерада дистрибуира под истом или сличном лиценцом. Ова лиценца дозвољава комерцијалну употребу дела и прерада. Слична је софтверским лиценцама, односно лиценцама отвореног кода.